Bioinspired 3D Cocultures of Human Skeletal Myoblasts and Motoneuron-like Cells to Investigate Neuromuscular Function *In Vitro*

A thesis submitted by

Thomas Anthony Dixon

In partial fulfillment of the requirements for the degree of

PhD

In

Cell, Molecular, and Developmental Biology

Tufts University

Sackler School of Graduate Biomedical Sciences

May 2017

Advisor: David Kaplan, PhD

Abstract:

The physical connection in the developing embryo between ventral horn motoneurons and skeletal muscle myoblasts is responsible for the creation of neuromuscular junctions (NMJs), which allow electrical signals from the spinal cord to be translated to mechanical work in contractile skeletal muscle. Pathology at the NMJ contributes to the spectrum of neuromuscular, motoneuron, and dystrophic disease. Improving *in vitro* tools that allow for recapitulation of the normal physiology of the neuromuscular connection enables researchers to better understand the development and maturation of NMJs. Further development of these tools and use of diseased cells will help to decipher mechanisms leading to disruption of the NMJ, and related peripheral nerve and skeletal muscle pathology. In this work, we describe a unique platform to coculture human skeletal muscle myoblast-seeded hydrogels suspended in between flexible cantilevers with integrated motoneuron-like cells derived from human induced neural stem cells. This platform is fully customizable using 3D freeform printing into standard lab tissue culture materials, and allows for quantifiable human myoblast alignment in 3D with precise motoneuron integration into preformed myotubes. The coculture method allows for observation and analysis of neurite outgrowth and myogenic differentiation in 3D with quantification of several parameters of muscle innervation and function. We demonstrated activation of muscle originated calcium transients in 3D constructs as well as some evidence of nerve originated contractions in a fully human 3D NMJ. Future refinements with increased cell specificity and external stimulation may lead to a high throughput method of neuromuscular analysis of patient derived cells.

Acknowledgements:

I thank lab members Will Cantley, Will Collins, Ashwin Sundarakrishnan and Lorenzo Tozzi for discussion and technique, and Caroline McCormick for help with cell culture and bioprinting. We also thank the following Tufts faculty for additional mentorship and guidance: Li Zeng, Lauren Black, Jim Schwob, and Eric Frank. I would also like to thank my supportive friends and family, and of course, David Kaplan for years of advising and providing a fascinating opportunity for research.

Table of Contents

List of Tables

List of Figures

List of Copyrighted Materials Produced by Author

1. **Evolution of Bioinks and Additive Manufacturing Technologies for 3D Bioprinting**
   Rod R. Jose, Maria J. Rodriguez, Thomas A. Dixon, Fiorenzo Omenetto, and David L. Kaplan
   ACS Biomaterials Science & Engineering **2016** *2* (10), 1662-1678
   DOI: 10.1021/acsbiomaterials.6b00088

List of Abbreviations

2.5D – Layered Cell Culture Technique

2D – Two-dimensional

2D FFT – Two Dimensional Fast Fourier Transform

3D – Three-Dimensional

3T3 (BALB/ or NIH/) – Immortalized mouse embryo fibroblast lines

AChR – Acetylcholine Receptor

BAM – BioArtificial Muscle

C2C12 – Immortalized murine myoblast line

CRISPR - Clustered Regularly Interspaced Short Palindromic Repeats

DAPI - 2-(4-amidinophenyl)-1H -indole-6-carboxamidine, blue nuclear stain

DMEM - Dulbecco's Modified Eagle's Medium

ECM – extracellular matrix

FGF – Fibroblast Growth Factor

GelMA – Gelatin Methacrylate

HAT - sodium hypoxanthine, aminopterin and thymidine

ICBS - integrated composite tissue/organ building system

MACS - Magnetic Cell Isolation and Cell Separation

mdECM - muscle decellularized extracellular matrix

MTU – Muscle Tendon Unit

MuSK – Muscle-Specific Kinase

NMJ – Neuromuscular Junction

PCL – Polycaprolactone

PEG – Polyethylene Glycol

PF – PEG-fibrinogen

PTFE - Polytetrafluoroethylene

PU - polyurethane

SCID - Severe Combined Immunodeficiency

SHH – Sonic Hedgehog (protein/pathway)

TCP – Tissue culture plastic

Chapter 1: Introduction

1.1 Formation and Pathophysiology of the Neuromuscular Junction In Vivo and the Need for In Vitro Tissue Engineering

The neuromuscular junction (NMJ) begins as a physical connection between the nervous and muscular systems in the embryo, and develops into a critical biological juncture that relays information efferently from the central nervous system to the body's motor system. Specifically defined, the NMJ in the adult is the area of synaptic contact between the terminal branches of the motoneuron and a specialized area of the muscle cell sarcolemma called the motor end-plate. The terminal branches of the motoneuron are enlarged in shape and called synaptic boutons, as they are rich in synaptic vesicles filled with the neurotransmitter acetylcholine. These synaptic boutons reside over invaginations in the sarcolemma named 'junctional folds,' which contain dense clusters of acetylcholine receptors (AChRs).

The developmental timing of the neuromuscular junction in humans is difficult to study directly due to ethical and technical issues surrounding the study of human embryos, but it is known that the development of neuromuscular junctions in humans begins approximately in the eight to tenth week of development [1,2] as motoneurons extend out of the ventral root of the developing spinal cord and contact acetylcholine receptors in postjunctional folds on myotubes in the laterally expanding myotome. Myotomes begin as a tissue layer in somites, bilateral blocks of mesoderm which form parallel to the anterior-posterior axis of the embryo [3], and eventually give rise to the muscular system. The clustering of acetylcholine receptors in myotubes is a complex interaction, hypothesized to be controlled by the action of Muscle-Specific Kinase

(MuSK), a tyrosine kinase receptor that binds to agrin, a proteoglycan released by motor neurons. Both MuSK and AChR are anchored into place by the structural/stabilizing proteins dystrophin and rapsyn [4].

Unfortunately, much can go wrong in this complex interchange between specialized cells, and neuromuscular diseases constitute a wide spectrum of human disease, including diseases of inherited and acquired origin. Neuromuscular diseases are often devastating illnesses for patients and families and are estimated to cost the US billions of dollars annually [5]. Although neuromuscular conditions include a wide range of illnesses, they are most often separated into genetic and autoimmune disorders.

Genetic neuromuscular conditions include spinal muscular atrophies, Duchenne muscular dystrophies, spinobulbar muscular atrophy, and congenital myasthenic syndromes (CMS). Spinal muscular atrophies are a complicated clinically heterogeneous group of debilitating disorders mostly with known genotypes. The spinal muscular atrophies are characterized by degeneration of lower motor neurons and muscular wasting. The most common and eponymous spinal muscular atrophy (SMA) is caused by a genetic defect in the telomeric copy of the SMN1 gene on chromosome 5. This gene mutation is well known to inhibit survival of lower motor neurons, but interestingly recent evidence has suggested that the gene defect may also be detrimental to skeletal muscle maturation [6]. Such evidence of complicated and interconnected disease progression highlights the need for controlled neuromuscular junction research in order to further elucidate mechanistic detail, especially relevant in the search for novel therapeutics. Similar in disease complexity and unclear mechanism are Duchenne muscular dystrophies (DMD), caused by mutations of the dystrophin gene on the X

chromosome. The dystrophin protein forms an integral part of the dystrophin-associated protein complex, or costamere, which connects the sacrolemma to the sarcomere in striated muscle. However, the dystrophin protein is also found in neuromuscular junctions [7] indicating a potentially multifaceted mechanism of disease. Similar to DMD, Spinobulbar muscular atrophy (as known as Kennedy's disease) is caused by a known gene mutation in the X chromosome, in this case the androgen receptor, which has survival effects on both motor neuron and skeletal muscle [8]. In the study of these complicated inherited neuromuscular conditions it is hard to overstate the translational advantage a reproducible *in vitro* human neuromuscular junction model would have, both in isolating neuronal, muscular, and junctional aspects of disease, as well as in the evaluation of novel therapeutic strategies.

Besides the inherited neuromuscular conditions, new *in vitro* screening tools and models are needed for the autoimmune neuromuscular conditions: myasthenia gravis and Lambert Eaton syndrome. These conditions are a spectrum of disorders related to an autoimmune humoral response against vital proteins of the neuromuscular junction. In myasthenia gravis, antibodies are directed against nicotinic acetylcholine receptors whereas in Lambert Eaton syndrome, the antibodies are directed against presynaptic voltage-gated calcium channels [9]. Promising new therapeutic strategies aimed at combating myasthenia gravis disease burden involve reducing the damage caused by antigenic modulation of the acetylcholine receptors and support proteins [10]. Such novel therapeutics would indeed benefit from the creation of an *in vitro* human neuromuscular junction model, especially one with easily quantifiable parameters of signal transduction strength and functionality.

An *in vitro* human neuromuscular junction model would not only be useful for disease studies, but also in examining aspects of normal human physiology, such as age-related sarcopenia, which has been modeled using several different gene manipulation mechanisms. Sarcopenia refers to degenerative loss of skeletal muscle mass and quality and is estimated to occur as a loss of 1-2% of muscle mass per year in all adult humans after age 50 [11]. Experimental models used to study sarcopenia include three dimensional (3D) collagen-based skeletal muscle constructs with multiple population doubled murine myoblasts, although such models are still preliminary [12]. Other experiments using *in vivo* stimulator cuffs in rats have shown that there are age-related changes in NMJ morphology, including changes in the motor endplate and a breakdown of the relationship between motor endplate and nerve terminal size. These studies also showed that electrical stimulation of the NMJ has potential to restore older NMJs to younger morphologies [13]. Adding to complex picture of sarcopenia, recent research has shown that cellular polarization and asymmetric localization of MAPK p38 signaling is responsible for the cell-autonomous loss of skeletal muscle in aged mice model [14]. This asymmetric localization of signaling pathways and cell polarization illustrates the need for 3D tissue models, which approach reconstitution of *in situ* conditions and eliminate two-dimensional (2D) substrate attachment effects. While most 3D tissue models are considered as prototypes or under development, research into 3D tissue models has already proved useful in evaluating cell polarity in epithelial tumor models [15].

1.2 Current 2D Myocyte Models with Transition to 3D Models

While 3D models have been recognized as a useful step in coculture, 2D models are the logical starting place for cell differentiation to specific tissue lineages and for cocultures, in particular for skeletal muscle model systems. While many models of human muscle systems have demonstrated limited differentiation capacities, recently the Hickman group confirmed advanced differentiation of cultured myotubes using a serum-free culture system with well-defined sarcomeric development, with cross striations and excitation-contraction coupling with apposition of T-tubules and ryanodine receptors [16]. Ryanodine receptors, which open in response to membrane depolarization from the sarcolemma into the T-tubule system, allow release of calcium ions into cytoplasm, initiating contractile machinery. Demonstrating ryanodine receptor apposition with T-tubules is important in that calcium ion fluxes have been shown to be different in aneurally and cocultured constructs [17], and the ability to localize ryanodine receptors and T-tubules is potentially responsible for the improved level of differentiation reported by the Hickman group as the first published evidence of human myotubes capable of spontaneous contraction in 2D [16]. While this novel system is often cited as the currently most-relevant 2D human skeletal muscle model [18–20], it is important to examine the development of 2D models in muscle cultures to understand how the field has evolved, and where the field is likely moving to fill in needed gaps in knowledge.

1.2.1 Overview and Challenges of Myocyte Models

2D culture of myoblasts is similar to 2D culture of many other adherent cells types, where cells are spread out and seeded on 2D tissue culture plastic (TCP) or a

coated surface, and surfaces exist inside tissue culture vessels with specific atmospheric environments. In 2D culture of skeletal muscle cells, differentiated adjacent myotubes have a tendency to align with the same orientation, forming 'patterns of myofiber clusters [16]'. However, as the myotubes are not aligned in individual wells or constructs, it becomes difficult to quantify contractions or alignment effects using 2D methods. There are also issues of stochastic properties of myotubes in 2D with variations of morphologies, widths, and interactions with 'randomly crossed' myotubes. However in a 2D patterned or more complex system, one could record intracellular calcium transients with more myotubes possessing uniform widths and morphologies [21]. Patterning, or micro-patterning techniques, which use 2D patterning to create more uniform measurements of nuclear and cytoskeletal alignment provide a number of benefits, including scalability from nanoscale to microscale, and control of substrate and mechanical features. However such techniques are usually not considered 3D models and are prone to effects of substrate attachment, limiting relevance to 3D tissue models [22].

3D muscle cultures usually involve encapsulation of myoblasts in fibrin, collagen, and matrigel, and such 3D cultures are generally considered more biomimetic, yet current models have a number of drawbacks which increase the difficulty of culture, and lead to less utilization in labs. These drawbacks include significantly higher cell numbers needed, difficulty in imaging, and less possibility for high-throughput screening as models become more complex to assemble[23]. Engineered constructs, or muscle bundles, have been created using diverse hydrogels including fibrin, Matrigel, hyaluron, or collagen [24–26]. Fibrin gels have been used as a substrate for human *in vitro* skeletal muscle engineering, and recent research has showed it is possible to optimize seeding densities of

human myoblasts to increase fusion index % and myotubes per microscope field [27]. However, fibrin gels are known to compact unpredictably, leading to restricted growth and spreading of encapsulating cells, limiting their potential for reproducible assays [28].

Another factor in deciding the substrate for myoblast seeding in both 2D and 3D is stiffness. In 2D the ideal stiffness of gels is thought to be 8-12kPa [29], however, the optimal hydrogel stiffness for 3D remains disputed and may vary depending on other culture factors. In addition, the cell type, such as derived primary cells or modified cell lines may change the requirements of 3D cultures. Engineered muscle constructs seeded from primary cells produce higher specific forces than cell line-derived constructs, indicating a possible function of supporting cell types found in muscle-derived or isolated cell populations [30,31].

The development of a clinically relevant NMJ model begins with the production of engineered human muscle constructs with a high degree of structural biomimicry to native skeletal muscle. The majority of the data on *in vitro* skeletal muscle biomaterials design and optimal growth conditions has been based on rodent muscle-derived-cells (MDCs) and C2C12 cell lines, which have recently been found to have phenotypic divergences indicating a lack of faithful recapitulation to the human myoblast response to biomaterial cues [32]. In addition there is a recently recognized 'striking excess' of human-specific gene expression deviation from rodent skeletal muscle, specifically in metabolic pathways, further indicating the lack of relevance of animal models to human muscle-related disease [33]. It is also recognized that there is a lack of data concerning the culture of human MDCs in biologically relevant matrices, and if physiological or disease model data from *in vitro* skeletal muscle research is to be translated clinically to humans, it is

imperative to further research on human tissue engineered models designed to structurally resemble human *in vivo* skeletal muscle [27,34].

Another concern with current models involves a lack of reliable and reproducible methods to control three-dimensional skeletal cell alignment [35]. This is troubling as unidirectionally aligned skeletal muscle cells are required for skeletal muscle fiber construction [36]. Furthermore, generation of effective and active contractile forces is dependent on muscle cell alignments, which is thought to initiate a cascade of cell organization of extracellular matrix deposition [35]. As developing a reproducibly high degree of muscle cell alignment in engineered muscle constructs is necessary for proper biomimicry of native skeletal muscle, and an *in vitro* neuromuscular junction model will not be clinically or translationally effective without developmentally relevant engineered muscle, establishing reproducible cell alignment in culture is our jumping off point [31].

1.2.2 Overview and Development of 3D Myocyte-Seeded Models with Alignment Generation

Several research groups have attempted to establish a recognized means of 3D culture of myoblasts, often with the goal of future culture types increasing in complexity, systems whose merits and drawbacks will be discussed further in the upcoming section. One method of culturing thicker 3D muscle tissues has been to stack monolayer aligned sheets of C2C12 cells grown on electrospun poly-caprolactone (PCL) nanofibers. These sheets can be stacked on top of each or sandwiched between layers of human umbilical vein cells (HUVECs) potentially increasing nutrient diffusion. While an interesting technique, it remains to be seen if the technique can be adapted to the demands of using human cells or be combined with specific nervous tissue [37].

Culturing C2C12 cells in 3D has been proven to have advantages of over monolayer cultures such as higher expression of adhesion proteins. In addition, C2C12 myoblasts in monolayer and 3D cultures exhibited significant differences in morphology and cytoskeletal organization, indicating a possible deviation between 2D cultures methods and *in vivo* cell behavior [38]. C2C12 culture in 3D with carbon nanotubes aligned in methacrylated gelatin (GelMA) hydrogels were also shown to be controllably differentiated through electrical stimulation in manner which could investigate the mechanisms of exercise- and insulin-induced glucose regulation through skeletal muscle. Theoretically such engineered tissue could be cheaper and less time consuming than animal experiments [39].

In other experiments neonatal rat myoblasts cast in 3D fibrin gels responded to miniagrin in a manner similar to what is found *in vivo,* where miniagrin treatment enhanced the formation of AChR clusters and upregulated and enhanced contractile machinery [40]. In further research, the Vandenburgh group developed 3D bioartificial muscle (BAMs) from green fluorescent protein (GFP)-transduced murine skeletal myoblasts suspended in a fibrin gel cast between two flexible posts. This passive tension from the silicone posts allows the myoblasts to align to the long axis of the culture system. The group used the BAM system to evaluate the effect of laminin and agrin on AChR clustering. They found that agrin alone was enough to induce formation of immature "oval plaque-shaped" AChR clusters, and that the addition of laminin enabled the AchRs to reach the mature and complex "pretzel-shaped" clusters. This research shows how useful *in vitro* modeling can be for determining normal physiological response to chemical signals, especially in the context of NMJ modeling [41].

Other methods of 3D myoblast culture have capitalized on emerging techniques such as 3D bioprinting, which uses 3D printing technologies to pattern biological cells or components. One technique used a tissue-specific muscle decellularized extracellular matrix (mdECM) bioink, which encapsulated C2C12 myoblasts utilizing an in-house cell-printing system called the integrated composite tissue/organ building system (ICBS). The bioprinted mdECM microenvironment in combination with the geometrical constraints in the muscle constructs provided cells with conditions for high viability, proliferation, and myotube formation with myogenic differentiation [42]. Another report of using bioprinting towards creating *in vitro* myoblast constructs combined C2C12 cells and NIH/3T3 cells with a 'distinct interface,' using thermoplastic printed to mimic the biological architecture of natural muscle and tendon. They found through 3D printing of the thermoplastic polyurethane, and PCL as structural materials they were able to retain cells through seven days in their original positions, which further self-organized into patterns consistent with muscle-tendon units (MTUs) [43]. A final bioprinting method used a photocurable PEG-fibrinogen (PF), in combination with sodium alginate, to encapsulate C2C12 cells with or without BALB/3T3, which partially degraded with in *in vivo* implantation experiments with immunocompromised SCID mice, and started becoming 'moderately substituted by arising myofibers [44].'

As opposed to characterization of C2C12 culture, there has been limited research into the characterization of human skeletal myoblasts on diverse and biocompatible substrates, Chaturvedi et al. found that some silk scaffolds resembled native muscle elasticity (12-15kPa) and were able to support myotube formation and alignment. Over the range of silk substrates from four Lepidoptera (silkworm) species it was found that

Bombxyii mori fibroin will be most useful for clinical applications involving skeletal muscle cells [45]. Unfortunately, there was limited alignment in patchy areas with this technique as myoblasts grew on porous surfaces stochastically in the absence of strain.

An additional 3D culture technique that had direct inspiration for experiments described later used the contractile force that muscle cells generate upon differentiation, which involves fixation of a scaffold, matrix, or hydrogel between anchor posts, creating predictable lines of isometric strain as cells pull against the stationary or flexible posts, sometimes referred to as artificial tendons. This cell-mediated internal tension promotes alignment along the principle axis of strain [46–49]. Heher, et al., built upon this technique and built a novel closed bioreactor system (MagneTissue) which applied adjustable strain regimes to C2C12 cells in freestanding fibrin gels after removal from casts. This 3D culture technique led to upregulation of structural genes important for muscle function and contractility after strain application [50]. A further advanced 3D integrated scaffold technique using PCL nanofiber mats produced 3D C2C12 tissue constructs, which were first electrospun then transferred to a polymer melt deposition system where the cells were cast with collagen and layered on edge fixation structures. The end point of these experiments show that cell supportive substrates are not necessary for cell contact guidance, and that fixed-edge structures along with nano-topographies can produce aligned cells, allowing researchers to decouple the effect of substrate attachment to alignment [51].

1.2.3 Reproducibility and Multiplexed Analysis of 3D Myocyte Cultures

Another factor that increases the utilization of skeletal muscle models in the ability for automated and multiplexed analysis. One technique that expands on the use of flexible cantilevers used neonatal rat myoblasts seeded onto a stereolithographically microfabricated silicon cantilever chip with an array of 32 cantilevers. Myotubes seeded on the cantilevers could be measured through a scanning program of a laser and photodetector. While useful in theory for high throughput detection of myotube functionality in the context of novel pathological and chemical responses [52], the technique suffers from 2D substrate attachment, limited alignment data, and lack of human cell use.

Another use of cantilevers towards translational systems was demonstrated by Lee, et al. in 2013 as they used a simple reduction in length of spacing between cantilevers supporting primary mouse myoblasts in collagen hydrogels to model skeletal muscle atrophy, as they noted decrease in cantilever spacing led to decrease in measured maximum isometric tetanic force, mean myofiber cross-sectional area, non-collagenous protein content and protein synthesis rate [53]. The same lab expanded on the cantilever model of bioartificial muscles (BAMs) by a transition to human muscle cells in co-culture with HUVECs and found some branching of HUVECs and early network formation with both 40% and 50% total cell percentage HUVECs [54]. While not explored to date, it was acknowledged that the clustering of AChRs and the effect of endothelial cells on AChR expression could be investigated with further refinements of this model [54].

More recently similar 3D casted constructs were used to test for similarity of cast human myoblast-seeded ‘myobundles’ to the response of pharmaceuticals in patients. These pharmaceuticals included chloroquine, where myobundles showed autophagic

myopathy observed in native muscle, and clenbuterol, where myofiber hypertrophy was observed at low doses and weakness observed at higher doses [55]. This human skeletal muscle in monoculture provides an improved tool for testing of pharmaceuticals and serves as a potential alternative to expensive animal studies. The method notably uses calcium signalling which could be combined with another optically-based assay (or neural co-culture) for improved relevance [55]. The most recent published report of the use of the myobundle expands on the clinical relevance and demonstrates lower oxygen requirements and respiration of the muscle cells in 3D culture as opposed to monolayers and the average myobundle basal respiration per volume was within the reference range of normal muscle at rest [56]. These analyses, along with the mitochondrial respiratory response to 20mM rotenone led the authors to suggest myobundles could be used to assess mitochondrial toxicity and possibly serve as a conduit between *in vitro* and *in vivo* testing is pharmaceutical development pipelines [56].

Many muscle-only or endothelial cell coculture models have used electrical stimulation as an alternative rather than neural stimulation to examine muscle function. One issue with this technique is the hazardous side effects of electrical stimulation may lead to decreased viability of long term culture, thus direct neural stimulation of muscle tissue is preferred [57]. To provide neural stimulation, neurons will have to contact areas of AChR aggregation on muscle tissue. In native muscle tissue AChRs are evenly distributed along myofibers at densities of ~ 10,000/μm^2. *In vitro* when motor neurons are integrated into myoblast-seeded cultures, axons contact myotubes randomly which induces a greater aggregation of AChRs in shallow beds on muscle fibers [58], forming the NMJ [59]. Functional maturation of AChRs is improved in neuron-muscle cocultures [60].

Similarly implanted constructs of rat skeletal muscle myoblasts in fibrin gels indicate the 'neurotization' of engineered muscle can increase force development and NMJ maturation [61]. Overall neural and muscle cell interaction and communication play a key role in skeletal muscle maturation and differentiation, which will result in higher-quality resemblance of engineered tissue to what is found *in vivo* and thus neural coculture is 'essential' to engineered both mature and functional tissues [57].

1.3 2D Myocyte-Neuron Models and Ongoing Need for 3D Human Model of NMJs

1.3.1 History and Evolution of Myocyte-Neuron Models

Perhaps the earliest known *ex vivo* coculture of muscle and nerve was in 1907, when Harrison et al isolated fragments of the medullary tube from frog embryos, as well as developing myotomes with pieces of medullary cord attached [62]. The next major step came in 1987, where a human muscle explant technique was developed allowing monolayers of human myocytes to emerge from 're-explanted explants' which started as $1mm^3$ biopsy sections. E13-14 rat embryo spinal cords with dorsal root ganglia remaining attached were placed on the muscle monolayer culture. This technique was developed as Duchenne muscular dystrophy, myotonic atrophy, myophosphorylase deficiency and muscle carnitine deficiency, presented defects which were not manifested in aneurally cultured muscle monolayer techniques [63–65]. The authors found that NMJs developed, although were present at different degrees of differentiation, with many mature NMJs present with Schwann cell apposition and deep postsynaptic folds [66].

One means of coculture that has been pursued by many labs in recent years involves microfluidic coculture systems, or chip cultures. This is partially due to the belief that the ability to tailor cell microenvironments individually may allow for closer

mimicry of physiological conditions. Chip culture was invented by Campenot in 1979 [67] and use of segregated chambers is often referred to as modified Campenot chambers. Tong, et al. used such a device with fluidically isolated cell seeding reservoirs allowing for separated culture of mouse primary motoneuron cells which could proliferate axons into C2C12-derived myotubes. Using this device, the group was able to track axons growing in 2D and offer some correlation through Ca^{2+} response in C2C12 myotubes [68]. Another similar chip model purportedly investigating the lower motor neuron NMJ circuit used segregated chambers of skeletal muscle cultures derived from hindlimb of postnatal day 2 (P2) rats, mixed spinal glial cells from P2 rats, and spinal motor neurons from E15 rats. This system was the first to show glial cell addition in chip culture to fill the role of Schwann cells at the NMJ. One issue involved with the chip culture was the lack of quantified alignment of myocytes as well as the substrate attachment, leading to difficulty analyzing potential contractions [69]. This chip model remains popular as Ionescu, et al. published a detailed procedure of a similar chip culture using primary murine cells. This chip model used Tetrodotoxin (TTX) to block neuronal stimulus and provided additional quantification of the morphological formation of NMJs [70].

One method of measuring contractions in chip-based systems occurred as Hickman, et al. expanded on the previously described multiplexed silicon cantilever system [52], as well as an advancement of the system using primary human myoblasts to replace animals cells [71] by seeding muscle cells with motoneurons isolated from E15 Sprague-Dawley rat fetuses. The planar co-culture was analyzed with a single-unit laser and photodetector system which detected myotube twitching from stimulation with glutamate and blocked with D-tubocurarine [72].

Additional advances in chip culture over recent years includes the development of a microelectrode array with gold mushroom-shaped microelectrodes which allows for analysis of intra- and extracellular potential recording in 2D monolayers of isolated rat myocytes [73]. While the culture was aneural, the author acknowledged that future uses could involve coculture of motoneurons and myotubes. This anticipated advance came in 2016 as Uzel, et al. described a chip culture that could be considered 3D culture as the channel contained membrane pillars where hydrogel-enscapsulated C2C12 cells, initially seeded as a long continuous gel, compacted around the pillars after two photon or manual ablation. These constructs were either stimulated by light through incorporation of transfected optogenetic culture or through a combination of glial and motor neuron cells isolated from mouse embryonic stem cells [74].

The next potential advance from the systems described come as human induced pluripotent stem cells are differentiated to relevant cell types comprising the NMJ. This use of human cells in 2D nerve-muscle coculture was pioneered in 2011 [75] and the pluripotent cell types has greatly expanded since 2015 [76], and currently many 2D neuron-muscle co-cultures exist which will be reviewed in the upcoming section, although none yet involve human motorneuron-myoblast culture in 3D.

1.3.2 Use of Human Cells in 2D NMJ Models

The first *in vitro* human neuromuscular junctions were formed in 2011 by the Vandenburgh group, who used satellite cells from patients undergoing voluntary muscle biopsies as the human skeletal muscle progenitor cells and used fetal spinal cord cells to form the human motor neuron progenitors. The group co-plated the two cell types on

trimethoxysilylpropyldiethylenetri-amine (DETA) coated glass coverslips using a published serum-free media, as exogenous serum can interfere with motorneuron growth and development, confound drug effects, and is generally not amenable for reproducible assays. The *in vitro* neuromuscular junctions were proven to exist by co-localization of immunostaining of BTX-488 (α-bungarotoxin), which binds to clustered AChRs on myotubes, and synaptophysin, a synaptic vesicle protein found in nerve cells. Myotubes were confirmed via phase contrast microscopy/video analysis and voltage/current clamp trace recordings were used to show the electrical activity of individual NMJs [75]. Unfortunately, this 2D culture model does not allow for measurement and quantification of motoneuron-originated muscular contractions as the cells are attached to the 2D substrate during cultivation and the skeletal myocytes are not aligned and fused unidirectionally as found in native skeletal muscle [77,78].

2D human coculture has expanded greatly since around 2015, as reports demonstrate cocultures can be derived from fully hiPSC-derived cell lines and can be optogenetically stimulated [79]. Demestre, et al. used a technique where myotubes and motor neurons both from embryonic rat isolation and human induced pluripotent stem cells could interact in 2D. For enhancement of myogenic cells, iPSC populations were labelled with anti-CD34 microbeads, and magnetic separation was carried out with magnetic-activated cell sorting (MACS). In coculture experiments hiPSC-derived motoneurons were differentiated through 14 days of 50ng/ml purmorphamine (shh agonist) [80]. Functional contact was shown through phase contrast images as well as co-localization of pre- and post-synaptic contacts in coculture.

A year later in 2016, Puttonen, et al. [81] showed the embryoid body-like spheres which are produced in addition to neurospheres from either human embryonic stem cells or human induced pluripotent stem cells will give rise to myotubes and neurons in neural proliferation media if spheres are maintained as adherent cultures after withdrawal of fibroblast growth factor (FGF). The significance of this is that cells derived from a single donor or individual could be differentiated into both the neuron and the muscle aspects of the neuromuscular connection *in vitro.* In 2D cultures of human derived neurons and muscle the authors found molecular machinery required for synaptic transmission present in myotubes, as well as an 'intimate interaction' with neural precursor cells/neurons during the whole period of development [81]. This research suggests that the fluidic isolation found in several chip cultures may not be necessary for successful functional neuron muscle co-culture.

Although there has been extensive development of animal models of skeletal muscle and engineered myoblast-seeded constructs from fibrin, collagens, and other polymeric gels, only recently have 3D innervated models of skeletal muscle been under development [82]. In general 3D innervated models begin with alignment of skeletal muscle, as alignment and syncytium formation allows 3D myotube cultures to be stimulated and produce a uniaxial response. In addition, this uniaxial alignment of cells is what it is found in myofibers *in vitro*. One prominent method of cell alignment used in monocultures (as discussed earlier), but also in many models of innervated skeletal muscle in development, was pioneered by Norman and Desai in 2005 whereby they used polydimethylsiloxane (PDMS) as a skeleton from which to seed cell-laden hydrogels.

This method controlled cellular alignment in human lung fibroblast-laden 3D hydrogels using physically predefined pathways or channels [83]. After manufacture of controlled width microchannels using microfabrication techniques, a fibroblast-seeded collagen matrix was cast around the channels, which functioned as a guide for the cells to grow in a confined 3D pattern. The human lung fibroblasts elongated and aligned along the direction of the channels [83], however, the applicability for tissue engineering applications was thought to be limited due to the enduring presence of the internal PDMS skeleton, as well as the reliance of feature size from PDMS micromolding techniques [84].

Five years later, Aubin, et al. demonstrated that cells could be encapsulated in hydrogels that self-organize without 'additional support or guidance,' and would form aligned 3D cellular networks through confinement in the appropriate microgeometrical conditions. As their technique did not require external physical pathways guiding the hydrogel, the work was the first direct method to use the cells' intrinsic potential to self-organize into functional 3D tissues in a hydrogel as the enscapsulated 3T3 cells were found to have an innate tendency to align along 'free surfaces,' as well as with their neighbors[84]. Interestingly this tendency, or 'intrinsic cellular potential to organize into aligned tissues *in vivo*' was demonstrated to not apply to all cell types, as evidenced by the behavior of Hep-G2 cells encapsulated in micropatterned hydrogels, which did not align *in vitro* and are not known to align *in vivo* [84]. Since publication in 2010, many systems have used fixed endpoints or artificial tendons to align cells *in vitro* and the next section concerns the use of this method in the creation of 3D *in vitro* models of innervated skeletal muscle, all of which at the time of writing do not contain fully human cells or are co-cultured with non-motoneuron cells.

1.3.3 3D NMJ Models Using Animal Cells

Larkin et al demonstrated one of the first 3D muscle-nerve constructs through co-culture with a monolayer of muscle cells isolated from rats and an added E15 fetal spinal cord explants. The authors used a self-organization system predating Aubin et al, yet using some similar features. In the system described by Larkin et al, a monolayer of rat myocytes plated on Sylgard-treated plates would be differentiated for two weeks before spinal cord explants from E15 fetal rats were pinned with a steel pin into the Sylgard. After an additional week of co-culture, monolayers with in-laid spinal cord extracts would spontaneously roll up and form cylindrical constructs. The co-cultured construct could then be tested through stimulation with microelectrodes, and functional connections be analyzed through neurofilament and bungarotoxin staining [85].

In 2013 a team of Japanese scientists sandwiched C2C12 murine myoblasts in a polydimethylsiloxane (PDMS) stamp and placed fetal brain-derived mouse neural stem cells (mNSCs) in neurosphere form on top of constructs after the maturation of the muscle cells. NMJs were shown to exist by immunostaining of clusters of AChRs as well as the delay of glutamic activation of contraction after curare treatment [86]. Curare is a potent neurotoxin, which competitively and reversibly inhibits AChRs, and glutamic acid is used analytically to potentiate or excite motor neurons. Thus if curare addition modulates the glutamic acid effect of activating the muscle construct, the group reasons the contractions must be circuited through NMJs.

An expansion on this technique of pinning individual constructs used self-organization of 3D tissues along anchor points [87]. This updated system used primary

muscle derived cells from P1 rats, and isolated motor neurons from E14 rat embryos, considered more towards fully *in vitro* innervation as opposed to spinal cord explants considered *ex vivo.* In this model, rodent motor neurons were found to frequently adopt a perpendicular tracking towards the tension axis of the myotubes. The authors suggested that the neurotrophic factors could potentially be overwhelming the mechanical signals which tend to align cells parallel to the axis of tension. The presence of added motorneurons had no purported effect of muscle precursor hypertrophy or cell fusion, however, it was noted that a striated pattern of Desmin immunostaining was found in a higher percentage of samples, possibly indicating a maturation effect of enhanced cytoskeletal organization on the myotubes [87].

In another method of allowing 2D cell assemblies to self-assemble in more complex 3D systems, Takahashi et al harvested myoblast monolayers which were then layered in three dimensions through detachment of monolayers and then stamping of layers on top of each other. To work towards more complex muscle cultures, the layered human myoblast monolayers were seeded with HUVECs and non-differentiated iPS-derived neurons. These endothelial cells formed some vascular-like branched networks through the layered cell sheet construct, and neural outgrowths were observed [88]. While a clear advancement on coculturing other human cell types along with myoblasts in 3D, the neurons were not meant to serve as innervating motor neurons, and no efforts were present to differentiate neurons towards a specific lineage to form specific connections with myotubes.

Other 3D systems in the years since Morimoto, et al. published a murine model of motor neuron-muscle cell 3D have used animal cells to create 3D culture systems meant

for to investigate the neuromuscular connection. In 2016, Smith, et al. used a 3D collagen-based model where primary muscle derived cells from P1 rat pups were encapsulated into a cell-collagen solution that was cast into a single-well culture slide with in-laid flotation bars serving as anchor points [89]. This model was an improvement over earlier models which used organotypic slices of central nervous system tissue, transected nerve tissue, or 'ill-defined' neurospheres [61,85,86] as they added defined motorneuron-like cells, isolated mixed ventral horn cells from E14 rat pups were pipetted directly onto the upper surface of the collagen gel. The ventral horn cells were shown to survive in co-culture for up to two weeks, with evidence of preliminary neuromuscular contacts. This model is thought to be well suited for investigating the basic biology underpinning NMJ formation including the response to mechanical strain and electrical stimulation [89], and is believed to have the potential through improvement through inclusion of terminal Schwann cells and transition to human co-cultures.

To incorporate Schwann cells into a 3D system Vilmont, et al. used a layered matrigel approach to combine isolated myoblasts from P7 pups with E13 embryo spinal cord explants with dorsal root ganglia attached. Muscle cells were first seeded in matrigel, and then additional matrigel was added on top. Lastly the explants with attached dorsal root ganglia were added 3 days after co-culturing. To look for potential Schwann cell incorporation through explant addition, constructs were stained for glial fibrillary acid protein (GFAP), and oligodendrocytic marker O4, which were found to be contacting axons [90]. The addition of dorsal root ganglia which contains dorsal sensory neurons is interesting as there has been some initial studies of co-culture of human muscle with human stem cell derived proprioceptive sensory neurons. Guo, et al.

demonstrated 2D coculture of induced intrafusal fibers from human satellite cells and human sensory neurons in a defined serum-free medium [91] in research that demonstrates a novel human-muscle neuron connection in 2D (table 1.1).

Table 1.1: Summary of Described Significant Aneural and Coculture Skeletal Muscle Models

Publication	*Culture Type*	*Cell Type*
	Aneural Muscle Models	
Guo, et al. 2014	2D monolayer	human primary skeletal myoblasts
Ahadian, et al. 2014	3D GelMA hydrogels with aligned carbon nanotubes	C2C12 myoblasts
Bian, et al. 2012	3D fibrin gels	Neonatal rat skeletal myoblasts
Wang, et al. 2013	3D fibrin cast between silicone posts	GFP-transduced murine skeletal myoblasts
Choi, et al. 2016	3D mdECM bioink	C2C12 myoblasts
Merceron, et al. 2015	3D PEG-fibrinogen, PU, PCL	C2C12 myoblasts, 3T3 fibroblasts
Chaturvedi, et al. 2016	*Lepidoptera* silk scaffolds[1]	Human skeletal myoblasts
Heher, et al. 2015	Magnetically actuated 3D fibrin gels	C2C12 myoblasts
Park, et al. 2014	collagen cast on electrospun PCL nanofiber mats	C2C12 myoblasts
Smith, et al 2014	Microscale silicon cantilevers	rat skeletal muscle satellite cells
Lee, et al. 2013	Collagen polymerized around silicone posts	primary mouse myoblasts
Gholobova, et al. 2015	Collagen polymerized around silicone posts	Human skeletal myoblasts, HUVECs
Madden, et al. 2015	Fibrin/matrigel in PDMS molds	Human skeletal myoblasts
Rabieh, et al. 2016	3D gold microelectrodes	Isolated rat myocytes
Takahashi, et al. 2015	Stacked cell sheets	Human myoblasts, iPSCs

Neural Coculture		
Harrison, et al. 1907	2D monolayer/medullary cord explant	Frog embryo myotome, medullary cord
Askanas, et al. 1987	Human monolayers, spinal cord explants	Human muscle monolayer, E13-14 rat embryo spinal cord explants
Tong, et al. 2014	2D dual-chamber chip	Mouse primary motoneurons/C2C12 myoblasts
Southam, et al. 2013	2D tri-chamber chip	Isolated P2 myoblasts, P2 spinal glial cells, spinal motor neuron E15
Ionescu, et al. 2016	2D dual-chamber	Primary murine myoblasts and GFP motoneuron explant
Smith, et al. 2014	Microscale silicon cantilevers	Human primary myoblasts, E15 rat motoneurons
Uzel, et al. 2016	2D tri-chamber chip	C2C12 myoblasts, mESC-derived glial cells motoneurons
Guo, et al. 2011	DETA-coated coverslips	Human skeletal muscle myoblasts, fetal spinal cord cells
Demestre, et al. 2015	2D monolayer	hiPSC derived myotubes, motor neurons
Puttonen, et al. 2016	2D monolayer	hESC derived myotubes, motor neurons
Larkin, et al. 2006	Self-assembled 3D fibrin gels steel pinned to coated dishes	Rat myocytes, E15 spinal cord explants
Morimoto, et al. 2013	Collagen gel cast between PDMS	C2C12 myoblasts, fetal brain-derived mouse neural stem cells
Martin, et al. 2015	Self-assembled 3D fibrin gels steel pinned to coated dishes	Primary MDCs P1 rats, E14 rat motor neurons
Smith, et al. 2016	Collagen cast between flotation bars	P1 rat MDCs, mixed ventral horn cells E14 rat pups
Vilmont, et al. 2016	Layered matrigel	P7 rat myoblast, E13 spinal cord explants

Guo, et al. 2017	2D monolayer	Human skeletal myoblasts, stem cell derived sensory neurons

[1]Four scaffolds derived from silk of four silkworms of the order Lepidoptera. Species include *Bombyx mori*, *Antheraea mylitta*, *Antheraea assamensis*, and *Samia ricini*

1.4 Hypothesis and Research Directions

What remains to be seen in the field is whether *in vitro* human neuromuscular junction tissue can be formed in a reproducible manner in a 3D environment that allows for precise analysis of structure and function. It is also unknown if such a tissue model will replicate the architecture and morphology of human *in vivo* innervated skeletal muscle and if integrated motoneuron-like cells will contact myotubes at points of AChR aggregation.

We hypothesized that we can form a functional human neuromuscular junction tissue model by implanting a tubular scaffold seeded with human motor neuron progenitors into a porous lamellar 3D scaffold with myotubes formed from human myoblasts undergoing cyclical mechanical stimulation. This model will provide a platform from which to study normal human physiology and aging, as well as hopefully a valuable tool both to uncover mysterious and complicated mechanisms of neuromuscular disease and to test novel therapeutic strategies for such diseases. Human myoblasts and human motor neuron progenitors have been available commercially, and satellite cells from disease mutation-carrying donors can be used to create human disease model muscle cells,

We chose to begin the design of the human skeletal myoblast seeded scaffold with a silk fibroin unidirectionally frozen scaffold, due to proven biocompatibility, tunable

properties such as stiffness and degradation rate [92] and lab expertise in use. This scaffold type is known to be porous and laminar, thus establishing a potential platform for inherently anisotropic muscle cells to elongate and align parallel to one another [39]. In addition, the biochemical and mechanical properties of the scaffold bulk can be tuned by altering the silk molecular weight and concentration or by adding other materials to the scaffold [93]. An especially relevant scaffold feature is pore size, as the pore size needed for optimal growth and differentiation of seeded cells depends on the biochemical and physical characteristics of the scaffold material. By varying the freezing agent, and thus the freezing gradient and rate, pore size can be honed in to optimal size for myoblast proliferation and growth.

To accomplish the first goal of aligning cells in 3D, we used a successive series of substrate designs for 3D culture of C2C12s and human myoblasts, including automated and sacrificial gel systems, and we finally used a gel compaction technique of printed silk anchor points or artificial tendons. Using this system we demonstrated reproducible alignment in human skeletal myoblasts with over 60% of myoblasts aligning within 20° of the gel long axis with three weeks of differentiation. Concurrently we showed that the skeletal myoblasts will exhibit exit from cycle, response to growth factors IGF-1 and recombinant agrin, and express AChRs in plaques in 2D

The next goals involved cocultures of motoneuron-like cells with myoblasts, with differentiation of both cell types towards expression of mature cell-specific machinery. As in myoblast alignment, a variety of methods including those using automation and cell segregation in 2D, 2.5D (layered technique) and 3D were explored. Differentiated C2C12s and human myoblasts were first cocultured with NG108-15 cell lines and later

hiNSC-derived motorneuron-like cells were cocultured along with human myoblasts. Using co-plating methods and 2.5D cell culture chips, human induced neural stem cell-derived neurites were found to extend through differentiated myotubes using specialized coculture media.

Transitioning to 3D coculture began as human 3D myoblast-seeded cultures were cocultured with microliter quantities of high density previously differentiated hiNSCs. Cultures were further differentiated with coculture media for an additional two weeks at which point cultures were shown to have integrating ChAT-positive neurites migrating through alpha-bungarotoxin positive myotubes. Interestingly bungarotoxin was diffusely distributed along myotubes, as has been seen in previous reports [94], and future work will involve methods to increase co-localization and mature plaque formation of alpha bungarotoxin.

To investigate the functionality of mono-cultured 3D human cell-derived constructs and cocultured constructs, stimulatory compounds were added in order to compare against baseline activation of calcium transients. Both mono- and cocultured constructs were found to be responsive to acetylcholine, and L-glutamic acid stimulation was used to investigate the neuronal stimulation of human myotubes. There was found to be some neural activation through L-glutamic acid, and in cocultured constructs there were some evidence of stimulation above baseline. Further experiments will seek to use optogenetic and other techniques to further elucidate cell specificity of activation.

Table 1.2: Variables, Outcome Measures and Completion of Major Aims

Variable Tested	**Method**	**Outcome Measure**	**Quantitative Metric – completion?**
Geometrical constraint, static strain delivery	Passive force: Solidworks modeling and 3D bioprinting of flexible cantilevers. Bioplotted and Bioprinted delivery at varyng morphologies.	Alignment of myoblasts in 3D matrix through 2D analysis of fluorescence images in Cell Profiler. Goal: >60% of myoblasts located within 20° of axis of strain.	Percentage of myoblasts oriented within 20° of axis of strain. *complete*
2D differentiation media of plated human skeletal myoblasts	hSKMs plated at $1*10^4$ cells per cm^2 and grown for 3 days with 28 days differentiation according to established protocols for differentiating primary human myoblasts.[95,96]	Exit from cell cycle through staining of MyoD, measure of cytoskeletal maturity through IF.	Percentage of myoblasts with nuclei that score as desmin+, and myoD+ as measured through CellProfiler *complete*
hiNSC-derived motoneuron-like cell integration with human myoblasts	Suspended gels: addition of neurons to 3D myoblast constructs. Plated culture: cell processes migrating through channels or moving through contacting printed gel.	Co-localization of acetylcholine receptor clusters and synaptic machinery, through bungarotoxin and ChAT staining.	Confocal analysis of cell specific processes *complete*
3D culture stimulation	Calcium response +/- muscle and neuronal stimulation and blocking agents	Functional muscle activation, specific neuron to muscle activation, successful blockade of neuromuscular transmission with curare	Live cell calcium signaling, twitch force measurement *Partially complete*

Chapter 2: Materials and Methods

2.1 Mono and Coculture Methods

Tissue Engineering Substrate - Silk fibroin solutions (hereafter referred to as silk) were extracted as in previously published procedures [97]. Briefly, silkworm cocoons were extracted in 0.02 M sodium carbonate, removing sericin coating from the fibers. Fibers were then rinsed in dH_2O, dissolved in 9.3 M lithium bromide (LiBr), and dialyzed against distilled water to remove LiBr. The resulting 7% w/v silk fibroin solutions were concentrated up to 40% w/v using air drying methods as needed and stored 4 °C until use. Other constituents of hydrogels include collagen type I and matrigel (materials from Sigma-Aldrich, St. Louis, MO).

Cell culture - NG108-15 neuronal cells were obtained from American Type Culture Collection (ATCC, Manassas, VA). The cells were cultured in humidified 37ºC/5% CO_2/95% air (v/v) environment in DMEM containing 10% (v/v) fetal bovine serum (FBS), 1% (v/v) L-glutamine, 1% (v/v) penicillin/streptomycin, 2% sodium hypoxanthine, aminopterin and thymidine (HAT) supplement (materials from Thermo Fisher, Waltham, MA). FBS was removed from the media when optimal cell density (~70 % confluence) was achieved to induce cell differentiation and neurite formation. Primary human myoblasts were cultured in growth medium (GM) containing DMEM supplemented with 10% fetal bovine serum, and 1% (v/v) penicillin/streptomycin (materials from Thermo Fisher, Waltham, MA). Confluence was kept below 80% during growth phase. A (1/40) dilution of matrigel in DMEM was used to coat expansion vessels.

Human induced neural stem cells (hiNSCs) [98] were induced from reprogramming factors OCT4, KLF4, SOX2, and cMYC in a polycistronic lentivirus. HiNSCs were differentiated towards cholinergic motoneuron-like cells with DMEM/F12, 1uM purmorphamine, and 1X B27/N2 for at least 12 days prior to coculture.

HiNSC Coculture - 3D cocultures were initiated as differentiated motoneuron-like cells were concentrated through trypsinization and centrifugation, after which 5μL of $1*10^7$ cells/mL were directly pipetted on top of 3D freestanding myoblast-seeded construct. Culture media was aspirated prior to neural cell incorporation for more precise addition and to enable cells to adhere to the constructs without being mixed in culture solution. After 10 minutes to allow for neural attachment, a 1:1 ratio of myoblast and neural differentiation was applied as coculture media, and cocultures were cultured up to an additional 14 days.

C2C12 Coculture - Cryopreserved NG108-15 (HB-12317) and C2C12 (CRL-1772) cell lines purchased from the American Type Culture Collection (ATCC) were cocultured in 1× DMEM (4.5 g/L glucose, L-glutamine and sodium pyruvate) supplemented with 10% (v/v) fetal bovine serum (FBS) (Invitrogen), 2% HAT supplement (Invitrogen), 100 units/mL penicillin, and 100 units/mL streptomycin (Invitrogen) at 37 °C, 5% CO_2. For differentiation, NG108-15 cells were seeded into at a density of ~20,000 cells per well. When serum-free medium was sued cells were differentiated in Neurobasal® medium supplemented with 2% B-27® Supplement, 2 mM Glutamax™, 100 units/mL penicillin/streptomycin (all from Invitrogen)). To induce motor neuron differentiation 2.5 μM purmorphamine (PUR) was added to the serum-free medium, and cells were incubated medium changes every 2 days.

2.2 Device Manufacture and Operation

Sacrificial Gelatin Culture Device - The delrin mold was milled using an 1/16" end mill for the negative cantilevers and #77 drill bit for the culture well walls. ABS molds were 3D printed using a Stratasys 1200es. Negative molds were used to cast the PDMS devices, which were physically removed from polyoxymethylene molds, or rinsed with acetone solvent to remove the sacrificial ABS. PDMS molds were cleaned with successive diH2O washes and autoclaving for at least 30 minutes. PTFE-coated stainless steel wires which would form channels when removed were threaded through the culture wall and cantilevers prior to autoclaving. Once removed from the autoclave, sterile heated 10% gelatin (Sigma) in growth media without serum was added to individual wells of the PDMS device with the liquid level above the removable PTFE-coated steel pins. After the gelatin is added, the device is cooled at 4ºC overnight. After cooling, the gelatin is stable at room temperature and the sacrificial channels are ready to be seeded after the PTFE-coated wires are removed manually with clamps. After channels were seeded with hydrogels described below, the device was placed in a humidified 37ºC incubator and the liquefied gelatin wass replaced by growth media after 30 to 60 minutes.

Bioprinting hydrogel arrays - Printing was performed using a custom built unit, with positioning of the print-head carriage accomplished by bi-polar 1.8º stepper motors driving translation lead screws in X, Y, Z and extrusion directions. STL files were designed in Solidworks and translated to printable GCODE using Repetier host software.

Scaffold Manufacture –Silk solution is placed in one side of a custom PDMS chamber, the two sides separated by a 1.0 mm conductive steel plate. During the unidirectional

freezing process, the other side of the PDMS chamber is filled with a freezing agent, from slow to fast: $CO_{2\,(l)}$ in 70% $_{v/v}$ EtOH/H_2O, $CO_{2\,(l)}$ in 100% EtOH, and $N_{2\,(l)}$. Scaffolds can be patterned with or without inlaid objects such as steel wires to provide conduits or optical media to provide ~1μm striations.

Cantilever fabrication – 40% silk fibroin solution (w/v) with 60-minute extraction time was loaded into a 3mL Nordson syringe and printed with a CellInk (Palo Alto, CA, USA) Inkredible+ bioprinter via the pneumatic syringe holder. Nanoclay solution (2.5g Laponite XLG in 50/50 ratio of PEG, dH_2O) was filled in the wells of six, eight, 12, or 24 well plates and the plates were loaded into the bioprinter plate holder. Code generated from slic3r, Repetier Host V1.6.1, with G-code modified with custom Python scripts were sent to the bioprinter and the constructs were printed with pneumatic extrusion through 20-28G syringe tips at pressures of 15-80 kPa (Video S1). After the printing process was complete, prints were left in nanoclay solution for up to 12 hours for silk polymerization (Video S2). Prints were subsequently washed with phosphate buffer solution (PBS) and left on a shaker plate overnight to remove nanoclay particles from silk. Prior to cell seeding, printed cantilevers were incubated at room temperature with 0.1% Pluronic F127 to reduce gel adhesion to the culture surface and then UV sterilized for 20 minutes. Final cantilever dimensions in eight-well plates measure 5mm high, 2mm wide, and 6mm across at widest point. The two cantilevers are separated by distance of 6mm and each cantilever sits atop a circular skirt with 1.5mm radius.

Physical Stimulation - Engineered tissue constructs were provided with static strain through attachment to optimized polydimethylsiloxane (PDMS) or printed silk fibroin cantilevers. Strain was calculated by deflection measurement of the cantilever from

neutral position. For modeling of mechanical stimulation of the engineered constructs a custom-built in house stepper motor driven linear actuator was built with stainless steel rods descending into culture wells to deflect cantilevers a quantifiable amount corresponding to specific forces applied to the tissue construct.

2.3 Imaging and Analysis

Immunostaining - Cells and tissue constructs were fixed in 3.7% paraformaldehyde in PBS for 10 minutes. Following fixation, samples were washed in PBS and then permeabilized in 0.1% Triton-X 100 and blocked in 1% bovine serum albumin for 1 hour prior to staining. When staining with Alexa Fluor 488 bungarotoxin conjugate constructs were stained pre- permeabilization to visualize surface receptors. In all other cases, desmin (1:200), myoD (1:200), alpha-actinin (1:200) (Thermo Fisher, Waltham, MA) were added after blocking solution and incubated overnight at 4°C. Corresponding secondary antibodies with conjugated Alexa flour 596 and Alexa 488 dyes were added after three washes with PBS for five minutes each. 0.1% (vol/vol) 4′,6-diamidino-2-phenylindole (DAPI) (Sigma Aldrich St Louis, MO, all others from Thermo Fisher, Waltham, MA) was diluted in PBS and added to the samples in the absence of light at room temperature after removal of the secondary antibody, and washed three times with PBS. Samples were either mounted on microscope slides or left in PBS to avoid sample drying. Images were acquired on Keyence BZ-X700 or Leica SP8 Microscopes and analyzed with ImageJ and CellProfiler (Broad Institute, Cambridge, MA).

Calcium Signaling and analysis - Live cell imaging was performed on the Keyence imaging system with a heated stage and 5% CO_2 environment. While some constructs

were able to be imaged *in situ*, in most analyses constructs were removed with micro tweezers and placed in an individual well with 1mL Hank's Buffered Salt Solution (HBSS). Acetylcholine chloride was added in a 100mM bolus of 10µL to the well containing the construct and recording commenced approximately 5s afterwards, after readjustment of the microscopy stage and enclosure. For these experiments recordings took place over 120s at 4-6 frames per second. Both mono- and cocultures were given the same acetylcholine bolus, although future experiments will add tubocurarine, which should diminish the transmission from nerve to muscle, and thus demonstrate to what degree nerves influence any calcium transient response.

To analyze calcium transients, recordings were saved as AVI files, and opened as an image stack in ImageJ. Z-projection of the image stacks with standard deviation displayed heat maps of cells with calcium responses. For quantification, randomly chosen muscle fibers were traced as regions of interest (ROIs) and then measured for fluorescence over the 120s study. Cellular fluorescence was normalized for the background, chosen as a dark area ROI, as well as baseline, which was established as an average of 5s at the end of recording. A representative recording for monoculture and co-culture is shown, with three responding cells traced over the recording.

Confocal Imaging - Confocal imaging was performed on an inverted Leica SP8 microscope equipped with white laser technology using a 10 or 20X water immersion objective with a numerical aperture of 1.0.

RT-PCR - Gene expression levels for MyoD, myogenin (MYOG), Muscle-specific kinase (MuSK), human agrin (AGRN), myostatin (MSTN), and Hypoxanthine-guanine phosphoribosyltransferase (HGPRT) were quantified by qPCR. In brief, total RNA was

extracted using RNEasy Mini Kit (Qiagen, Valenica, CA), eluted and quantified. The RNA extracted was reverse transcribred to cDNA in a 20 uL reaction using iScript Advanced CDNA Synthesis Kit (Bio-Rad, Hercules, CA). Quantitative RT-PCR of cDNA (∼10 ng/µl) was performed using assays containing fluorescent hybridization probes (SYBR: Thermo Fisher, Waltham, MA). Reactions were incubated at 95°C for 10 min and amplification was carried out on samples with 2 min incubation at 50°C, followed by 50 cycles of 15 s at 95°C and 1 min at 60°C. The reaction for RT-PCR was processed in a 10 µl solution containing 1X Universal PCR Master Mix (Thermo Fisher) with 2 µl cDNA samples. RNA expression was compared to experimental controls using HGPRT as a reference gene. Primers had the following sequences: TGCCACAACGGACGACTTC Human MyoD1-F 5'-CGGGTCCAGGTCTTCGAA-3' Human MyoD1-R 5'-CACTCCCTCACCTCCATCGT-3', Human myogenin-F 5'-CATCTGGGAAGGCCACAGA-3', Human myogenin-R 5'-CTGGTTGCCTTCAGCGGAA-3', MUSK-F 5'-CTGCACACATGAAAGTAGCCA-3', MUSK-R 5'-GTCCTGCGTCTGCAAGAAGAG-3', AGRN-F 5'-CTCGCATTCGTTGCTGTAGG-3' AGRN-R 5'-ACCCCTGCCTAACCACATC-3', PAX7-F 5'-GCGGCAAAGAATCTTGGAGAC-3', PAX7-R 5'-TCCTCAGTAAACTTCGTCTGGA-3', MSTN-F 5'-CTGCTGTCATCCCTCTGGA-3', MSTN-R 5'-CCTGGCGTCGTGATTAGTGAT-3', HPRT-1-F 5'-AGACGTTCAGTCCTGTCCATAA-3', HPRT-1-R 5'-GGAGCGAGATCCCTCCAAAAT-3', GAPDH-F 5'-GGCTGTTGTCATACTTCTCATGG-3' GAPDH-R.

Statistics – All statistical analyses were performed in the text were performed with GraphPad Prism 6. As indicated throughout paired or unpaired Student's *t* test was used where appropriate, and for the comparison of three or more groups we used ordinary one-way ANOVA followed by Dunnet's multiple comparisons test. Kolmogorox-Smirov normality test was used where appropriate. N.s = not significant, * $p < 0.05$ level, Error bars are given as mean ± SEM.

Chapter 3: Results

3.1 Unidirectionally Frozen Scaffolds for Human Myoblast Culture

The first model system adapted for use as a NMJ model system is a silk fibroin unidirectionally frozen scaffold. The scaffold type is known to be porous and lamellar, thus has potential to allow inherently anisotropic muscle cells to elongate and align parallel to one another. In addition, the biochemical and mechanical properties of the scaffold bulk can be tuned by altering the silk molecular weight and concentration or by adding other materials to the scaffold. An especially relevant scaffold feature is pore size, as the pore size needed for optimal growth and differentiation of seeded cells depends on the biochemical and physical characteristics of the scaffold material. By varying the freezing agent, and thus the freezing gradient and rate, pore size can be honed in to optimal size for myoblast proliferation and growth [92].

3.1.1 Manufacturing and Coating Method for Cell Adhesion

The scaffold production starts with aqueous silk, prepared as described previously [97]. The silk is placed in one side of a custom PDMS chamber, the two sides separated by a 1.0 mm conductive steel plate. During the unidirectional freezing process, the other side of the PDMS chamber is filled with a freezing agent, usually one of three agents, from slow to fast: $CO_{2\,(l)}$ in 70% $_{v/v}$ EtOH/H_2O, $CO_{2\,(l)}$ in 100% EtOH, and $N_{2\,(l)}$. In our contexts $CO_{2\,(l)}$ in 70% $_{v/v}$ EtOH/H_2O was used a freezing agent due to prior studies illustrating >100μm pores. One of the first steps was to test the ultrastructure formed during different coating conditions as a microscale surface roughness has been shown to lead to better cell adhesion in silk blend scaffolds [99]. Silk scaffolds were prepared in bulk

using the anisotropic freezing mechanism leading to lamellar scaffolds and coating procedures with sterile culture gelatin and Geltrex® applied to silk scaffolds after lyophilization and prior to sputter coating for scanning electron microscopy (SEM) prep. Scaffolds were analysed at both milli- and microscale resolution to ensure lamellae would fit the short axis of myocytes at around ~10μm and could display microscale roughness similar to what is found in webbed morphology of perimysium native skeletal muscle[100] and theoretically would lead to increased cell adhesion. Gelatin and Geltrex® were both found to have coatings of silk that changed the ultrastructure and had room between lamellae for cells to integrate (figure 3.1A). It was also shown that optical media could be used to imprint microscale resolution onto cells at micron channels which have been shown (figure 3.1B).

After the lyophilization process, the scaffolds can be either water-vapor or methanol annealed to increase the β-sheet percentage of the silk fibroin protein for scaffold stability [97]. The scaffolds can then be rehydrated in culture media before seeding via direct pipetting of cells or premixing of cells with extracellular matrix gel or laminin, both of which can be added to increase cell adhesion to the silk scaffold.

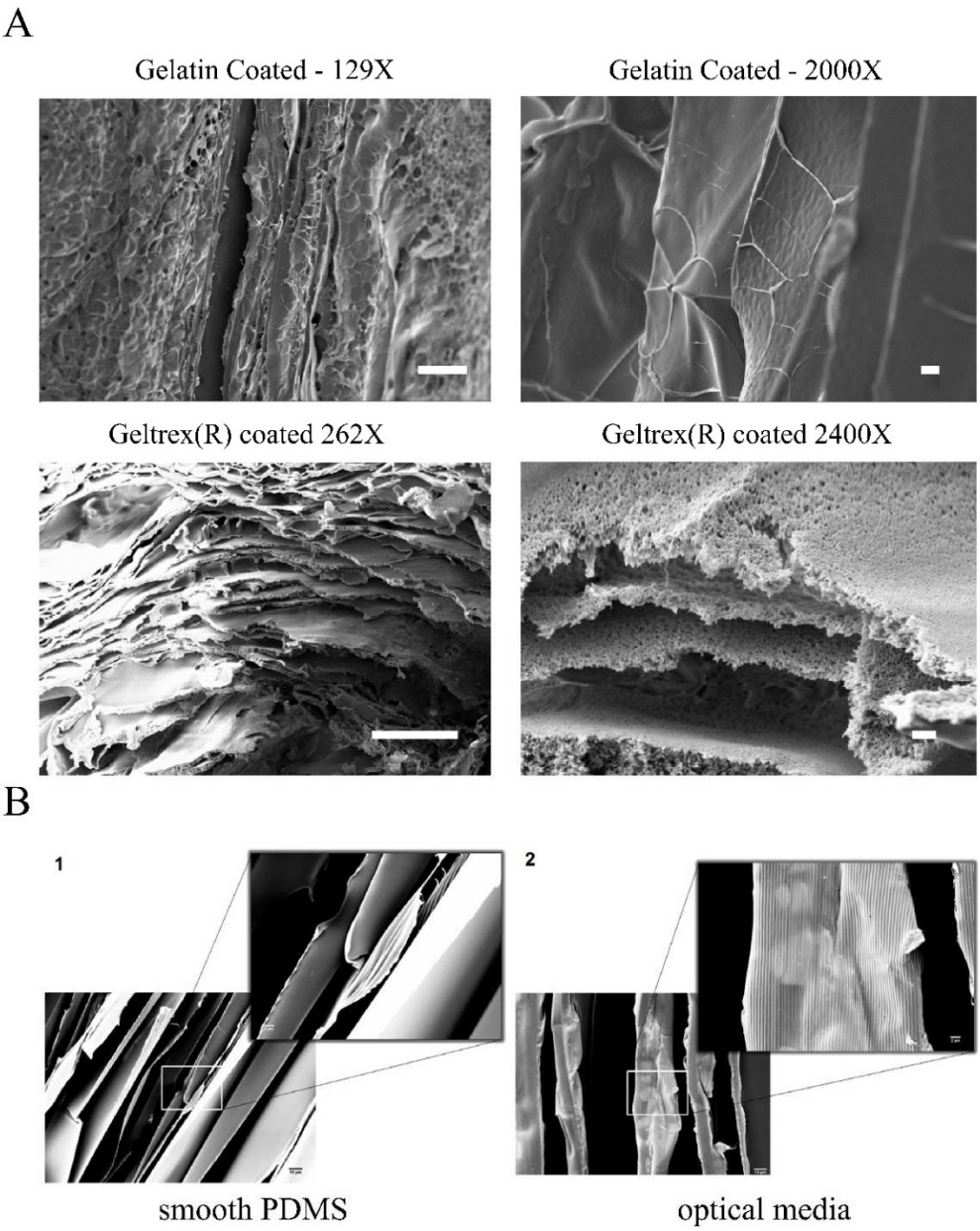

Figure 3.1: Silk Scaffold Coating and Patterned Casting for Skeletal Muscle Tissue Engineering. (A) Two common coating substrates applied to lamellar frozen silk scaffolds at two magnifications viewed with Scanning Electron Microscopy (SEM). Sterile 2% gelatin in H_2O (Sigma-Aldrich, St. Louis, MO) applied to silk scaffolds at 10µL per cm^2 surface area. Geltrex® Matrix (Thermo Fisher, Waltham, MA) applied at 50µL per cm^2 surface area in manufacturer recommended protocol. Scale bars: 100µm (left), 2 µm (right). (B) Non-patterned and patterned scaffolds shown via SEM. Bottom right: 505x magnification of laminar folds of directionally frozen silk scaffold. Scale bar 10 µm. Top right (inset): 1950x magnification of smooth surface of laminar folds. Scale bar: 2µm. 2. Bottom left: 505x magnification of laminar folds of silk scaffold seeded on micropatterned optical media surface. Scale bar 5µm. Top right (inset). 1950x magnification of micropatterned lamina. Ridge spacing ~ 1.5µm. Scale bar 2 µm. Images from preliminary data.

The scaffold morphology was designed from the beginning to incorporate the ability for co-culture, where after maturation of the human myofiber tissue scaffold through tension between fixed artificial tendons [101], tubular neuronal scaffolds will be dropped into a central pocket in the scaffold. The innervated myoblast-seeded scaffolds will be set on two suitably spaced PDMS attachment posts of known radius, length, and elastic modulus, allowing the moment of inertia of the posts to be calculated, and the post deflection used to evaluate the force generated [102]. To confirm the force/deflection angle function, force transducers can be used to deflect the attachment posts and calibrate force measurements. Attachment post deflection in captured images can be used to covert deflection to force in μNewtons. Using this program, contractions derived from electrical stimulation or spontaneous will be video-analyzed for measurement of contraction force vs. elongation past length of zero tension. Passive scaffold forces and active contraction-produced forces will be analyzed to produce force-length and force-frequency relationships. Using these data combined with geometric analysis of tissue constructs will allow comparison of specific tetanic force per muscle cross-sectional area to be compared to the state-of-the-art engineered muscle tissue [103].

3.1.2 Scaffold Design for Myoblast Alignment and Neural Coculture

The tubular scaffold theoretically will have cholinergic neural cells incubated in neural induction media, which will form connections through co-culture in preformed pockets in the human myofiber tissue scaffolds. To form the tubular scaffolds the use the "dipped-silk" or "gel-spun" tubes [97] or rolled decellularized tendon slices is employed, all biocompatible candidates for neural tissue engineering and axon growth, which have also been shown to be useful in nerve conduit engineering [104,105]. During the design process, human embryonic stem cell (hESC)-derived motor neuron progenitors (Lonza, Portsmouth, NH) were planned to seed the tubular scaffolds and incubate in a spinner flask with MotorBlast™ (Lonza, Portsmouth, NH) media for maintenance of the motor neuron progenitors. After the insertion of the tubular neuronal scaffolds into the myoblast-seeded scaffolds, we would switch the media to the serum-free co-culture system developed by the Vandenburgh group [75] The coculture is also designed to be in multi-well format, intended to increase reproducibility and minimize variance between constructs, a potential for individually made constructs with hand-set anchors or minutien pins (figure 3.2A).

The scaffolds were formed as the aqueous silk side of the chamber has in place a custom designed, machine fabricated CNC mold from a Solidworks part (.sldprt) design of the routed positive scaffold mold array. Each individual "dog-bone" unit produces one scaffold. The larger two holes are for mechanical stimulation using polytetrafluoroethylene (PTFE) coated wires and the smaller center hole mold ensures the silk scaffold is formed into a shape designed for stretching with a pocket for a neuronal scaffold placed in the center (figure 3.2B). The CNC mold is the positive shape and

produces a negative mold (figure 3.2B) out of SORTA-Clear® 40 silicone (Smooth-On, Macungie, PA), which is more flexible and durable than PDMS, making it suitable for molding and removing frozen scaffolds. After freezing, the scaffolds are removed from the mold and put in a lyophilizer for 3 days. After this point they are stable and can be placed into room-temperature aqueous solution (figure 3.2C). Scaffolds samples were examined pre-seeding to ensure lamellar structure and proper spacing for myoblast growth, where the pore diameter and geometry could be varied through freezing methods. Anisotropic morphology from unidirectional freezing was hypothesized to lead to myoblast proliferation, and the custom-molded tissue scaffolds are to be seeded human skeletal myoblasts (Thermo Fisher #A12555, Waltham, MA), guaranteed 50% myogenic index after two days. Scaffolds were first incubated in PBS with Pen/Strep 24hrs prior to seeding to ensure sterility.

To test the potential of anisotropic morphology leading to directed myoblast proliferation, 12 tissue scaffolds, with and without addition of reduced growth factor matrix, were seeded at 15 million cells/mL. Scaffolds were first incubated first in growth media for two days, followed by differentiation media for five days, with media changed every 48 hours.

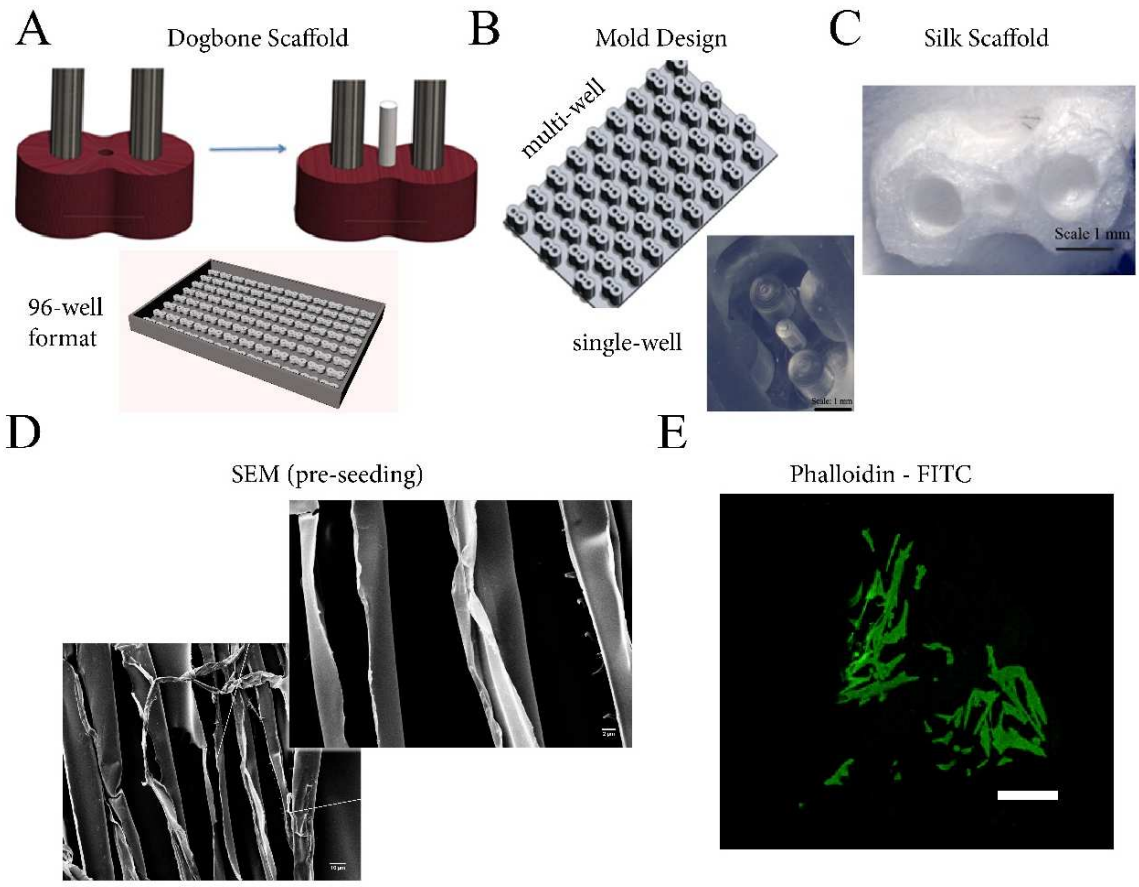

Figure 3.2: Frozen Lamellar Silk Scaffolds for Mechanical Stimulation and Innervation of Skeletal Myocytes. (A) Schematic of myoblast scaffold (red), artificial tendons (metallic chrome), tubular neuronal scaffold (white). 96-well format of arrayed supported scaffold shown below. (B) Solidworks (DS Solidworks Corporation, Waltham, MA) design of multi-well mold for frozen scaffold with magnified view of single scaffold on bottom right. Scale bar 1mm. (C) View of dogbone scaffold removed from mold prior to seeding. Scale bar 1mm. (D) SEM of lyophilized silk scaffolds showing lamellar pattern for myoblast alignment. Scale bar 10µm (bottom left), 2µm (top right). (E) FITC-phallodin stained human skeletal myoblasts (Thermo Fisher, Waltham, MA) stained after differentiation for seven days. Scale bar 100 µm.

Scaffolds were examined after one week through confocal microscopy visualization of FITC-phalloidin staining. Although scaffolds visualized through SEM had laminar patterning (figure 3.2D), seeded cells had seemingly random distributions and did not show the aligned morphology necessary for biomimicry of *in vivo* muscle tissue.

As we found that cells were randomly oriented on lamellar sheets, we wanted to examine how myoblasts proliferated on 2D surfaces with similar surface coatings as used in coating 3D culture scaffolds. We coated culture plates with thick and thin gelatin plating protocols, as well as Geltrex matrix coating, similar to what was applied to silk fibroin seeded scaffolds. Randomly chosen brightfield images were taken at day 4, 8, and 12 (figure 3.3A), and at the end of the study the ImageJ plugin 'angiogenesis analyzer,' designed to look at length and branching of cell networks, was used to evaluate myoblast growth in 2D (figure 3.3B). It was found that tissue culture plastic (TCP) had a lower degree of branching and total length of growth at days 4 and 8, but had non-significant differences at day 12. This is likely due to cells filling in and becoming fully confluent at the exponential growth phase and reaching a critical limit of growth. However, the expedited growth phase with gelatin and geltrex warranted further pursuit of the mechanisms governing human skeletal muscles interactions with extracellular matrix component based gels.

While we continued to explore scaffold-based methods to align human myoblasts, due to evidence of cell alignment in gels with tensioned contact points a transition to gel-based systems with softer matrices was sought to align human myoblasts in a manner amenable to downstream neural scaffold integration.

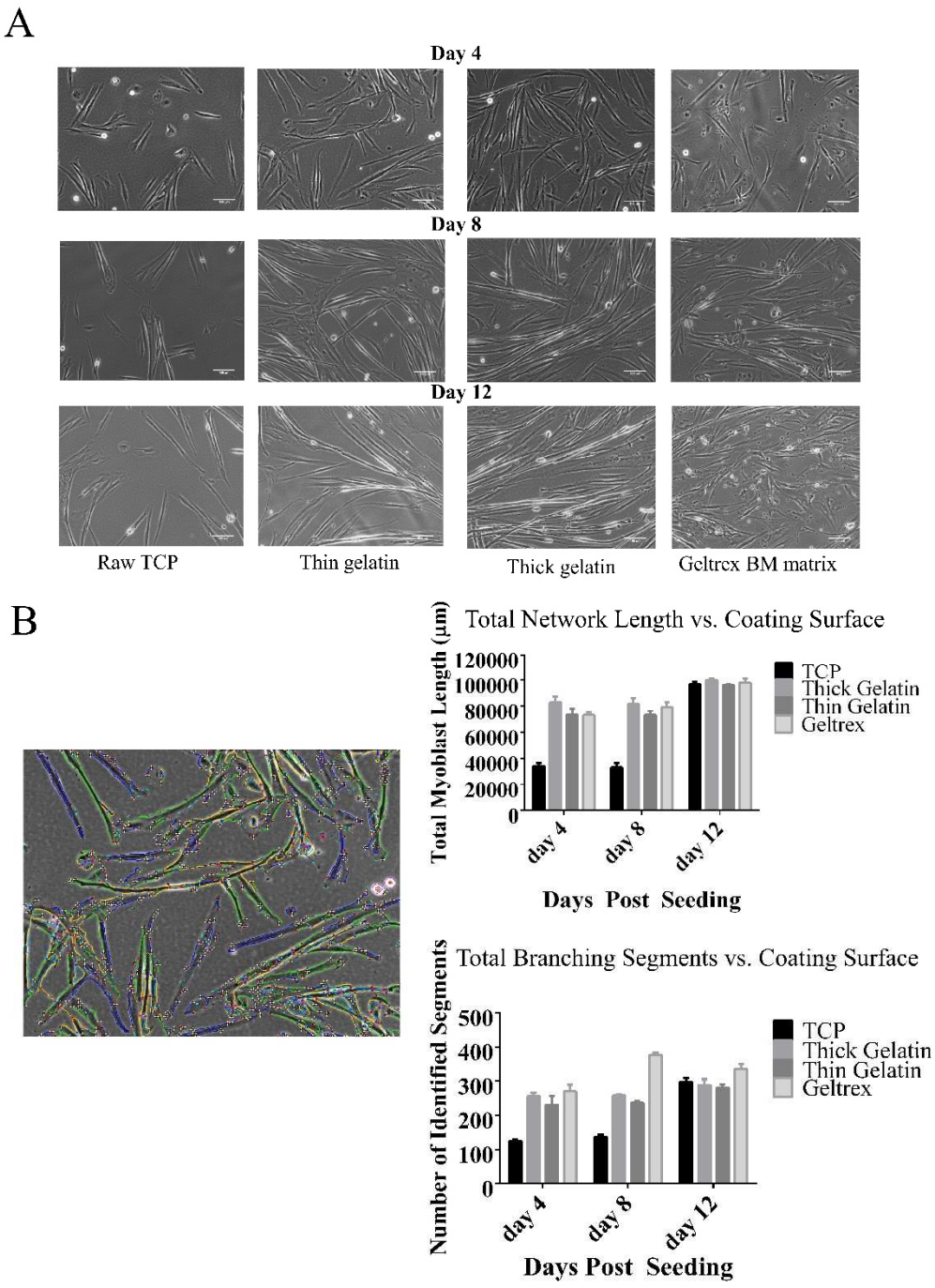

Figure 3.3: Primary Human Myoblast Growth and Segmentation on Coated 2D surfaces. (A) Representative brightfield microscopy of four different surface conditions at three regular timepoints. (B) Angiogenesis Analyzer for ImageJ sample output (left), showing identified and profiled branch points. Total combined length of cells showed for four different seeding conditions at days 4, 8, 12 (top left) and number of identified branches for same seeding conditions at same timepoints (top right). TCP – tissue culture plastic.

3.2 Effect of Extracellular Matrix Surfaces and Gels on Myoblast Growth and Morphology

3.2.1 Static Growth in Collagen and Collagen-Matrigel 3D Cultures

To begin to explore the viability of human skeletal muscles embedded in commonly used tissue culture substrates we seeded 200μL of $1*10^6$ human muscle cells/mL into six-well plates and then grew constructs in two days in growth media followed by six days in differentiation media. At the end of the eight days, cells we incubated in fluorescein diacete/propidium iodide (live/dead) and imaged 3D gels on fluorescence microscopes.

Human muscle cells appear to be aligned circumferentially around edge of gel bundle, potentially indicating mechanical compaction forces. Cells also showed isotropic network formation in blends of collagen/matrigel. Dead cells were common in cores of gel constructs, however necrotic cores were more common in 3D gels without matrigel (figure 3.4). Given the concentric alignment around the periphery of 3D gels it was thought that gel embedding may be a useful tool for studying application on tensile stress or other stimuli on myoblast alignment.

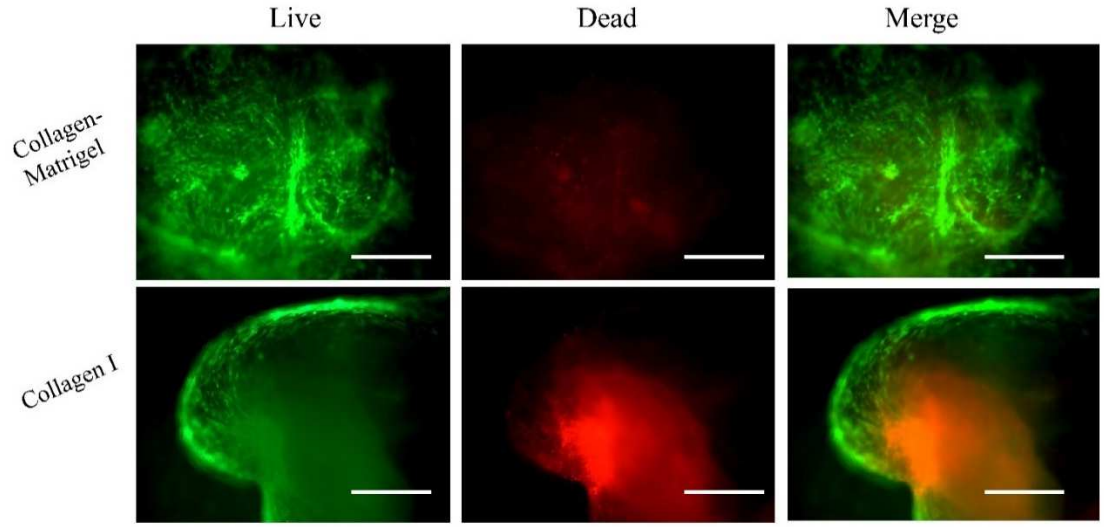

Figure 3.4: Human Skeletal Myoblast Growth in Static Cultured Collagen and Collagen/matrigel. Human myoblasts seeded at $1*10^6$ cells/mL. Live/dead stain performed after eight days in growth media. Live cells stained green with fluorescein diacetate, dead cells stained red with propidium iodide. Collagen-matrigel consists of 2mg/mL collagen at 5:4 ratio of collagen : matrigel. Collagen I consists of 2mg/mL collagen, with no added matrigel. Scale bar 250μm.

3.2.2 Automated Systems for Embedded Gel Culture in Myoblasts

To examine the effect of embedding cells in gels we examined methods of cell encapsulation with a high throughput array method. We used a custom developed bioplotting method to first look into agarose and gelatin blends, common substrates for *in vitro* gel encapsulation [106]. Bioplotting is thought of as a controlled array deposition of biologic deposition inside a gel substrate, and cell-plotting is considered a similar method for placing cells on top of a cell substrate for automated imaging. Other similar methods to be discussed in later sections include bioprinting and cell-printing, used to create arbitrary geometries (figure 3.5A).

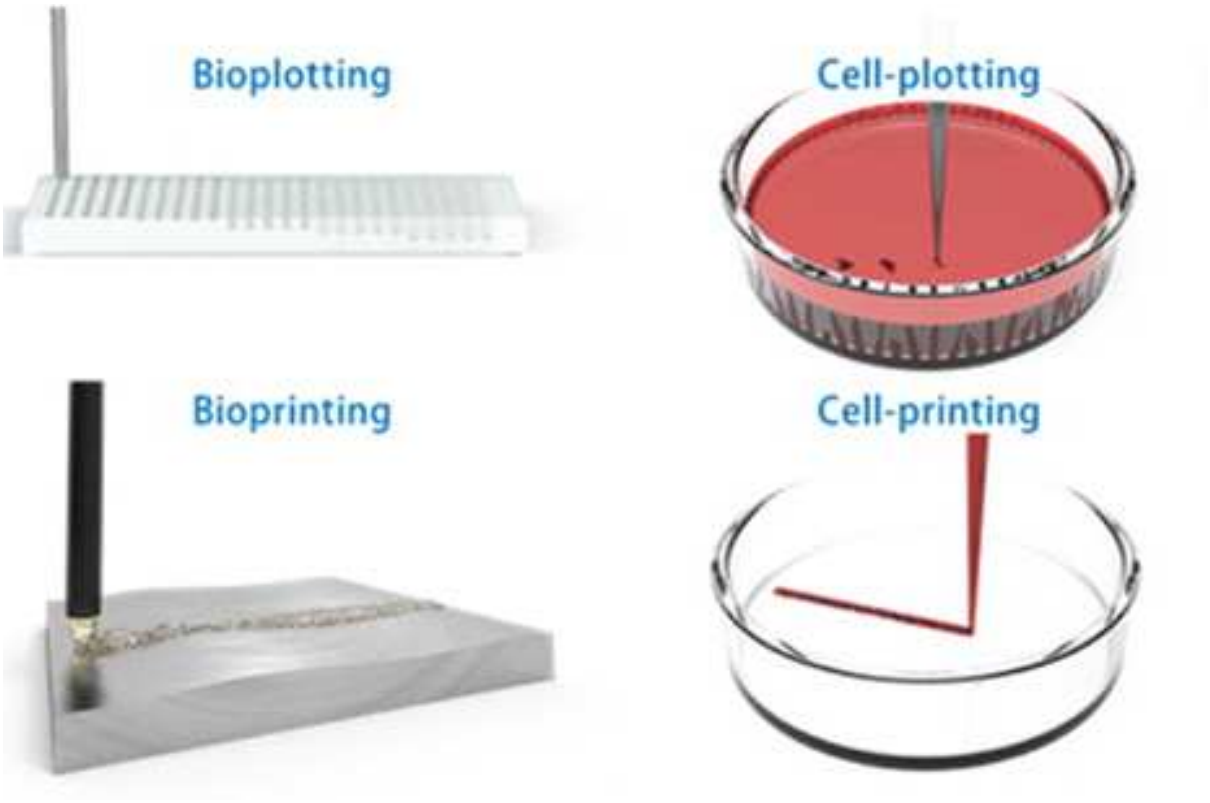

Figure 3.5: Automated 3D Biological Patterning Systems and Nomenclature. Illustrations display the differences between bioplotting and bioprinting strategies. Bio- vs. Cell- indicates biological materials versus living cells. 'Plotting' systems use array deposition while 'printing' systems build from filament. Reprinted with permission from Jose, Dixon, et al. 2016[107]. Copyright (2017) American Chemical Society.

The next step of examining the interface of encapsulated myoblasts involved ways to evaluate the viability of collagen/matrigel hydrogels and other gel blends in a high-throughput manner, through enscapsulation in agarose/gelatin blends shown to have healthy encapsulation of multiple cell types [106]. A robotic deposition system developed in house was used to separate bundles of cells or cells embedded in hydrogels on an array-based system that could be examined through dissecting scope or fluorescence microscopes. Gels were loaded into a 3mL syringe, and a 27 gauge (G) side port dispensing tip was used to inject cell-laden hydrogels at varying gel depths (figure 3.6a) and separated in square arrays at 250μm, 500μm, and 1.0 mm injection spacing. A side port dispensing tip, with rounded off tip was used to avoid clogging and gel disturbance during injection of cell-laden hydrogel. Myoblasts were first encapsulated in collagen-matrigel hydrogels and then programmed to deposit micro-scale quantities of hydrogels 200μm below the surface with varying the E-steps, a programming metric corresponding to actuation of the cantilever to depress the syringe plunger. Each step corresponds to approximately ~10nL of liquid with ~10 cells per nL assuming equal mixing of $1*10^6$ cells/mL of hydrogel. Live-dead staining and brightfield staining were used to examine cell bundles in ag50 (1.5% (w/v) agarose and 1.5% (w/v) gelatin) at 250 and 500μm spacing (figure 3.6c). At 500μm spacing it appeared gel bundles were better resolved than at 250μm, possibly due to less gel disturbance. It was also found that ag75 (0.75% (w/v) gelatin and 2.25% (w/v) agarose), had a higher degree of gel cracking, with cells moving through cracks in between gel bundles. In both gel blends and spacing, cell viability appeared to be at acceptable levels, although there appeared to be some degree of cell death in the center of gel bundles (figure 3.6c, 6d).

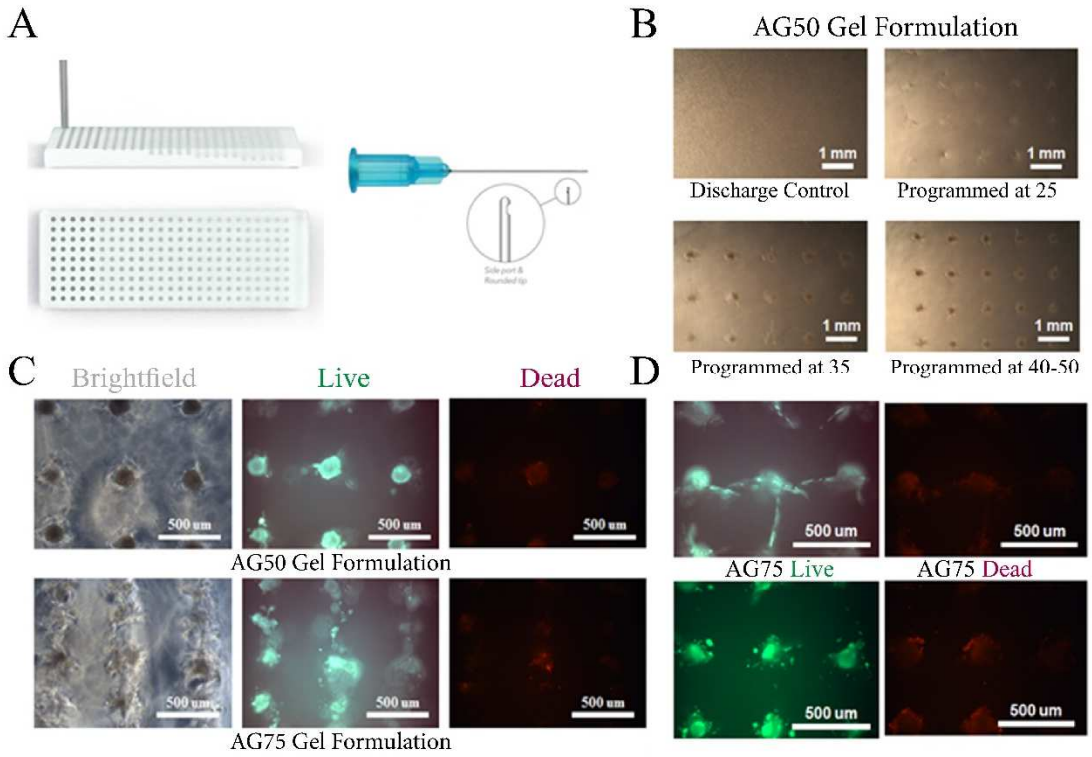

Figure 3.6: Bioplotted C2C12 Myoblasts as Proof of Concept for Mechanical Manipulation and Gel Encapsulation. (a) Schematic for bioprinting into gel media at various depths to test for viability in cell encapsulation. 27 gauge side port needle type shown on right. (b) Dissecting scope photographs of cell bundles programmed at relative extrusion volumes corresponding to E-steps on cantilevered syringe piston. Each step is equivalent to ~10nL of liquid with ~10 cells per nL. AG50 indicates gel composition of 50:50 ratio of 1.5% (w/v) agarose and 1.5% (w/v) gelatin in phosphate-buffered saline (PBS). AG75 refers to 0.75% (w/v) gelatin and 2.25% (w/v) agarose. Scale bar 1mm. (c) Bioplotted bundles of cells shown with 500µm spacing (top) and 250 spacing (bottom) in brightfield (left) live imaging (fluorescein diacetate, green, center) and dead stain (propidium iodide, red, right). (d) Bioplotted bundles of cells in AG75 gel encapsulation. Scale bar 500µms.

To expand the automated method of delivery of myoblasts, and eventually combine myoblasts interspersed with neurons, we deposited 1 million C2C12 cells/ mL plotted in arrays of straight lines with the custom made robotic delivery system, also using rounded tip, side port dispensing needles, Cells were again imaged with brightfield and live imaging. After two days of incubation of growth media we visualized cell bundles in the ag50 encapsulation matrix and live cells appeared to grow in elongated clusters through the crevasses creating by dispensing needle tip movement (figure 3.7A,B), although the live staining method made it difficult to determine the precise morphology of the live cells, specifically if they existed in syncytia or aligned cell clusters. To examine and quantify the alignment created by robotic extrusion in linear patterns with C2C12 fluorescent images are converted to square images in 8-bit and then processed with 2D Fast Fourier Transform (FFT). The oval plot plugin of the 2D Fast Fourier Transform is analyzed by intensity by degree showing relative alignment by degree orientation, shown in from 0 to 360˚ (figure 3.7C).

Although myoblasts appear to be expanded to some degree, the system of deposition requires better homogenous seeding of cells, possibly with increased mixing beforehand. It is also important to look at cell morphology as opposed to viability en bloc as an expanded and aligned phenotype is critical for an improved 3D NMJ model.

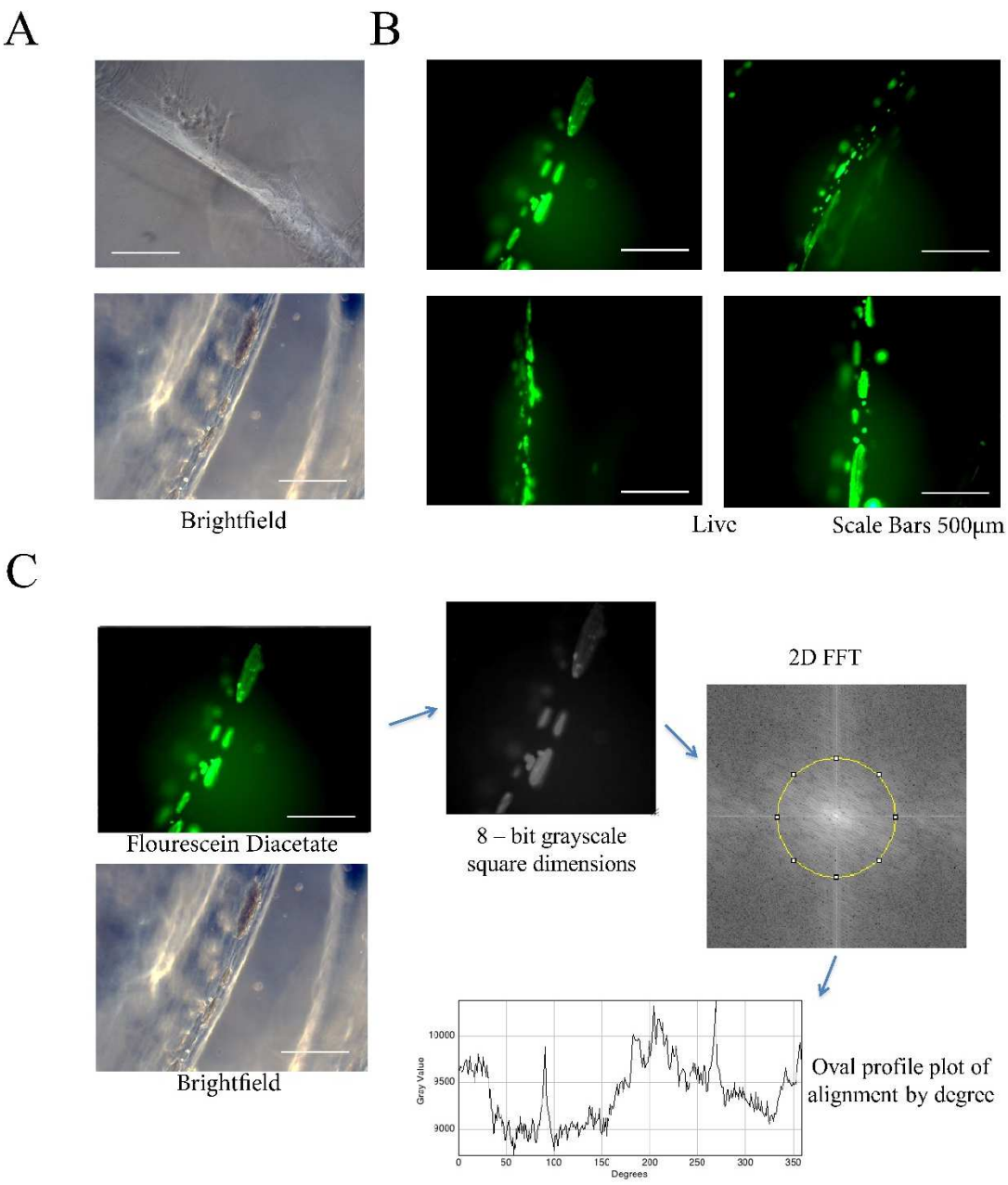

Figure 3.7: Murine Myoblast Cell Elongation and Alignment in Encapsulated Gels and 3D Suspended Gels. (A) Brightfield imaging of cells found in gel crevasse left by linear movement of robotically controlled syringe. Cells imaged two days after robotic extrusion. Scale bars 500µm (top) 250µm (bottom). (B) Live cell imaging of myoblasts encapsulated in AG50 after two days of culture in growth media. Scale bars 500µm. (C) Flow schematic for quantification of alignment in encapsulated myoblasts. Images are converted to square images in 8-bit and then processed with 2D Fast Fourier Transform (FFT). The oval plot of Fast Fourier Transform is analyzed by intensity by degree showing relative alignment by degree orientation, shown in from 0 to 360̊.

3.2.3 Alignment Analysis of Embedded Gel Culture in Myoblasts

While there appeared to be some degree of alignment within gel blends indicated by peaks on the alignment chart, there were two directions taken. One was to increase the specificity of the alignment process using ImageJ, and the other was the ensure more even distribution of embedded myoblasts. To examine the 2D FFT method for use in both monoculture and 3D culture we examined C2C12 myoblasts in monolayers and 3D culture. C2C12 myoblasts were cultured on 2D monolayers in eight days, after which we took a square grayscale image from live stain shown on left with image transformation by 2D FFT and overlaid oval profile plot in center which calculated frequency of alignment by degree from 0 to 360̊ (figure 3.8a). We also used C2C12 myoblasts cultured in 3D culture for 8 days in previously described 5:4 collagen/matrigel blend for cell enscapulation with live stain shown on left with image transformation by 2D FFT and overlaid oval plot in center, and alignment plot from 0 to 360̊ (figure 3.8b).

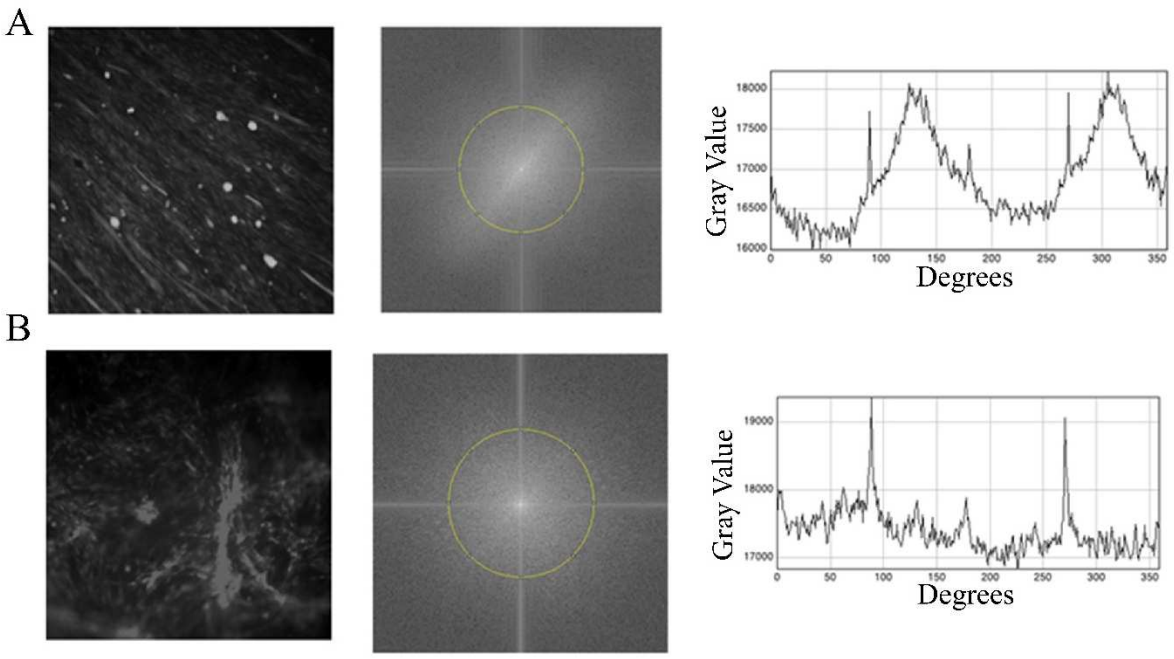

Figure 3.8: Proof of Concept of Alignment Detection with 2D FFT Method with C2C12 Myoblasts in Monolayers and 3D Culture. (A) C2C12 myoblasts were cultured on 2D monolayers in eight days. 2D grayscale image from live stain shown on left with image transformation by 2D FFT and overlaid oval plot in center. Graph on right depicts frequency of alignment by degree from 0 to 360̊ determined through oval plot plugin in ImageJ. (B) C2C12 myoblasts cultured in 3D culture for 8 days in previously described 5:4 collagen/matrigel blend for cell encapsulation with live stain shown on left with image transformation by 2D FFT and overlaid oval plot in center, and alignment plot from 0 to 360̊ shown on right.

Examining the oval plots it appears that region of 2D monoculture have aligned cells, due to the inherent nature of myoblast growth, however 3D culture blends showed spectral flatness and pseudo-random alignment. One feature of the profile plot was peaks at 90 and 270°. We used a fine-tuned 2D FFT and oval profile plot methods to find reproducible methods of determining alignment of myoblasts in culture and sought ways to eliminate vertical and horizontal artifacts of imaging, through a manual deconvolution method (figure 5.1), which could be made into an automated macro in future aims. Using the manual deconvolution method, it appears the peaks at 90 and 270° are decreased, leading to better alignment signal resolution.

3.3 Differentiation and Alignment of 3D Cultured Myoblasts

3.3.1 Growth and Differentiation of C2C12 Myoblasts in Engineered 3D Hydrogels

To further attempt to create bioprinted 3D myoblast cultures we adapted techniques used to create 3D bioprinted muscle [43] where hot extrusion tips where used to create patterned thermoplastic and extrusion tips were used to pattern cell aggregates on top of support agar (figure 3.11A). The experiment started with expanding C2C12 myoblasts in growth medium in DMEM plus 10% fetal bovine serum. Myoblasts were then encapsulated into similar collagen-matrigel 1% silk hydrogels as found in the 3D constructs mentioned above.

For extrusion based bioprinting, bioinks are loaded into a syringe, which has an extrusion mechanism, which will extrude the inks as dictated by 3D design, while simultaneously the printer positions the extruder tip to recreate the 3D object. Objects can be printed with or without support material which serves to physically constrain the printed part and provide mechanical support while the construct is crosslinking and undergoing gel-solution transition (figure 3.9A). The collagen crosslinking works as neutralized collagen is loaded into the syringe and then extruded and incubated at 37°C for 30 minutes to an hour before addition of growth media. After culture for up to five days C2C12 culture showed definite spacing using the bioprinted technique on top of support agar, with viability at two different culture densities (figure 3.9B). Using this technique to print lines of C2C12 embedded silk-collagen hydrogen spaced 1mm apart, C2C12 cultures have been differentiated for two weeks, showing fusion into myotubes along the axis of printing, as illustrated by alpha-actinin staining, an advanced differentiation marker [24].

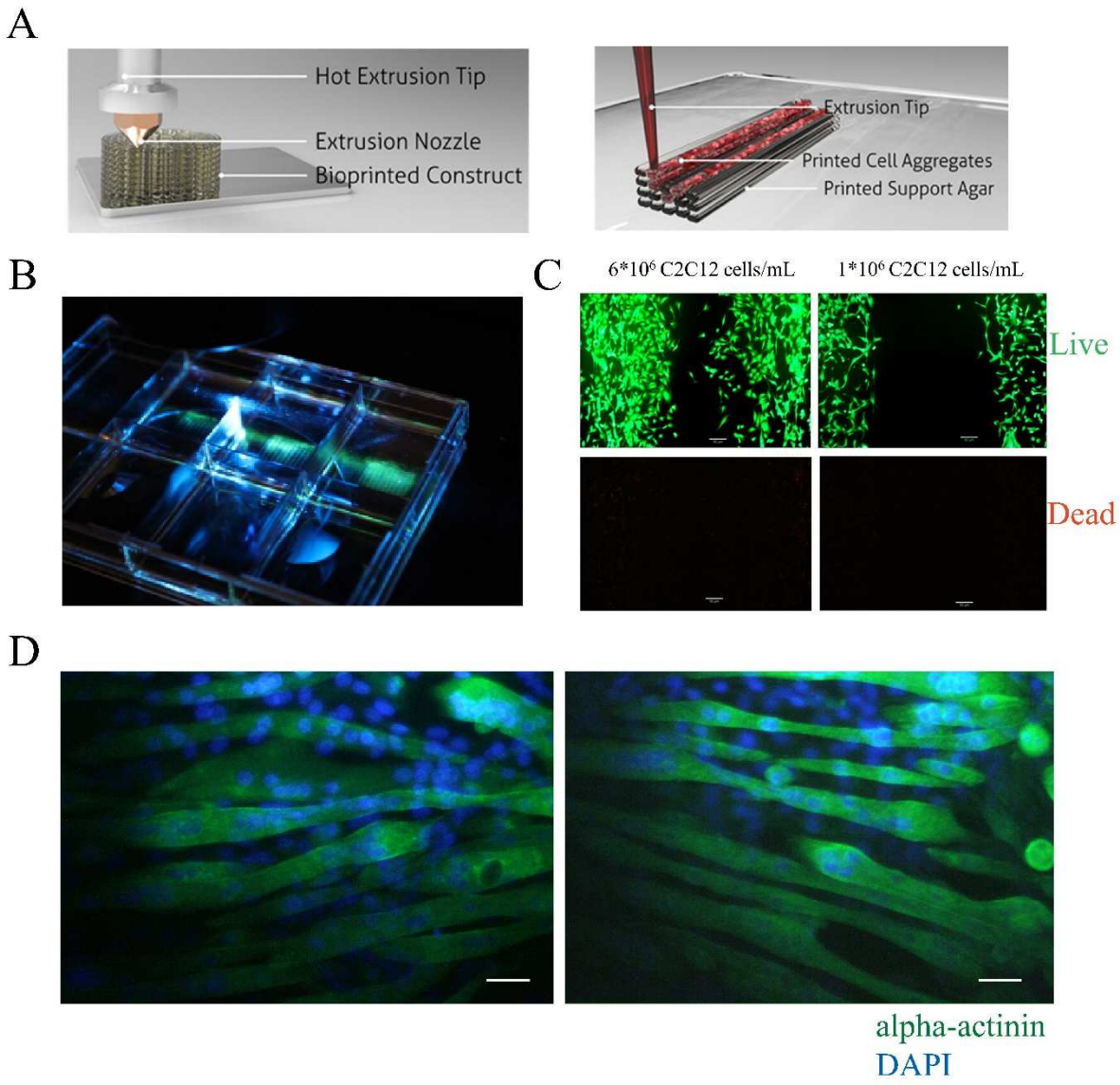

Figure 3.9: Myotube Formation Through Bioprinted Coculture. (A) Schematic of a FDM printing process (left), and schematic of the 3D cell-printing process which directly extrudes cellular aggregates a 3D building blocks on support material (right). Reprinted with permission from Jose, Dixon, et al. 2016[107]. Copyright (2017) American Chemical Society. (B) Image of array bioprinted myoblast lines printed 500µm apart in an 8-well plate. (C) Live/dead staining (fluorescein diacetate-green, propidium iodide – red) of C2C12 cells printed at different densities after two days. Scale bar 50µm. (D) Fluorescence image of bioprinted C2C12 cells differentiated for 5 days and stained with α-actinin, to indicate differentiation towards mature muscle. Scale bar 10µm.

It was recognized that a method to create aligned myoblasts using well integrated and homogeneously seeded hydrogels was needed that built on automated systems, and was able to create multiple constructs seeded from one batch. This system also needed to have a downstream method that could be used to integrate neurons with minimal disturbance to the initial design of 3D myoblast culture and alignment.

In transitioning from plated 3D gel culture, we developed a means of injecting an extracellular matrix-enriched collagen-silk hydrogel through sacrificial channels in a polydimethylsiloxane (PDMS) mold, allowing the cell-infused hydrogel to polymerize after seeding at 37°C in an incubator. This system is based on previous engineering methods using sacrificial gelatin cavities to show reproducible C2C12 alignment [108]. We sought to update the technique published by Neal, et al. through using sacrificial channels through flexible cantilevers (figure 3.10a) so that the cantilevers provide an artificial tendon for the polymerized gel to pull against. We also designed the molds to produce innervations with sacrificial channels manufactured orthogonal to the channels running through the silicone cantilevers, designed to hold myoblast-laden gels. The schematic and setup of the 3D gel cross design is to reproduce the interface between the developing ventral nerve root and the extending myotome *in utero*. The ventral nerve roots of humans have a wide range of cross-sectional area, although it also found that roots are divided into up to 40 fascicles [109], thus nerve roots may be present in the micro- to submillimeter diameter range. While these developing tissues are physically and interconnected by interstitial fluid, there is likely a microenvironment enveloping each tissue dictating its developmental course. Thus, I wanted to explore a method to spatially

segregate the two tissue types while still maintaining proximity, as a means to control for what the role of physical tissue contact is on *in vitro* coculture.

The system is also extendable to downstream neuronal cell culture as two gel types can polymerize and encapsulate cells, and thus we aim to demonstrate and have shown viable growth of motorneuron-like cell lines and extension of myoblast cells in an anisotropic manner. The co-culture will be applied as polytetrafluoroethylene (PTFE)-coated wires pulled through the mold in two directions, leaving sacrificial channels.

The system of sterile bioreactor development begins once the cast PDMS is removed from the negative mold, and the PTFE-coated wires are inserted. After sterilization through autoclaving and ultraviolet light, sterile 10% gelatin w/v in culture media is added to the mold. The gelatin is gelled at 4°C after which the PTFE-coated wires can be removed and hydrogel solutions can be inserted in two directions, with the longest dimension being suspended between two posts. The PTFE-coated stainless rods forming the two channels (meeting at 90°) were removed at the same time that two cell-laden gels are prepared, and then various cell types are injected into the channels in both directions simultaneously (figure 3.10A). The format for creating crossed sacrificial gels is expanded to a 24-well plate format for syringe-loading of suspended gels by using a molding technique that can produce a 24 well plate format based on existing dimensions for 24 well plate culture.

The full 24 well negative mold was fabricated through machined CNC milling of Delrin® blocks and PDMS was poured over the negative mold, degassed and polymerized at 60°C for four hours. Once the PDMS is removed (figure 3.10B), the PTFE-coated wires are reinserted and after sterilization through autoclaving and

ultraviolet light, sterile 10% gelatin w/v in culture media is added to the mold (figure 3.10B). The gelatin is gelled at 4°C after which the PTFE-coated wires can be removed and hydrogel solutions can be inserted in two directions, with the longest dimension being suspended between two posts (figure 3.10B).

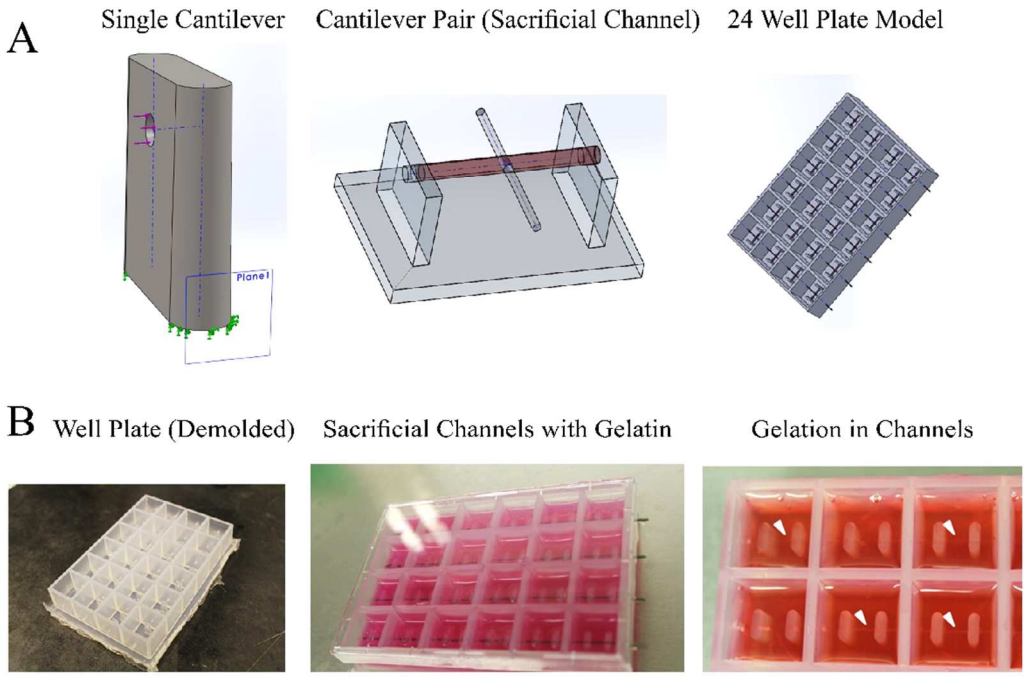

Figure 3.10: Passive Tension Methods for Fabricating Free-Standing Gel Constructs from Sacrifical Gelatin PDMS molds. (A) (left) Cantilever deflection from single cantilever in Solidworks (Solidworks, Waltham, MA) with red arrows depicting areas of contact with muscle gel and green arrows showing forces on cantilever base. Cantilever pair model shown in center with red gel indicating final placement of myoblast-seeded gel, and transparent gel indicating neuronal-seeded gel. 24 well plate model used for creating negative mold (left) showing inlaid wires for forming sacrificial channels. (B) Well plate shown removed from mold after solidification at 60℃ for four hours (left). 24-well plate shown with PTFE-coated wires in green, gelatin type A solution filling up wells in red (center). After wires are removed hydrogel solutions are added into the sacrificial channels, and after plate in incubated at 37℃ for 30 minutes, hydrogels can be seen in crossed channels, with gel crosses polymerized together shown by white arrows (right). Scale bar 5mm.

After the 24-well plate format for syringe loading of suspended gels was proven to be possible through proof-of-concept gelation of collagen into gel-crossed structures in the incubator, further directions aimed to create 96-well molds with the ability for *in situ* imaging, including the possibility of parallel perfusion. There were also efforts to automate with syringe deposition of hydrogels through bioprinter loading, and initial tests tested the possibility of this with two-well model systems (figure 5.2).

This system presents some benefits as well as challenges for future studies. The first benefit is that molds could theoretically be reused as PDMS can be autoclaved sterilized and washed with diH_2O for subsequent seeding. However, one challenge is that the gels seem to have limited stability between the cantilevers, potentially limiting the feasibility of longer term culture. Another challenge is whether the designed system creates enough tensile force to form a higher degree of differentiation in myotubes. This limitation could theoretically be tuned by altering machining of cantilever dimensions, and through increasing adhesion in the area of gel attachment to PDMS cantilevers. Despite the drawbacks, this system allows for use in multiple gel and cell types, to be discussed later in co-culture experiments.

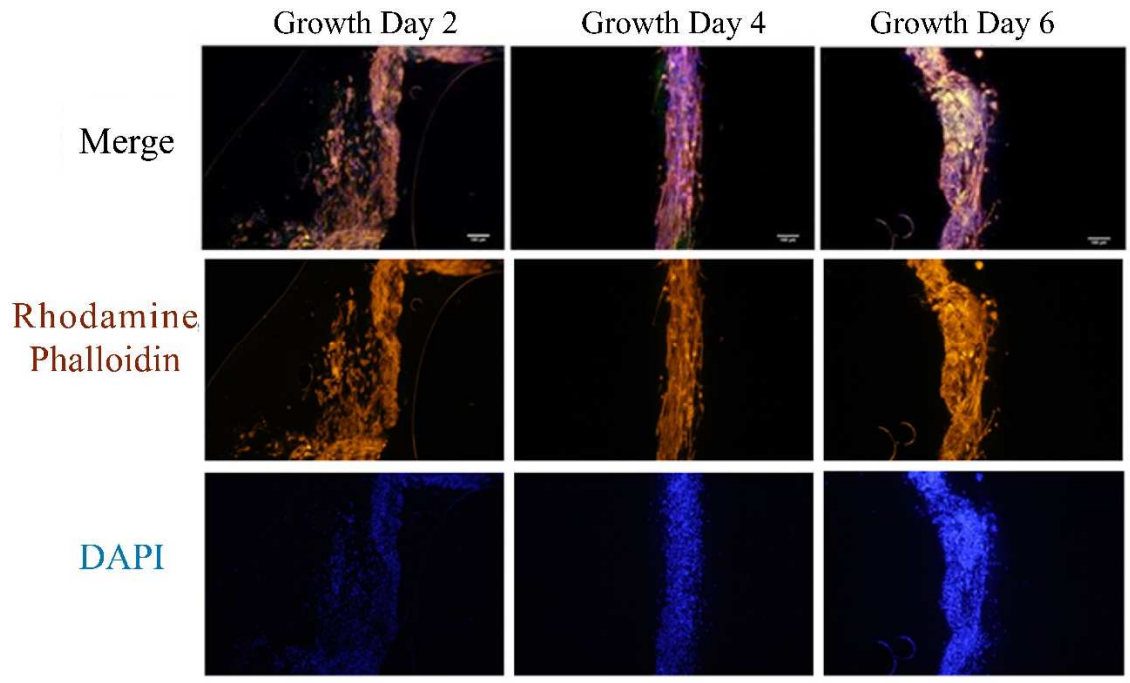

Figure 3.11: Representative Phallodin/DAPI Imaging of Free-Standing C2C12 Gel Embedded Constructs from Sacrifical Gelatin PDMS molds. C2C12 Cells suspended in gel bundles through gelation in sacrificial channels. C2C12 cells were seeded at $1*10^6$ cells/mL hydrogel, using the sacrificial channel method, and fixed at three timepoints to visualize cytoskeletal alignment in silk-collagen hydrogels. Constructs were stained for rhodamine-phallodin, and DAPI, then mounted on slides and imaged through fluorescence microscopy. Merged views of representative samples shown on top with rhodamine phalloidin and DAPI shown below. Scale bars100μm (top).

The specific goal of successful formation 3D culture of myoblasts in hydrogels is to determine reproducible and robust methods aligning myoblasts in 3D matrices. From previous experiments seeding myoblasts in collagen gels I had learned that the best starting density is approximately 1-6*10^6 myoblasts/mL of hydrogel. I carried out 3D cultures at 1.0*10^6 cells/mL starting density with sacrifice of constructs at two day timepoints with sacrificial channel bioreactor. Cells in constructs after two days appeared loosely adherent and partially extended, whereas in day 4 constructs had fascicle-like appearance with longer, thick extensions of cells noted through fourier transform analysis. At day 6 cells appeared overgrown and tortuous (figure 3.11), indicating a need for differentiation through serum withdrawal prior to over-confluence of myoblasts. If cells undergo differentiation around day 4, it is possible that there will be less expansion of cell types and more cell fusion into myotubes, lessening the tortuosity of overgrown myocytes. Similar timecourse experiments were also repeated with human myoblasts toward the final goal of a 3D innervated cell model.

3.3.2 Characterization and Differentiation of Human Primary Skeletal Muscle Myoblasts

C2C12 myoblast cultures are useful as model systems for determining factors influencing myoblast elongation and fusion, however human myoblasts are inherently more relevant to translational studies. To test the suitability of human myoblasts for myogenic differentiation, primary skeletal myoblasts were purchased commercially and expanded per manufacturer's recommendation.

Human myoblasts are seeded on common substrates in 2D and differentiated according to common serum withdrawal protocols [54]. These cells are analyzed by

immunofluorescence (IF) for differentiation factors including MyoD, Myf5 and myogenin as well as cytoskeleton markers such as desmin, actin, and alpha-actinin. Myoblasts population are typically ~90% positive for myoD, and Myf5 after three days of differentiation although desmin expression varies between a range of 50-80% based on a number of factors, such as passage number, length of culture, serum percentage, and surface coating (2D culture) [50,110].

The first step after beginning culture of primary human myoblasts was to confirm that the cells are in fact myogenic and will form myotubes, with a known differentiation marker timing after exit from the cell cycle. In the first experiment to accomplish this aim, I seeded human myoblasts from Sigma (A12555, St. Louis, MO) in 2D on collagen I coated wells at $1*10^4$ cells per cm^2 and grew them according to established protocols for differentiating primary human myoblasts [95,96]. As per protocol cells were seeded in growth media for five days followed by three days of differentiation media. Cells were analyzed via immunofluorescence for positive staining of desmin and myoD, and multinucleated desmin positive myotubes were present as well as myoD expression at over >90% as shown by previous timecourse studies of primary human muscle cells (figure 3.12A,B) characterized to display a phenotype for exit from the quiescent myoblast stage and into mature desmin-positive myotube state with nuclear expression of the differentiation marker MyoD (figure 3.12A) [95]. The next step was to see how expression of desmin was affected by different 2D substrates, which would give a preliminary picture of changes to desmin positivity when cells were encapsulated in different 3D hydrogel environments.

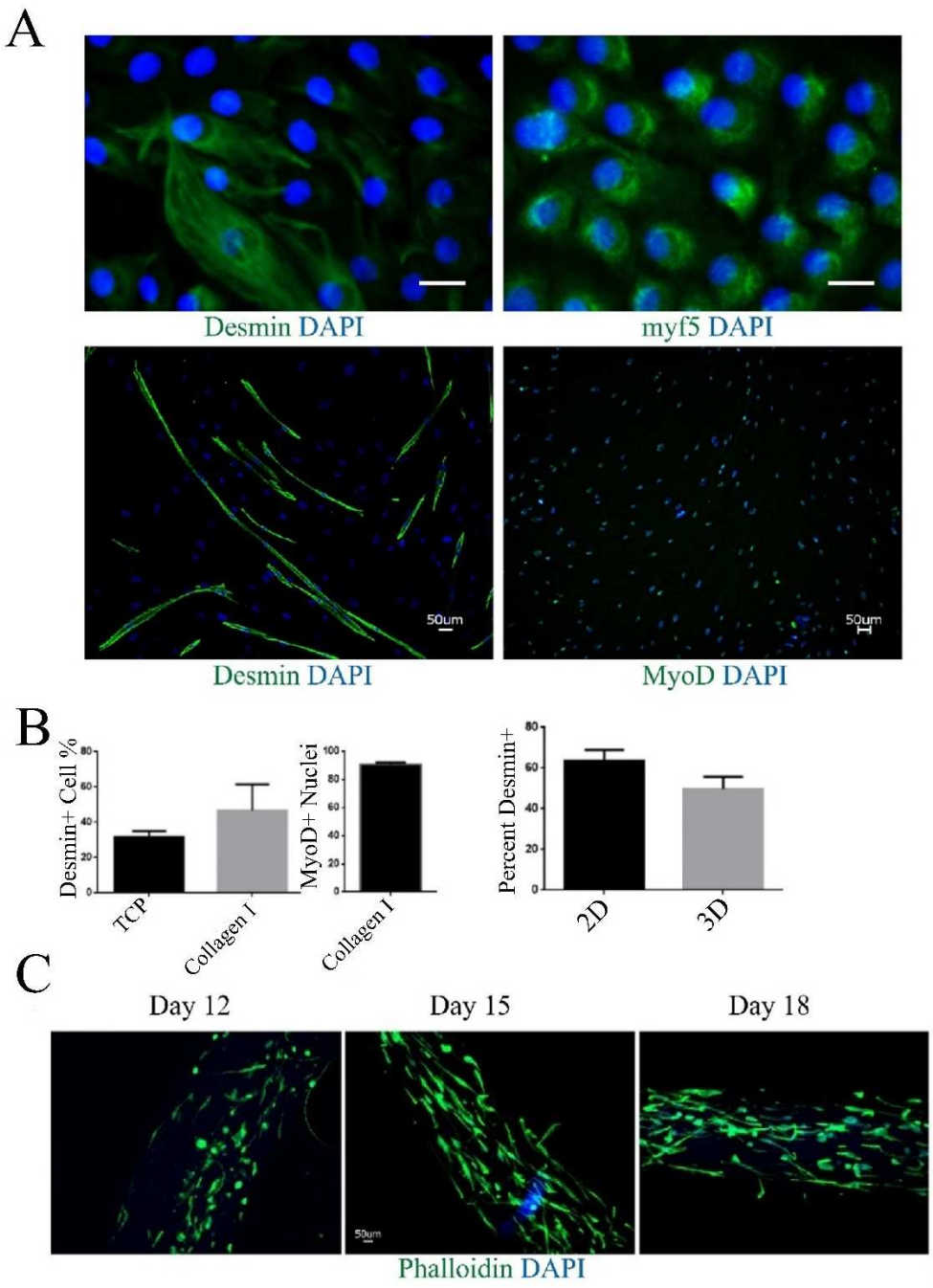

Figure 3.12: Characterization and Alignment of Human Myoblasts in 2D and 3D Culture. (A)(top) IF imaging of human myoblasts grown on 2D collagen show Desmin and myf5 expression after growth media for 5 days and differentiation media for 3 days. Scale bar 15µm. IF imaging (bottom) of human myoblasts seeded in 2D collagen gels in growth media for 5 days, followed by 3 days of differentiation media, express the muscle-specific cytoskeletal protein desmin (left), and show nuclear co-localization of the differentiation factor MyoD. Scale bar 50µm. (B) Desmin, MyoD percent positive nuclei quantitated via CellProfiler (Broad Institute, Cambridge, MA) on (left) (B) Percent Desmin+ nuclei in 2D and 3D culture. (C) Time course of human myoblasts expanding in 3D culture over 18 days. Scale bar 50µm.

Repeating the previous experiment with one group on tissue culture plastic and the experimental group grown on a coating of collagen I and analyzing for percentage of desmin positive cells show that there was a suggested increase of desmin positive nuclei with the collagen I coating (figure 3.12B). This led us to believe that the myogenic purity was increased with contact with collagen I in culture conditions, and further experiments sought to look at the difference in desmin positive nuclei when cells were grown in 2D collagen I coating, or in a collagen I 3D hydrogel. These cells are then seeded in experimental conditions including novel plated silk hydrogels and hydrogels in 3D culture, using the same analysis as above. After many trials in 3D with high percentage Desmin myoblasts gels composed of 2% silk, 2mg/mL collagen I, and 8% matrigel (hereafter referred to as silk/collagen) have been optimized for the purpose of human skeletal myoblasts (hSKM) differentiation upon polymerization with simultaneous optimization of timing and composition of growth and differentiation media, with over 50% Desmin+ nuclei in 3D culture. To test the effect of 2D vs. 3D enscapsulated cells in silk/collagen, cells were once again grown in the same myogenic conditions as previously described in 2D and the percentage of nuclei that were desmin positive was analyzed via immunofluorescence. The difference showed a trend but was below statistical significance (figure 3.12B). Overall many things are known to effect myogenic purity, measured both through positive desmin staining and MyoD+ nuclei at 3 days post differentiation. These factors include levels of senescent myoblasts, growth substrate, passage number, and culture factors [111]. To test proof-of-concept that human myoblasts would be aligned when suspended in 3D silk collagen hydrogels in a manner similar to

C2C12 model cells, silk-collagen hydrogels were seeded at a cell density of $2*10^6$ hSKMs/mL, extending myoblasts with high cell viability were found to extend throughout the gel in the axis parallel to the channel up until day 18 in growth media in 3D suspended gels (figure 3.12C). Qualitatively cells appear most aligned and congruent around day 15 which is the timepoint at which further differentiation studies will switch to differentiation media.

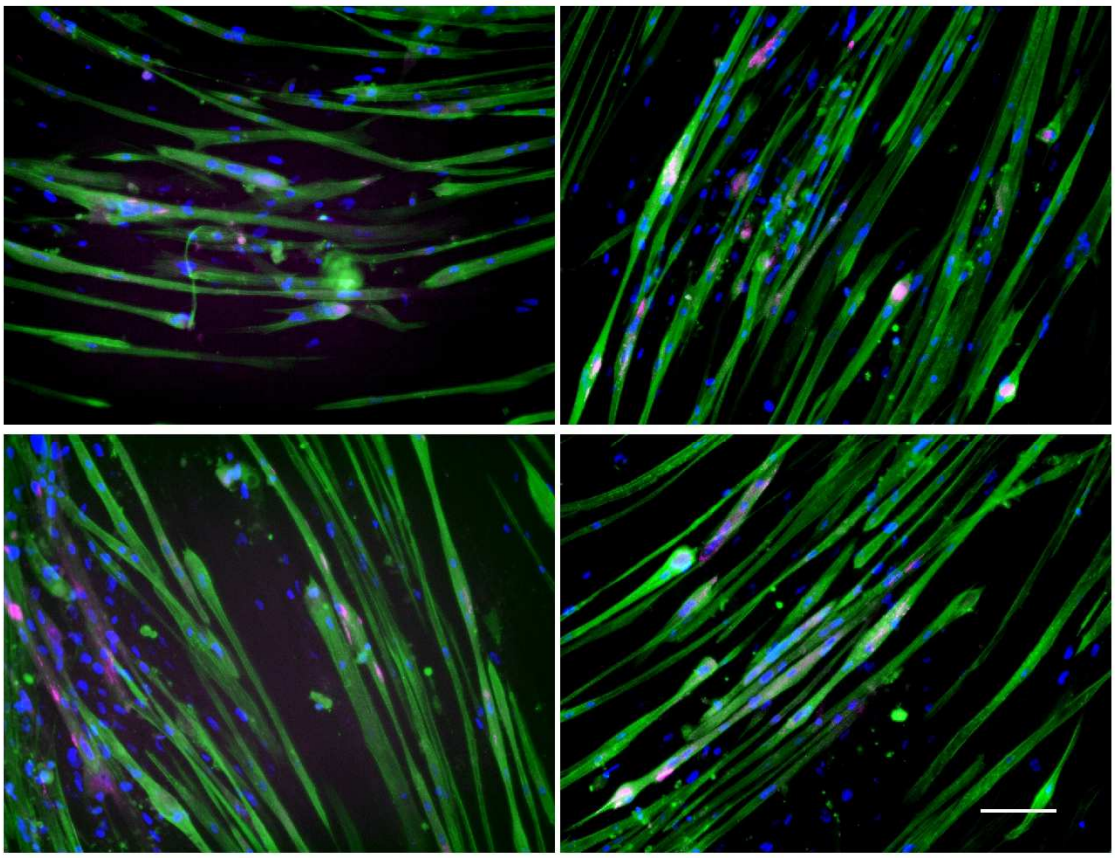

Figure 3.13: 2D Maturation of Human Myoblasts plated in Silk/Collagen I gel with Potential for Innervation. Human skeletal myoblasts (hSKMs) differentiated for four weeks displayed positive α-BTX (pink) staining in multi-nucleated myotubes. Multinucleated myotubes display α-actinin (green) staining throughout differentiated myotube. hSKMs differentiated for four weeks under the same conditions displayed punctate alpha-bungarotoxin staining (pink) in multinuclear myotubes with nuclei stained with DAPI (blue) scale bars 200μm.

To test if human myoblast cultures would present cellular machinery available for innervation, hSKMs were grown on thin silk-collagen coatings and expanded for 3 days in growth and analyzed after an additional 28 days in culture in mono-culture to determine if alpha-bungarotoxin was colocalized in plaque patterns. We found alpha bungarotoxin expression was generally low-level, although in several instances there was distinct plaque formation on highly differentiated alpha-actinin positive myotubes (figure 3.13). To determine if common small molecule signaling molecules could be added to differentiation conditions to increase plaque formation we first added agrin and IGF-1 at 40mU and 25nM IGF-1, respectively, for seven days after previous seven days of differentiation. 2D cultures were again examined for AChR expression and myosin heavy chain (MHC), although it was difficult to determine a difference in immunofluorescence (figure 3.14).

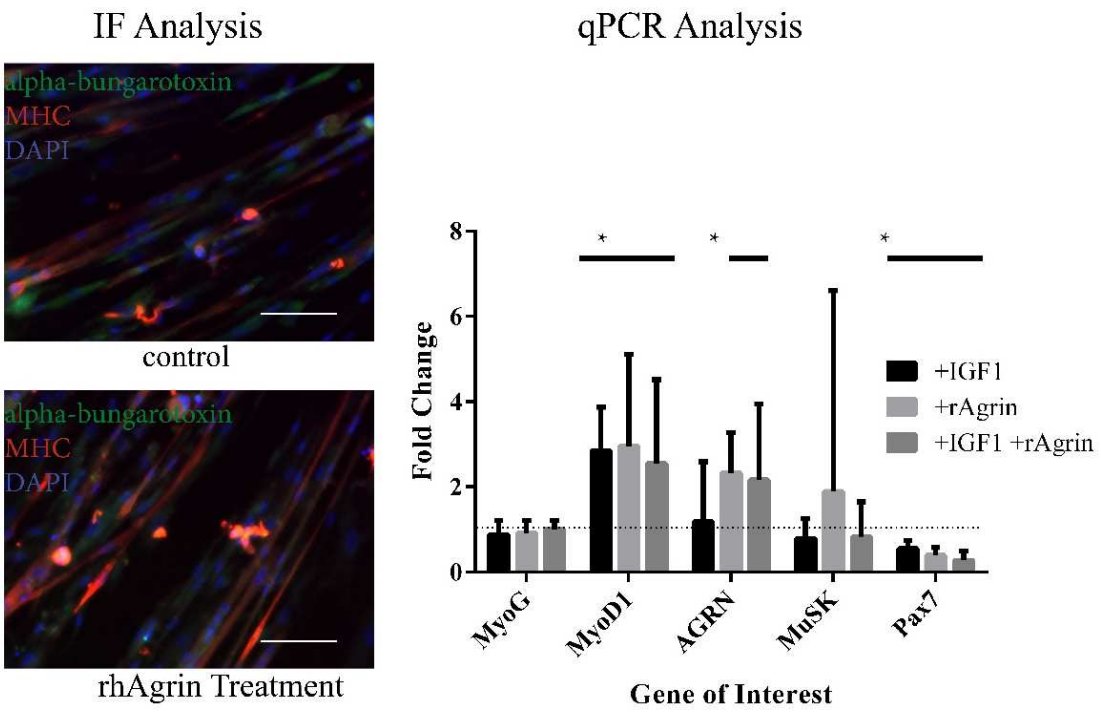

Figure 3.14: Myogenic Response of Difference Human Skeletal Myoblasts to rAgrin and IGF-1. (left) IF imaging of hSKMs plated in 2D silk/collagen gels with 1% silk fibroin with 2mg/mL collagen I treatment beginning day 7 and carrying on for 7 days of differentiation. Muscle differentiation related genes MYOG, MyoD, AGRN, MuSK, Pax7 quantified with qPCR at day 14, 7 days after beginning of 25nM IGF-1, 40mU rAgrin treatment. Significance of fold change with asterisk indicates $p<0.05$.

These human myoblasts cells were also assayed via qPCR for a panel of myogenic and differentiation markers specific to innervation including MyoD, myogenin, AGRN, Pax7 and MuSK. The transcription factors MyoD and MyoG are useful for determining the differentiation stage and cell cycle that the cells are fixed in at the time of staining. Initial results are suggestive that at MyoD is upregulated in treatment with 25nM IGF-1, 40mU rhAgrin (recombinant human agrin), or both in combination. Musk and agrn are both used in acetylcholine receptor clustering and AGRN showed an increased with +rAgrin treatment (figure 3.14). Pax7 is necessary for the transition out of quiescent satellite cells and thus a downregulation is unsurprising for the addition of commonly used muscle differentiation molecules.

3.3.3 Freeform Fabricated Silk Cantilevers for 3D Human Myoblast Suspension

There were difficulties in maintaining long-term cultures as constructs would not always adhere to hydrophobic PDMS, and the need for a customized PDMS plate had occasional sterility issues. To combat these issues, a system of submerged freeform silk cantilevers was used in a bath direct-write approach (figure 3.15) to build cantilevers capable of sustaining cell-laden hydrogels.

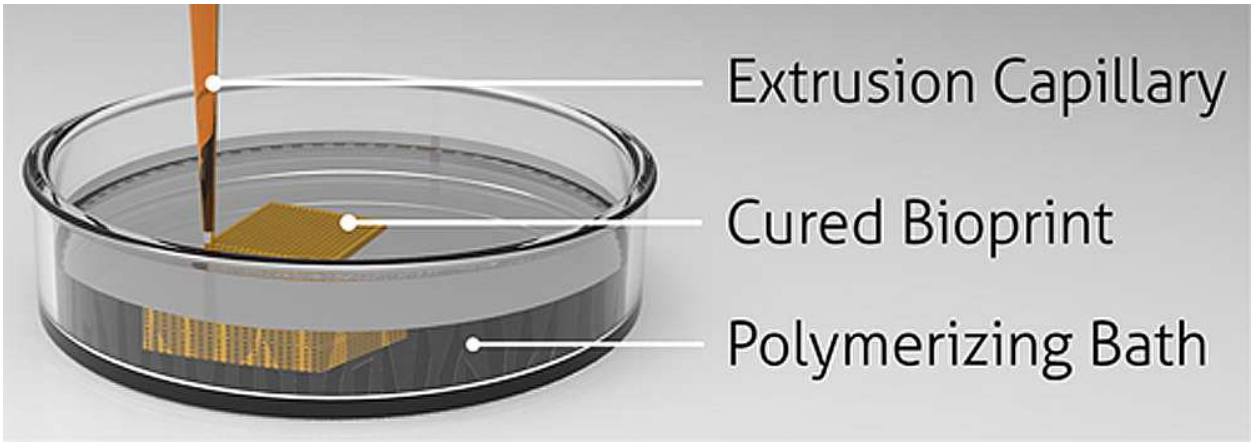

Figure 3.15: Submerged Additive Manufacturing Schematic of Freeform Silk Bioprinting. Schematic of a curable bioink being deposited into a bath of polymerizing solution using a direct-write approach. Reprinted with permission from Jose, Dixon, et al. 2016[107]. Copyright (2017) American Chemical Society.

We adjusted the previous flexible cantilever strategy due to difficulties maintaining longer term cultures, but retained much of the morphology and sizing of the cantilevers to allow for similar gel compaction as in the injectable sacrificial (or fugitive) gelatin cavity strategy. In the newly created system, hydrogels can be mixed and seeded around custom designed and 3D printed natural biomaterial cantilevers and then polymerized with thermal gelation at 37℃ to form 3D suspended constructs which compact and align cells progressively four days after seeding. We began the cantilever design ensuring that flexible polymeric cantilevers can be displaced with micronewton forces without unacceptable stress points (figure 3.16A). The cantilever was designed so that compacting gels would not slide off the flexible cantilevers but would rather be anchored by the T-shaped cantilever acting as a flexible cantilever (figure 3.16B). The cantilevers were printed using 35-45% silk fibroin solution (w/v) with 60-minute extraction time loaded into a 3mL Nordson syringe and connected to a CellInk Inkredible+ bioprinter via the pneumatic syringe holder. Nanoclay solution (2.5g Laponite XLG in 50/50 ratio of PEG, dH_2O) was filled in the wells of 6, 8, 12, or 24-well

plates and the plates were loaded into the bioprinter plate holder. Code generated from slic3r and Repetier Host, with G-code modified with custom Python scripts were sent to the bioprinter and the constructs were printed with 20-28G syringe tips. After the printing process was complete, prints were left in nanoclay solution for 12 hours for silk polymerization. Prints were subsequently washed with phosphate buffer solution (PBS) and left on a shaker plate overnight. Prior to cell seeding, printed cantilevers were incubated at room temperature with 0.1% Pluronic F127 for one hour to reduce gel adhesion to culture surface and then UV sterilized for 20 minutes (figure 3.16C). In pilot studies of primary human myoblasts seeded in silk/collagen gels at densities ranging from $1\text{-}3*10^6$ cells/mL with 50μL of solution per mm^2 of seeded culture surface, we applied differentiation media to constructs for up to two weeks to demonstrate alignment would occur in similar ways to the previous method using flexible cantilevers. Constructs were analyzed by IF and viewed in confocal microscopy with alpha-bungarotoxin staining, as well as 2D in fluorescence microscopy (figure 3.16D, E). Following pilot studies, differentiation protocols were used for the full four weeks, as had been demonstrated in previous aims to express localized alpha-bungarotoxin on multinucleated desmin-positive myotubes.

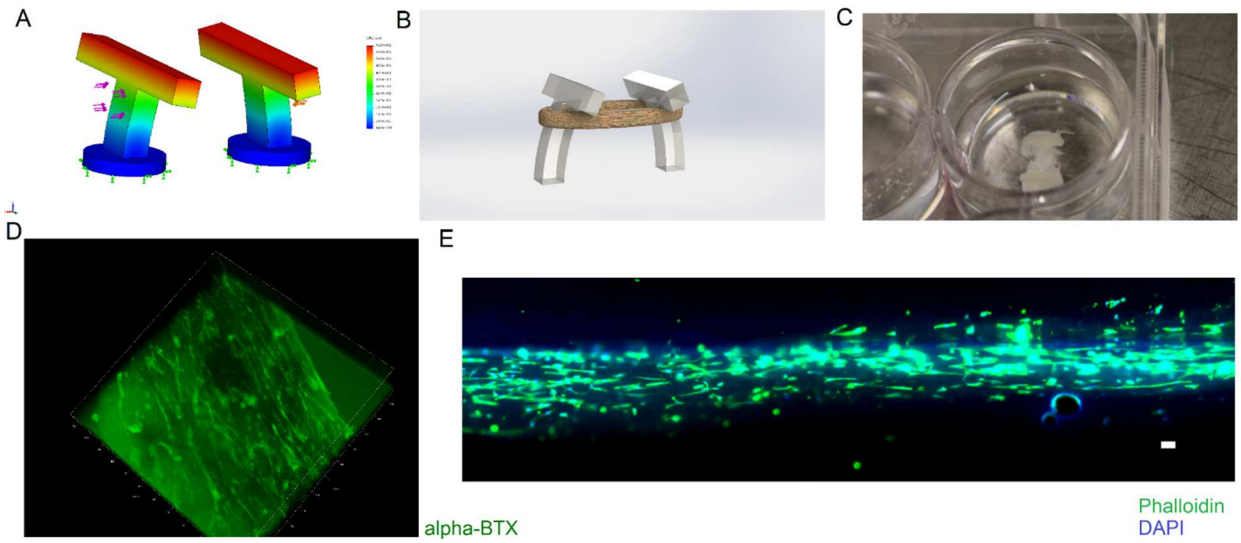

Figure 3.16: Modeling and *In Vitro* Analysis of Dynamically Loaded 3D Myoblast Cultures. A. Solidworks assembly (.sldasm) of conceptual cantilever displacement for maintaining a suspended myoblast-laden gel. Forces are modeled with arrows on individual cantilever to predict force dynamics and expected displacement B. KeyShot display depicting single cantilever pair with compacted myoblast laden gel. C. Printed cantilever pair in 24 well plate loaded with silk-collagen blend gel for myoblast encapsulation. D. Confocal Z stack of conjugated Alexa Flour 488 alpha-bungarotoxin depicting maturity of cell-hydrogel constructs. E. Human myoblasts grown in 3D suspended culture with representative phalloidin/DAPI staining of myoblasts day four post-seeding in suspended culture. Scale bars: 50µm

To validate the new system, it is necessary to show the cantilevers provide fixed cues for the myoblasts to align parallel to one another. This parallel alignment of myoblasts allows myotube fusion to move closer to recapitulating the parallel ordered architecture of native muscle [55]. At a cell density of $2*10^6$ hSKMs/mL, extending myoblasts were found to extend throughout parallel to the long axis of the gel, after four weeks in differentiation media. Using four separate samples from the same custom printed plate, a high degree of anisotropic elongation was determined using CellProfiler from the Broad Institute. A total of 2243 cells in four separate samples were distributed from -90° to 90° (absolute cell orientation) into 20° bins and each sample was individually analyzed for percentage of cells within 40° of the mode orientation, which was determined in each instance to be orientated along the long axis of the gel (figure 3.17A). Constructs also showed an improved density from previous experiments, as well as elongation throughout the gel covering over 3-5mm along the length of the construct, approximating the distance between the printed silk cantilevers (figure 3.17B). This technique also demonstrates the potential for multiplexed analysis of 3D culture in plastic wells which have been previously optimized for standard cell culture techniques, shown as four separate samples in an eight-well plate (figure 3.17C)

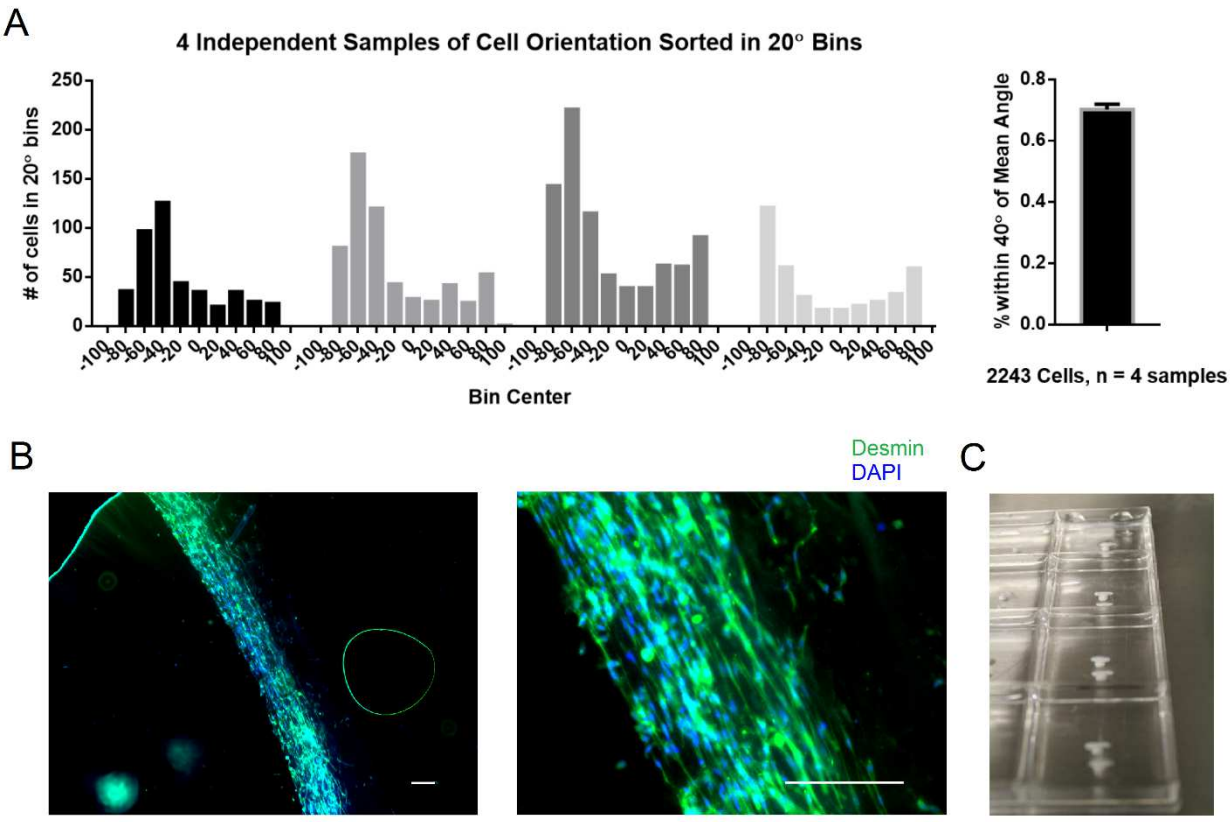

Figure 3.17: Cell growth and anisotropic elongation in engineered silk/collagen hydrogels. (A) Four individual histograms with profiled cell orientations from -90˚ to 90˚ in bin sizes encompassing 20˚ with the bin center depicted on the axis. The percentage of cells following within 40˚ of the mode orientation in each sample is shown as an average with n=4 (right). (B) IF of mounted myoblast-seeded gel differentiated four weeks shown at 4x (left), 20x (right) with desmin staining depicting cell orientation, and cell angles based on DAPI staining. Cell orientation workflow from CellProfiler (Broad Institute, Cambridge, MA). (C) Photograph of 4-wells with 3D printed silk cantilevers used in an 8-well plate to elongation and align myoblasts using static tension from compacting silk/collagen hydrogels. Scale bars 200μm.

Further fine-tuning of the 3D printing system, covering reproducibly and efficiency through adjustments in both hardware and software, as well as consultation with the lead designers of the bioprinter (Cellink, Gothenburg, Sweden) enables our lab to reliably provide an arbitrary morphology and sizing of the natural polymer cantilevers to allow for repeatable gel compaction, and the technique has been used in 6, 8, 12, and 24 well tissue culture plates (Figure 3.18).

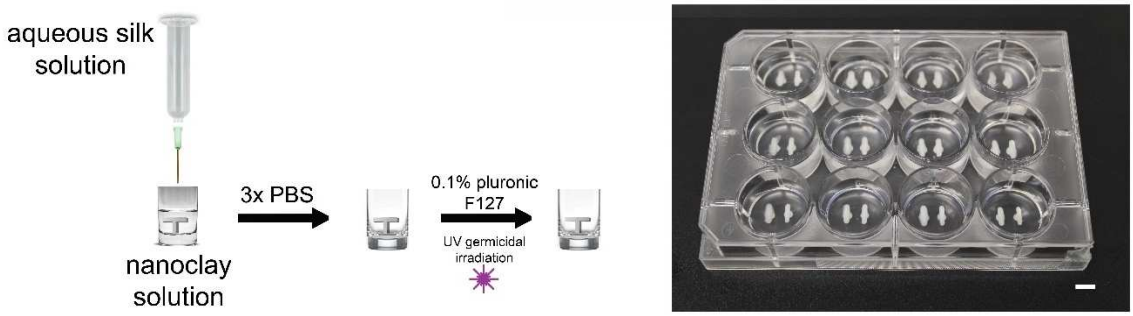

Figure 3.18: Freeform Fabrication of In-laid Silk Cantilevers in Tissue culture-ware. (left) 3D printing strategy for physically crosslinking aqueous silk into cantilever pair in tissue culture well with post-printing washing, and sterile preparation for cell seeding. (right) Photograph of 12 well plate with replicated cantilever pairs for medium throughput study. Scale bars: 6mm (bottom right)

As it yet unknown exactly what creates the theoretically reproducible alignment in human cell-based constructs, tensile stimulation by static strain was tested as the 3D tissues compacting in passive compaction around of T-shaped cantilevers are compared to seeded 3D hydrogels polymerized on the bottom of an empty well. In one group, hydrogels were seeded around 3D printed silk cantilevers, allowing the 3D suspended hydrogels to compact between the flexible cantilevers, whereas the other group gels compacted in the wells and formed condensed constructs. Both groups of engineered tissues were incubated in differentiation media and sacrificed at three points spanning three weeks and then stained with cytoskeletal markers to view alignment. Silk printing was performed in 12-well plates (figure 3.18).

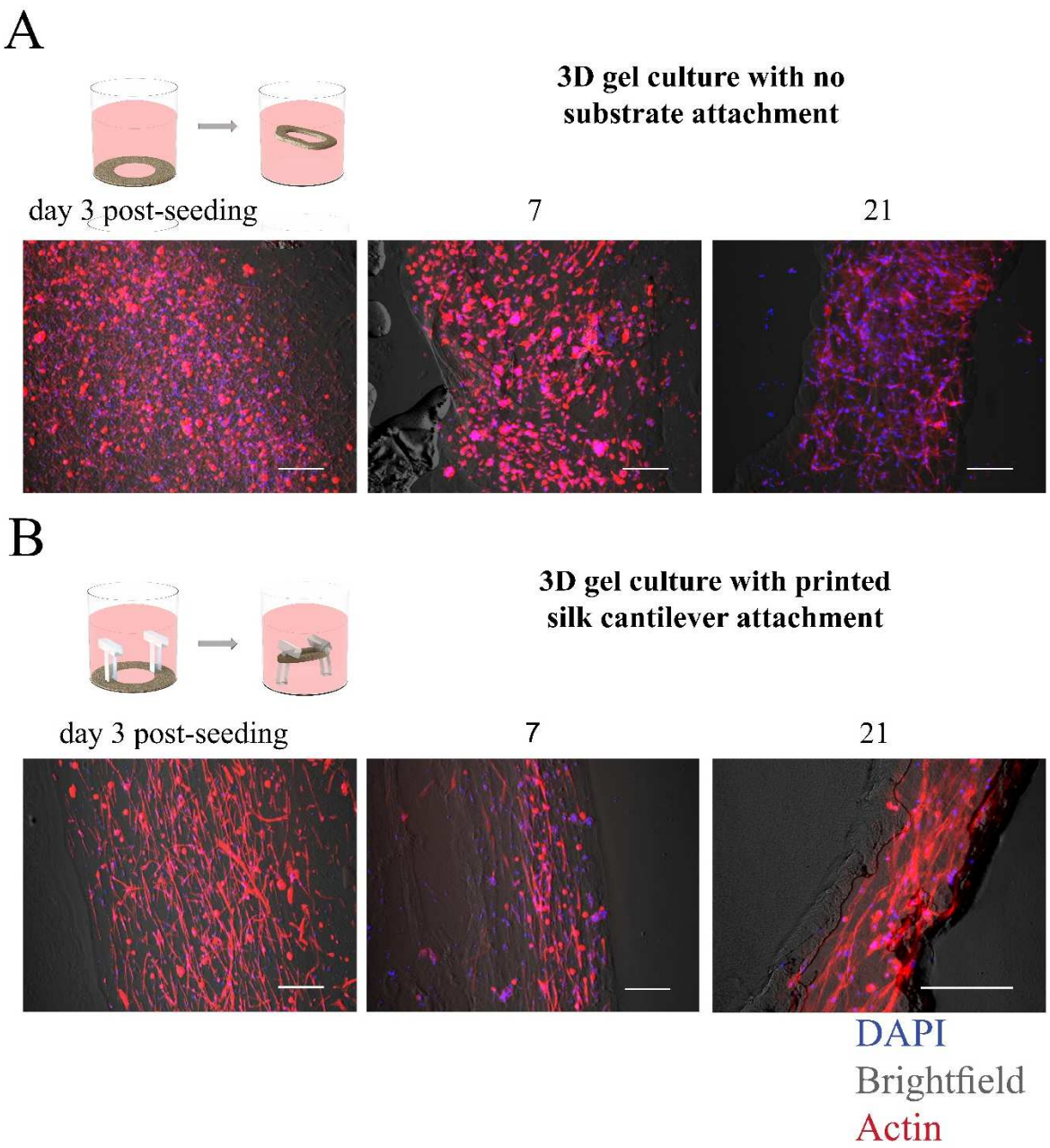

Figure 3.19: Cell growth and anisotropic elongation in engineered silk/collagen hydrogels with and without substrate attachment in culture plates (A) Representative IF of mounted myoblast-seeded gels differentiated at time points of three, seven, 14, and 21 days after seeding shown at 10x with phalloidin (actin) and DAPI staining. Hydrogel-seeded constructs in this series used standard 3D plated culture techniques with no substrate for gel compaction. (B) Representative IF of mounted myoblast-seeded gels differentiated at time points of three, seven, 14, and 21 days after seeding shown at 10x with phalloidin (actin) and DAPI staining. Hydrogel-seeded constructs in this series compacted around 3D printed cantilevers. Scale bars 200μm.

A total of 12,553 in cells in 24 separate samples were distributed from -90˚ to 90˚ into 20˚ bins and each sample was individually analyzed for the percentage of cells falling within 20˚ of the orientation along the long axis of the gel. Constructs were then stained with cytoskeletal and nuclear markers (figure 3.19) and were analyzed through CellProfiler (Broad Institute, Cambridge, MA) and GraphPad Prism 6 (Graphpad, CA, USA).

Cells were first scored and outlined by colocalization of cytoskeletal staining with identified nuclei and then analyzed for orientation from -90˚ to -90˚ with respect to the long gel axis. Cells were analyzed for frequency distribution in Prism with an n=3 for each condition at each timepoint. In the printed group at least 60% of cells had an orientation angle within 20º of the tension axis of the tissue through 21 days post-seeding, significantly higher than unattached controls without printed substrates at all timepoints (figure 3.20).

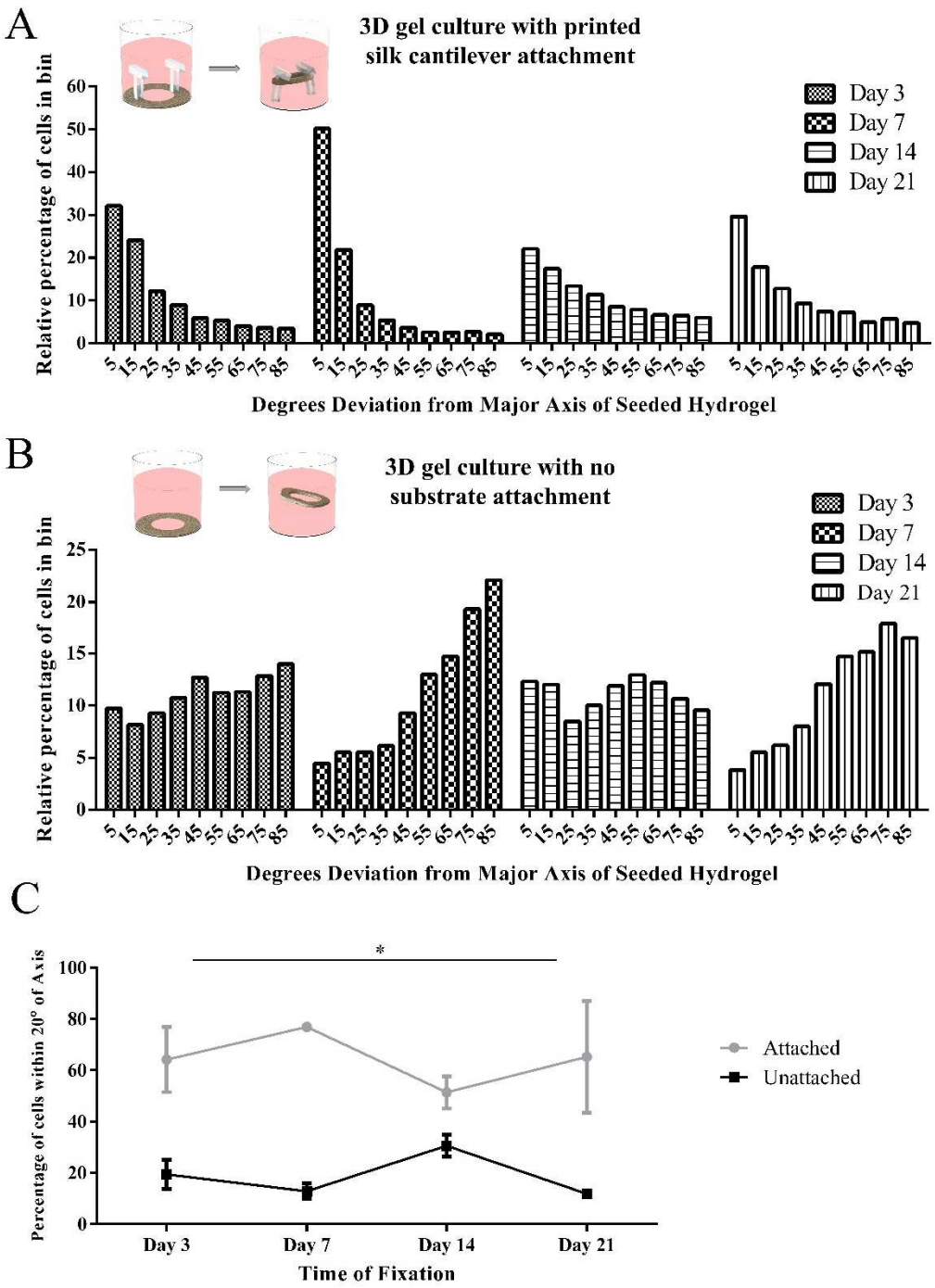

Figure 3.20: Quantification of anisotropic elongation in engineered silk/collagen hydrogels. (A) Four individual histograms with relative cell orientation to long axis of printed substrate attached 3D hydrogel in 10° at four sacrificial time points. Each time point had n=3 independent samples with the following combined binned cell count: 3048 cells (day 3), 1252 cells (day 7), 998 cells (day 14), 522 cells (day 21). The Y axis indicates the percentage of cells falling into bins with corresponding bin center ticked on x axis. (B) Four individual histograms with relative cell orientation to long axis of 3D hydrogel without printed substrate ('unattached') in 10° bins at four time points. Each time point had

n=3 independent samples with the following combined binned cell count: 3006 cells (day 3), 1304 cells (day 7), 649 cells (day 14), 1774 cells (day 21). As above, Y axis indicates percentage of cells falling into bin with corresponding bin center ticked on x axis. Sample were sacrificed in both groups from cells batch seeded in the same passage. (C) Row statistics of percentage of total binned cells falling within 20° of long gel axis with 'attached' samples from (A) shown in red, with 'unattached' samples from (B) shown in blue. Statistical significance at all time points determined using the Holm-Sidak method, with alpha=5.000%.

The initial strategy for designing a 3D coculture of human myoblasts and neurons began as a scaffold was designed with addition of conduits for mechanical stretch, media flow, or external scaffold addition. Silk biomaterial tubes and hydrogels provide excellent biocompatible candidates for neural tissue engineering and axon fasciculation[105,112], thus the plan was to combine silk scaffolds with nerve guidance conduits derived from bovine tendons, which have been shown to have potential use for nerve regeneration. We would use these established substrates for neuron growth in a co-construct with the developed human myoblasts scaffolds to form co-cultures of human cells in a reproducible 3D NMJ model. Initial trials of this technique led to anisotropically oriented cells, thus gel based systems were sought, as they had previously been shown to align C2C12 cells.

After culturing static 3D gels and bioprinted and bioplotted C2C12 cells to test for alignment, we used fluorescent stains to enable microscopy of cell-laden constructs as a means to compare cell morphology seen in brightfield microscopy. The most successful means of patterning and reproducibly aligning cells was forming combinations of collagen I/matrigel and silk in empty cavities formed from removal of steel pins set in chilled gelatin. The 24-well plate format of growing the sacrificial channel was shown to align cells, and only suffered from stability of gels in longer term culture.

Human skeletal muscle myoblasts were shown to align in sacrificial gelatin-derived channels, and myoblasts were shown to properly express differentiation markers. Human myoblasts were assayed via qPCR for expression of myogenic and differentiation markers specific to innervation including MyoD, myogenin, AGRN, Pax7 and MuSK. Myoblasts with treatment of rAgrin and IGF-1 had upregulation of MyoD, and downregulation of the queiescent marker Pax7, as expected with movement down the terminal myogenic differentiation lineage. Myoblasts also showed expression of AChRs through long term differentiation.

To overcome issues with the sacrificial gelatin system, hydrogels were seeded around 3D printed silk cantilevers, allowing the 3D suspended hydrogels to compact between the flexible cantilevers, which enable constructs to be analyzed for differentiation and innervation in later studies. Engineered tissues were incubated in culture media anywhere from 24 hours to four weeks and stained for specific myogenic markers via immunofluorescence and analyzed with customizable software. A high degree of anisotropic elongation was determined using CellProfiler from the Broad Institute from myoblast gels seeded using this method, and gels around printed cantilevers, were compared to gels with no in well substrate. Overall, these results suggest that modern patterning and additive manufacturing techniques can be applied to human myoblast culture in 3D, and such techniques may be useful for subsequent innervation with human motoneuron-like cells.

3.4 Neuron-Muscle Coculture Towards 3D Human NMJ Model

The principle behind combining motoneuron-like cells with human constructs is inspired by embryonic development as ventral nerve roots extend processes into developing myotomes, as well as by a number of like-minded works (using animal-derived cells), most of which seek to introduce neurons with extending processes into muscle cell-seeded constructs, which have already begun the process of differentiation in myotubes [76,86,89]. In this section, we expand on 3D muscle cultures developed in the prior section by controlled introduction of motoneuron-like cells in environments which allow propagation of neurite extensions as well as synaptic connection with differentiation muscle systems.

In early work to generate cholinergic motoneuron-like cells which could be cocultured with C2C12 model systems and human myoblasts, NG 108-15 cells were used as surrogates for motoneurons in coculture as they have a cholinergic phenotype, they are known to induce acetylcholine aggregates in coculture, and they have been established in models of neuromuscular toxicity [113,114]. NG 108-15 cells are differentiated in DMEM with 1X sodium hypoxanthine, aminopterin and thymidine (HAT), and HS [115], or Neurobasal media, HAT and serum free B27 supplement [113]. Differentiation towards motorneuron-like cell lineage can be achieved with a combination of 5 μM retinoic acid, and 2.5 μM purmorphamine (agonist of sonic hedgehog, shh). After differentiation for four days in culture, early evidence of neurite outbranching is evident, with spiny branches visible at higher magnification through fluorescence staining (figure 3.21A). Other methods to examine NG108-15 cell growth were also explored, from standard brightfield microscopy (figure 3.21B) to sputter coating and viewing in SEM (figure 3.21C). SEM techniques were explored as several SEM studies have been used to explore

the ultrastructure of the NMJ and determine the nature of extending neural contacts, as well as specific morphology of postjunctional folds [116,117]. Using SEM we could determine extension of processes of differentiating NG108-15 cells, although it is likely sputter coating and dehydrating processes lead to artifacts and other difficulties in viewing, thus IF and confocal techniques were used in further analyses.

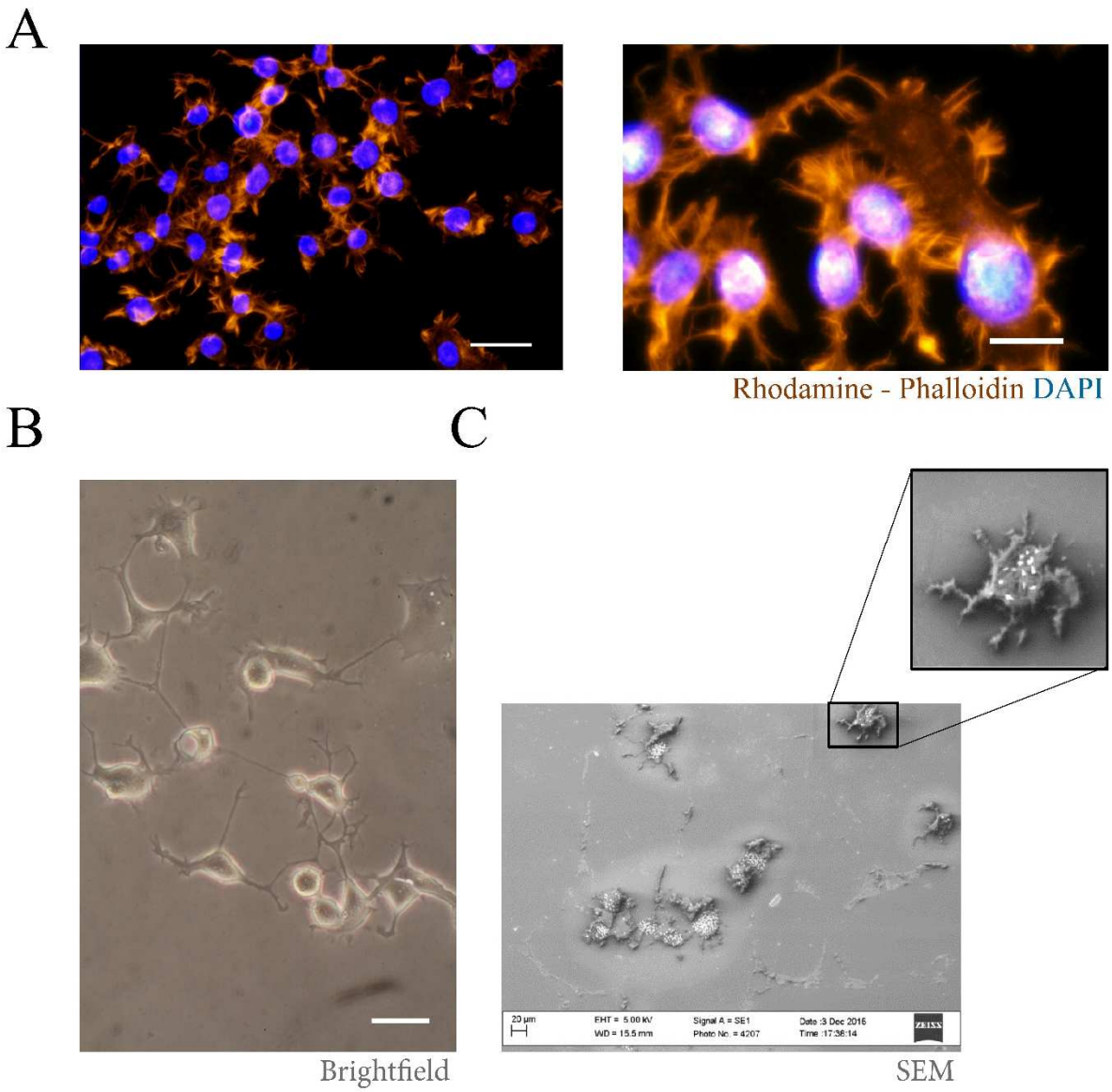

Figure 3.21: Visualization of NG108-15 Neural Outgrowth. (A) NG108-15 cells differentiation in Neurobasal media with serum free B27 supplement after four days visualized through actin staining (Rhodamine-Phalloidin : gold/red), and nuclear (DAPI) staining. Scale Bar 30µm (left), 15 µm right). (B) NG108-15 cells seeded on tissue culture plastic and viewed through brightfield, scale bar 15 µm. (C) Sputter-coated NG108-15 cells viewed through SEM. Scale bar (bottom left: 20 µm)

3.4.1 NG108-15 Coculture with Myoblasts

After demonstration of NG108-15 growth and neurite extension in 2D culture, NG108-15 cells were differentiated for 4 days and added to preformed C2C12 myotubes (cultured in differentiation conditions for seven days prior) to look for evidence of myotube maturation in the presence of NG108-15, and possible early NMJ formation through co-localization of cytoskeletal proteins. Using phalloidin stains for actin, visualized NG108-15 cells retained their spiny morphology and were seen to contact myotubes and show bright actin staining at points of contact (figure 3.22A). For further visualizations, NG108-15 cells identified through phase-contrast round and spiny morphology in brightfield, and staining for AChRs was performed through conjugated alpha-bungarotoxin, which demonstrated brightness and putative contact points on myotubes with rounded, spiny cells, suggested to be neurons. In these experiments NG108-15 cells were not exposed to cell tracking dyes and thus relied upon differences in cell morphology. This led to difficulty determining contact points, and was thus an imperfect method which was built upon by examination of cell-specific fluorescent staining in later experiments.

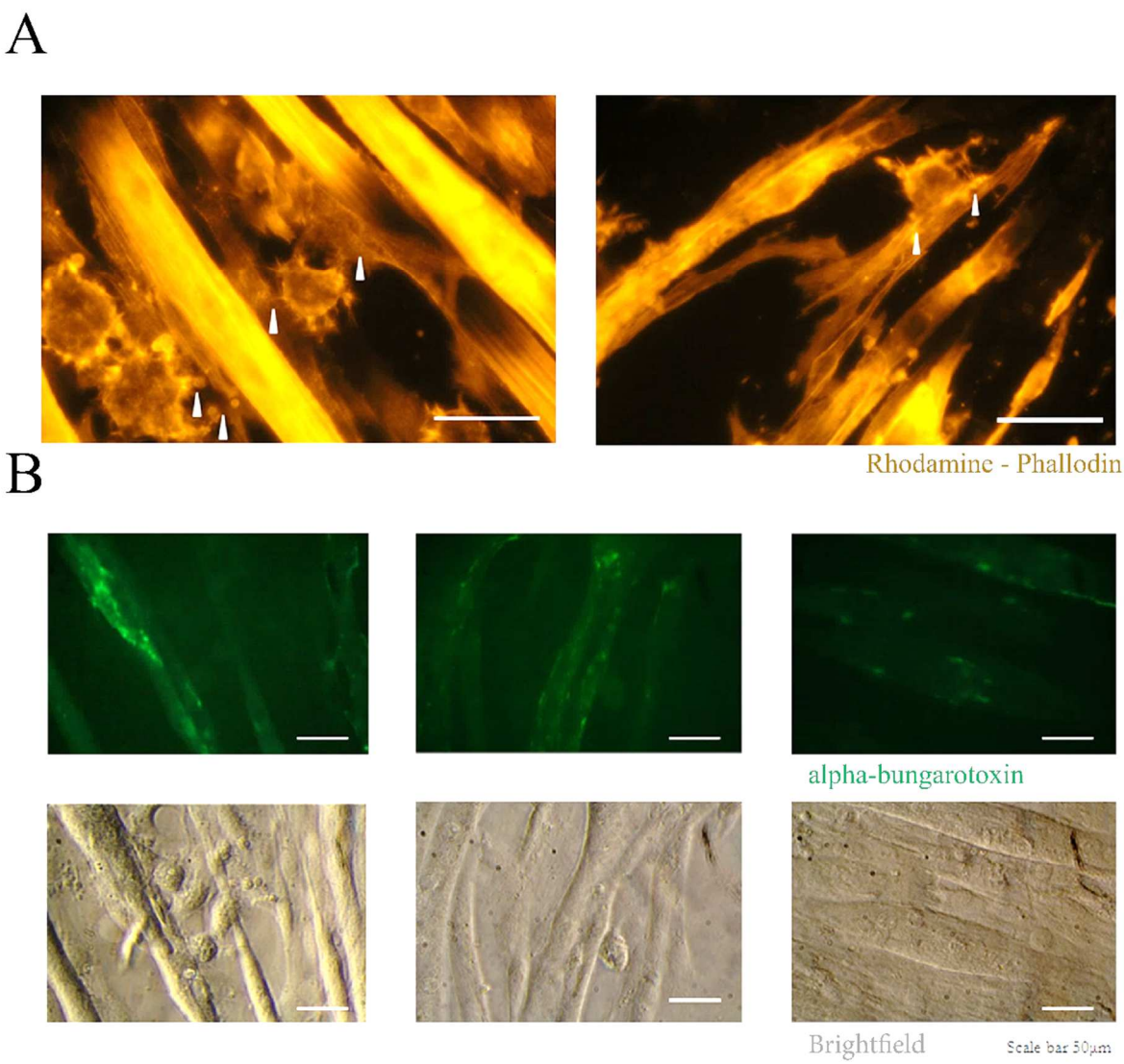

Figure 3.22: Visualization of Putative NG108-15 Outgrowth and Contact with Formed Myotubes. NG108-15 cells differentiation in Neurobasal media with serum free B27 supplement after four days, were added to C2C12 myotubes in 2D after one week of differentiation and visualized after three additional days in coculture. (A) NG108-15 cells identified via their rounded morphology were visualized with contact on C2C12 myotubes through non-cell specific actin staining. Scale bar 50µm (B) Contact of NG108 through C2C12 myotubes also visualized through brightfield and fluorescence through alpha-bungarotoxin seeding with three representative samples in both brightfield and FITC fluorescence. Scale bar 50µm.

The phallodin and alpha-bungarotoxin stain proved to be a useful cytoskeletal visualization method to determine neuronal/myocyte contact points and acetylcholine receptor clustering in 2D as there was an aberrance or highlighted point of the myotube actin skeleton where the neurite from the NG-108 cell contacts (figure 3.22A), and early results suggested contact with spiny cells elicited clustering of AChRs on myotubes (figure 3.22B). However, at this stage it is difficult to decouple the effect of NG108-15 addition with AChR clustering in live imaging, thus there is still a need to increase visualization and quantifiability of neuromuscular junctions in culture. To test further for viability of NG108-15 coculture, demonstration of viable growth in 3D culture similar to what the cells will experience when cocultured with differentiating myoblasts is sought.

3.4.2 NG108-15 Growth in Engineered Silk Collagen Hydrogels

This aim also pursues evidence for motorneuron-like cell survival in engineered 3D hydrogels, as in a manner similar to 3D culture of myoblasts, fibrous 3D structures are thought to better resemble the physiological microenvironment of motoneurons than coated tissue culture plastic [118]. Lastly, initial co-culture in 2D is an important sub-aim to showing plausibly of providing a culture environment and media where these two cells types can be viable and healthy while in contact with each other, given the different media requirements than in monoculture.

To move towards controlled culture of motorneuron-like cells and myotubes in silk-collagen hydrogels, the sacrificial channel technique which first showed elongation of C2C12 myoblasts as a proof of concept (figure 3.11) was used to encapsulate NG108-15

motorneuron-like cells, to show the system could be expanded to multiple cell types and potentially be used to contact orthogonally oriented cell-specific seeded suspended gels.

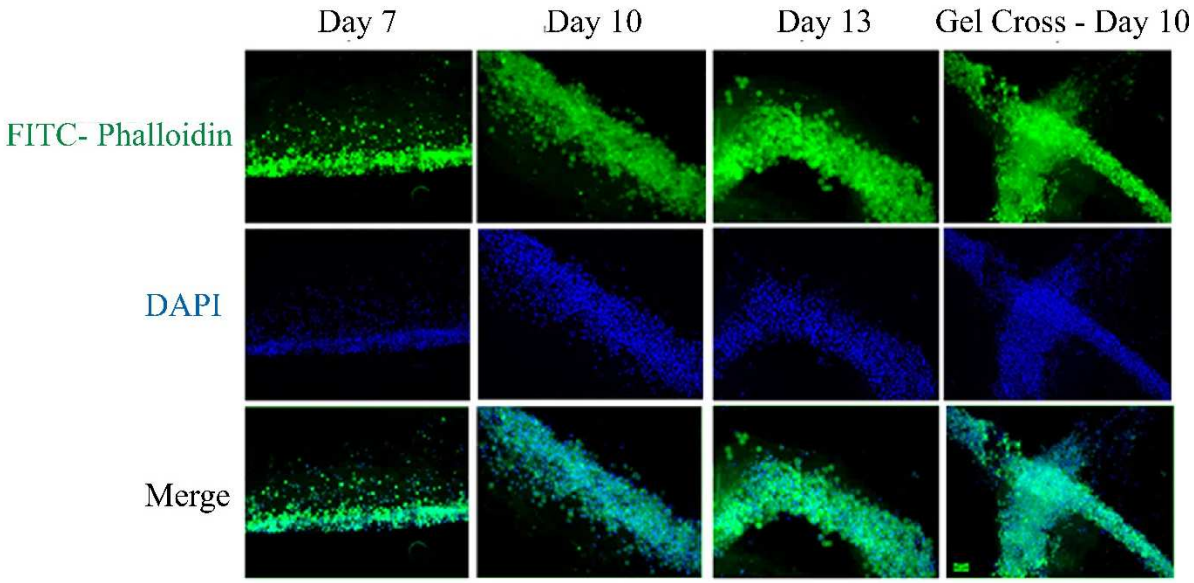

Figure 3.23: NG 108-15 Cells Suspended in Gel Crosses Through Gelation in Sacrificial Channels. NG108-15 cells were seeded at $5*10^5$cells/mL hydrogel, using the sacrificial channel method, and fixed at various timepoints to visualize neural outgrowth in silk-collagen hydrogels. Constructs were stained for FITC-phallodin and then mounted on slides and imaged through fluorescence. Scale bar 50µm (green, bottom right).

After growth in neural differentiation media for two weeks and fixed at segregated timepoints, NG108-15 cells were found to have a high degree of cell body expansion through dense DAPI (nuclei) staining and cytoskeletal staining, however, little neurite extension through the 3D construct was seen upon imaging with fluorescence, which was not immediately clear whether due to growth conditions or microscopy techniques (figure 3.23).

As it is likely necessary for neuronal cells to undergo further differentiation with neurite outgrowth inside the gel, another way to view 3D encapsulation of NG 108-15 cells with potentially better visualization was sought. We used the bioprinting approach,

as constructs can be visualized *in situ*, similar to those used with C2C12 cells (figure 3.9). This approach was first used to pattern both myoblasts and motoneuron cell lines independently, and then began initial trials patterning two cell types in separate bioinks individually.

3.4.3 Bioprinting Systems for Patterning and Coculturing NMJ Model Cell Lines

In first experiments towards cocultured bioprinting, C2C12 myoblasts were printed as discussed earlier and carried out with differentiation conditions for 14 days, at which point they were stained with alpha-bungarotoxin to look for evidence of acetylcholine clustering, which indicates the potential for coculture with motorneuron-like cell lines [115]. C2C12 myotubes appeared to have overall low level alpha bungarotoxin staining, with evidence of clustering of acetylcholine receptor in foci indicating immature neuromuscular junctions in the absence of coculture (figure 3.24a). NG108-15 cells were grown in bioprinted culture with well-defined lines in similar techniques (Figure 3.24b). Lastly, cocultured cells have been printed although the technique although due to technical difficulties in simultaneous polymerization and patterning of the bioinks, the cells were found to have spread past their margin of printing (figure 3.24). Cocultures were stained with FITC-phalloidin, which stains actin in both neuronal and muscle cells, however is useful as fused myotubes and differentiating neuronal precursors have distinct, non-overlapping morphologies, and can be distinguished (though not definitively) via fluorescence microscopy through differences in contrast and morphology. Myotubes generally have long parallel-aligned actin fibers, whereas neuronal cells are roughly spherical with short to medium spindly processes,

which look a little bit like sea urchins. While the prints do not show precise morphology, they have proved useful in determining co-culture media which is compatible with both cell types. Inability to fully segregate the extending NG108-15 cells and developing myocytes in this context led to using of other cell segregation techniques, as discussed in further sections.

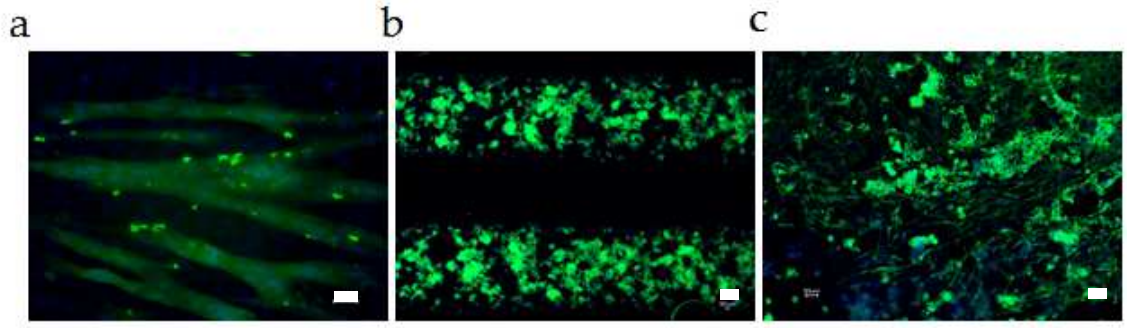

Figure 3.24: Mono and Coculture of Bioprinted C2C12 and NG108-15 Model Neuromuscular Junction Cells types. (a) Alexa 555 conjugated α-bungarotoxin was added to C2C12 myotubes after 14 days in differentiation media. Scale bar 50 μm. (b) NG108-15 cells were seeded at $5*10^5$cells/mL hydrogel and stained with FITC-phallodin at day 8 post printing. Scale bar 50 μm. (c) FITC-phalloidin stain of C2C12 cells and NG-108 cells at day 8 post printing. Scale bar 50 μm.

3.4.4 2.5D Cultures Systems for Examining Specific Interactions Between Differentiating Myoblasts and Motoneuron-like Cells

One method explored for investigating the vitality of neuron/muscle co-cultures with controllable interactions between cell types uses silk films, which have provided a means to grow a large number of cell types, and more recently work (with Lorenzo Tozzi, postdoctoral associate) has focused on using films as coculture devices, whereby different cell types may be seeded and grown on opposing faces of the film. This transwell system can be considered a 2.5D system, as microfluidic gel-embedded cell methods are sometimes referred to 3D culture [74], but often are referred to as 2.5D culture,

where cells are seeded on or into a thin layer of other extracellular matrix [119], or other fabricated multilayered thin channels [120].

Using this silk film transwell system there is the potential to vary pore sizes in the film allowing a balance between migration of cell components and media exchange between the lower and upper faces. Higher pore sizes (up to 10um) will theoretically allow larger cell extensions and cell bodies to migrate while allowing more media exchange, and smaller pore sizes have less fluid exchange allowing for segregation of media components but have more restricted cell passage [121].

NG108-15 cells were first shown to be successfully cocultured with hSKMs in plated gel culture with thin silk-collagen gels cast in well plates (Figure 3.25A), with hSKMs differentiated 12 days prior to 4 days of coculture. The next step was to see if the NG108-15 could extend processes through the silk film allow direct visualization of neuronal processes with myoblast cell layers. Silk films were first seeded inverted with myoblasts, and then NG108-15 cells were added in the well on top of the silk film.

Silk films with 10μm pores showed growth of human myoblasts in a gel layer, but had limited evidence of neural growth, possibly due to washing off in IF preparation, as neurons were seen previously via brightfield microscopy. Further experiments focused on using cell tracking dyes to visualize movement of two cell types in the few days following seeding. These cell tracking experiments showed that there was healthy human myoblast growth in the 3D layer. However, when the films were visualized for cell specificity with whole-mount staining, it appeared that the NG108 motorneuron-like cells had out-competed the myoblasts and spread throughout the gel. On closer examination of the stained films, it appears that the motorneurons are in fact occupying the pore spaces

in the film and moreover in a semi regular square array (figure 3.25B). This result has led me to shift my focus to potentially employing silk films as means to provide regularly spaced motorneurons for addition to a myoblast seeded scaffold for innervation in 3D.

The next step to complete the aim of a controllable means of culture of motoneuron-like cells with differentiating myoblasts was to transition to an all human cell model. Differentiated human induced neural stem cells are known to show terminal neuronal differentiation and not expand in culture (expansion is present in NG108-15 cell lines). These coculture studies began using human induced neural stem cells (hiNSCs) induced from reprogramming factors OCT4, KLF4, SOX2, and cMYC in a polycistronic lentivirus [98]. These hiNSCs produce Tuj1 positive neurites upon expansion and differentiation and are NCAM, ChAT and β-III tubulin positive after 14 days of differentiation with 1μM purmorphamine on both poly-D-lysine and collagen I coated culture-ware (figure 3.26).

After the differentiation conditions were established; human myoblast cultures were mixed with hiNSCs in gels with culture media reflective of myoblast growth with the addition of purmorphamine. Many media types were not conducive to positive growth and extension of both cell types, however it was found that high glucose DMEM with first 10% fetal bovine serum for 6 days followed by differentiation with 2% horse serum, and 1μm purmorphamine during growth and differentiation, produced Tuj1 positive extending neurites comingled with desmin-positive myoblasts after 12 days growth and 4 days differentiation. After 12 days differentiation, the ratio of hiNSCs/human myoblasts increased, possibly due to myoblast senescence in longer term culture (figure 3.25C). This plated 3D co-cultured gel provides a starting place for additional controlled dynamic

3D cultures and allows differentiation conditions is used to adapt to 3D suspended gels, as well as printed and culture chip protocols.

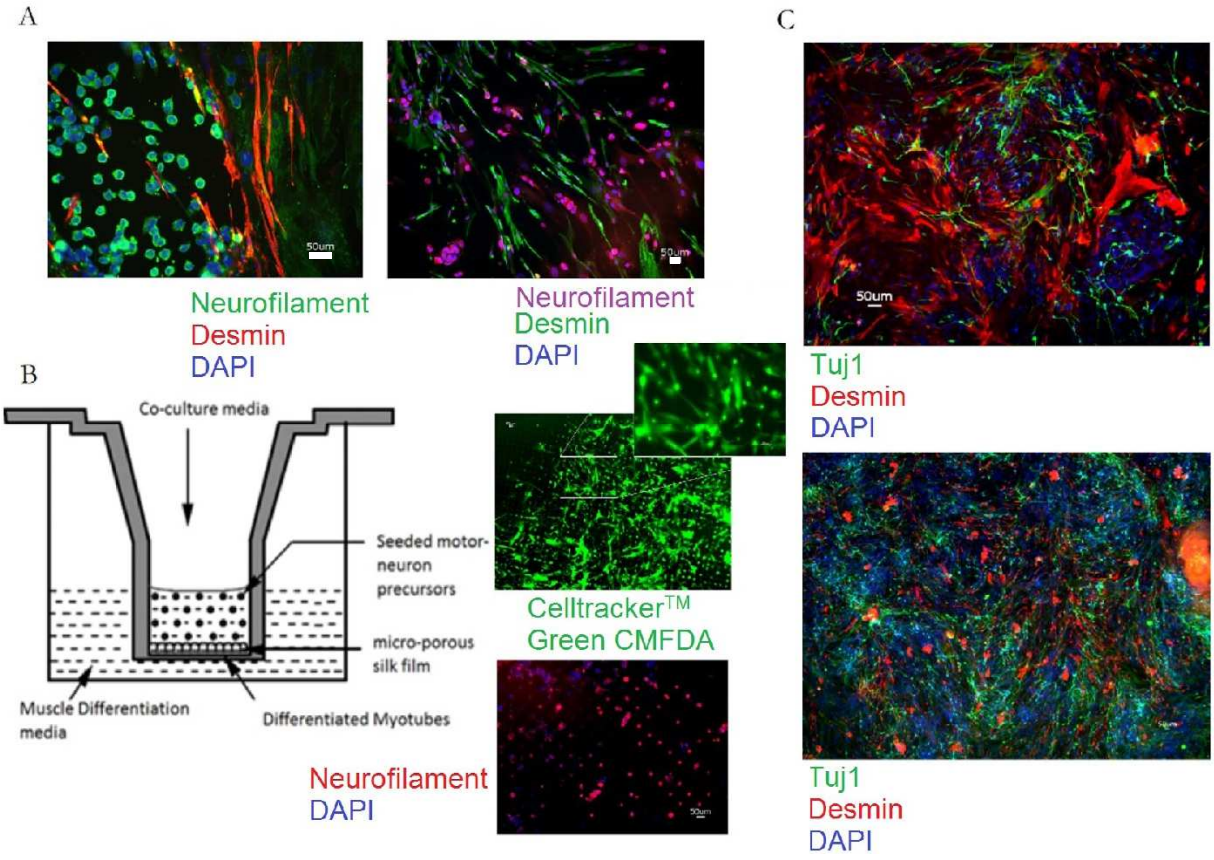

Figure 3.25: Plated Cocultures in 3D Gels and 2.5D Coculture in Silk Films. (A) IF images of NG108 cells and human myoblasts grown in silk/collagen blends for 12 days of growth and 4 days of differentiation. Image on right shows optimized trial with cell ratios adjusted and motorneuron agonist factors added. (B) (left) Schematic of NG108 and human skeletal muscle cell culture on opposite sides of micro-porous silk film. (top right) Human myoblasts stained with green cell tracking dye showed spread of myoblasts on surface of silk film. (bottom right) Neural cells stained with neurofilament (red) and nuclear stain (DAPI, blue) showed potential presence of cell bodies in arrays of pores present on the silk films. (C) 3D co-plated gels optimized for human coculture, grown for 12 days in growth media and 4 days in differentiation media (top), and 12 days in differentiation media (bottom). Neurons stained green for Tuj1 (beta-III tubulin) and differentiating myoblasts stained red for desmin, nuclear stain blue (DAPI). Scales bars 50μm

The primary coculture strategy has been to combine hiNSCs and hSKMs in silk-collagen hydrogels and inject into sacrificial channels in the same method as with hSKM only gels, followed by differentiation in media identical to 3D plated culture. After 14 days in culture in heterogenous cell-laden gels, TUJ1 positive hiNSCs were found comingled with desmin and alpha-bungarotoxin positive hSKMs, however, there was limited spatial segregation of cell types, and both cell types showed sub-optimal differentiation (figure 3.27A). In IF analysis of the patterned heterogenous cell-laden gels, NF positive hiNSC-derived motorneuron-like cells were found comingled with desmin and alpha-bungarotoxin positive hSKMs. At higher resolution, however, staining for alpha-bungarotoxin proved to be inconclusive and thus was not included in imaging results.

To examine the effect of having the cocultured cells contacting within the same fluidic environment, we used a commercial chip-based coculture platform, where the neuronal cell and myoblast-laden hydrogels could interact through pores of 100 microns, allowing extensions of cell processes, but not cell bodies, to contact the adjacent cell compartment.

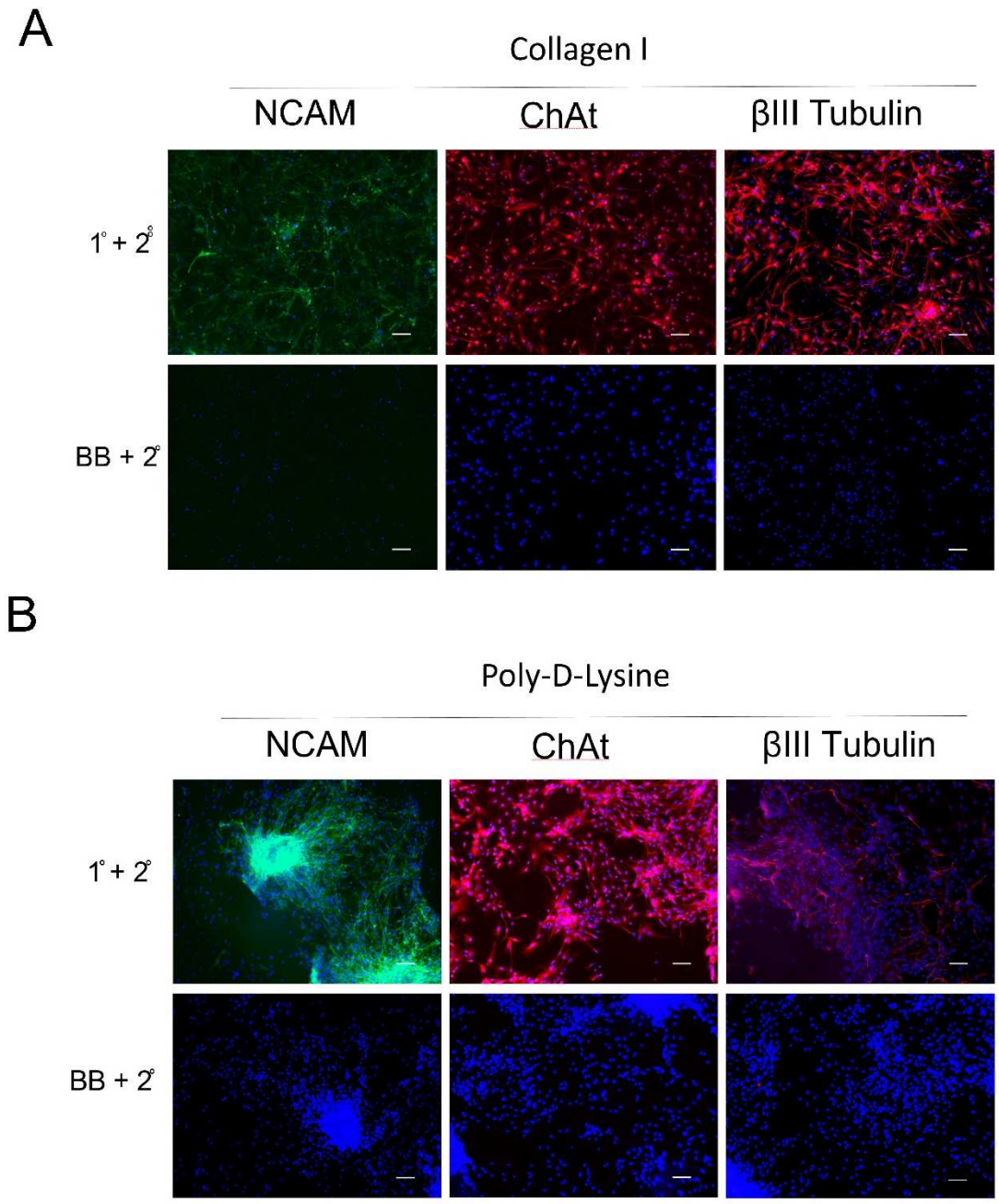

Figure 3.26: 2D Differentiation of Motorneuron-like Cells for Coculture with Human Myoblasts. IF images of hiNSCs grown on collagen I (Col I) and Poly-D-Lysine (PDL) after 14 days of differentiation. Cells are stained for NCAM, ChAT and βIII tubulin (Tuj1 antibody). Top row shows primary and secondary antibodies and the bottom row shows cells incubated with blocking buffer (BB) and secondary antibody. Bottom row included to detect for non-specific staining due to potentially low signal expression from neural markers. Microscopic field is approximately 0.7mm^2 in area. Scales bars 100µm.

To investigate the culture conditions affecting controlled migration of motorneuron-like cells to differentiated 3D myoblast cultures a 2.5D coculture chip with two cell culture channels and one middle gel channel was used which would allow extending neurites to be visualized live in real-time. This system serves two purposes: the first is to control for the effect of 3D substrate suspension as the gels used are identical to those used in suspended 3D culture, and the second is to have a platform to visualize the movement of motoneuron-like cells across the barrier (which is the same gel composition as the 3D suspended gels) in real time. The coculture chip works with a central channel that can be loaded with hydrogel; and leaves two peripheral channels which can be coated with extracellular matrix and then seeded with individual cells types. Over time, depending on the stiffness and compaction of the interior gel, proliferative cells will migrate across the interior central region and contact the opposing cell channel through regularly spaced openings in a manner similar to the silk film above. In the commercial chip-based coculture platform, neuronal cell and myoblast-laden hydrogels are theorized to interact through pores of 100 microns, allowing extensions of cell processes through the interior gel compartment, but not cell bodies, to contact the adjacent cell compartment.

To investigate the interactions of human myoblasts and neural cells using the cell culture chip from AIM biotech [122], the central region was loaded with a silk-collagen hydrogel analogous to those used in 3D suspended culture and then plated hSKMs on one flank, followed one day later by seeding of hiNSCs. The chip can be observed during live culture by brightfield microscopy and then can be stained by IF to detect cell specificity and morphology. Despite some technical difficulties with staining, myoblasts were found

to have extended throughout their individual channels, and hiNSCs spread throughout the center channel dependent on silk concentration. Neurite extensions were found to have entered the myoblast channel and co-localized on desmin-positive myoblasts (figure 3.27B).

Human myoblast cultures were first loaded into one side of the media chamber in the 3D chip culture with 10μL of $1*10^6$ cells/mL per chamber and differentiated for 14 days after 3 days in growth media. Myoblasts were showed to differentiate into desmin-positive multinucleated myotubes which elongated along the long axis of the chip culture with a high degree of anisotropy. These cells were found to expand along the course of the 10.5mm channel, although there remained little evidence of alpha-bungarotoxin localized staining. At this point after 17 days total in culture, hiNSC-derived motorneuron-like cells were added at $1*10^5$ cells/mL in 10μL/chamber and incubated in a spatially segregated manner with purmorphamine-containing serum-free media. phenol-red free DMEM with 1% horse serum on the myoblast side and serum-free B27/N2 on the opposing channel, produced NF-positive extending neurites comingling with desmin-positive myoblasts after 14 days of co-culture differentiation.

In these chip samples, colocalization and connection of extending processes from motorneuron-like cells could be observed in phase contrast microscopy, although cell specificity could only be suggested from differential contrast and morphology noted from previous viewing of motorneuron-like cells. Upon IF imaging processes of motorneuron-like cells were confirmed to cross into cell chambers occupied by differentiated myotubes (figure 3.27B), although further analysis is needed to confirm that the phenotype of the motorneuron-like cell in this context, as it is possible the serum found in the human

myoblast differentiation media could transition the hiNSC-derived cells to a more glial phenotype.

Using this technique of loading human myoblasts and human induced neural stem cell-derived motorneuron-like cells in chip culture allows one to follow the health and extension of cultures in real-time with brightfield or phase contrast microscopy, providing a reasonable proxy for evaluating gels before downstream transition to more complex 3D cultures. Overall the chip-based 2.5D co-cultured gel provides a starting place for additional controlled dynamic 3D cultures and allows determination of differentiation conditions which will be adapted to 3D suspended co-cultured gels.

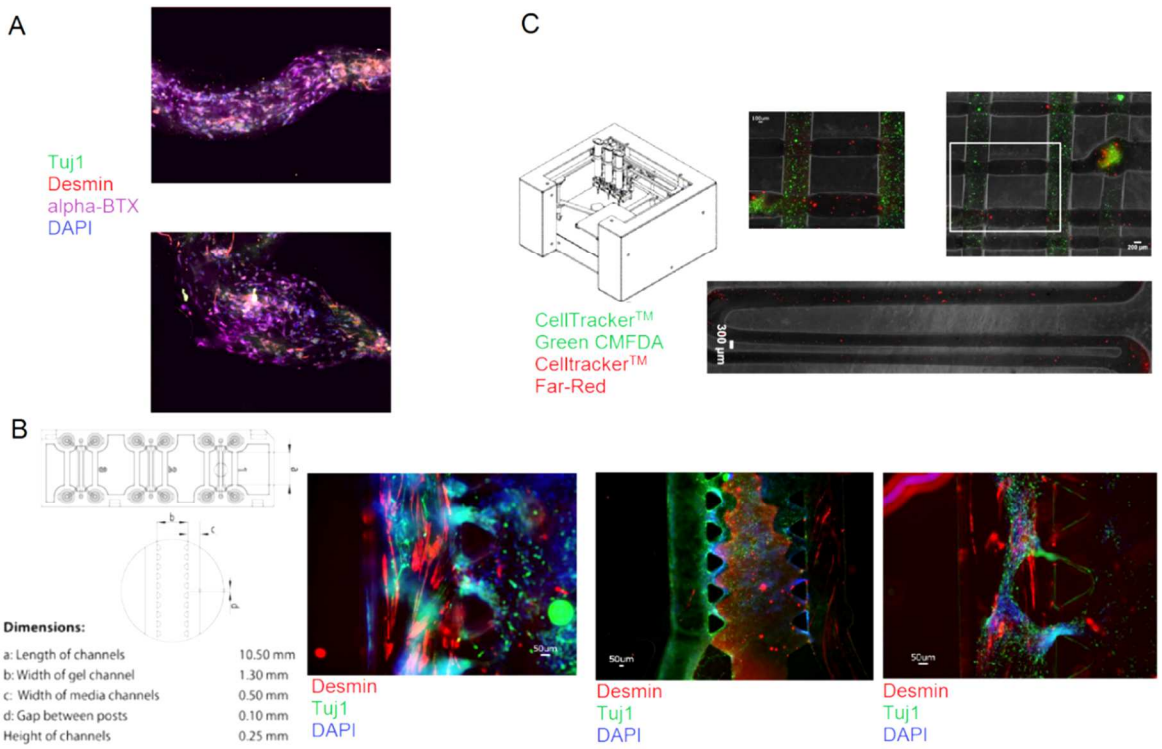

Figure 3.27: Heterogeneous and Spatially Segregated 3D Interactions of Skeletal Myoblasts and Motorneurons. (A) Heterogenous 3D co-culture gels grown for 14 days in suspended 3D culture, top and bottom show independent trials with four color stain (B) Co-culture chip (far left) schematic from AIM biotech website (http://www.aimbiotech.com/) (left to right), IF images of: myoblast channel with integrating hiNSCs from opposing channel, large-field view of chip with hiNSC channel on left and hSKM channel on right, and close-view of hiNSCs invading hSKM due to inner gel breakdown. Scale bars 50µm. (C) (left) schematic of Scientist (Fab@Home, Seraph Robotics) 3D printer, with fluorescent images of cell-tracking dyes one-day post printing (top right) and profilometry lines (bottom) showing current resolution of printing technique.

In further research, to test the potential for patterning the myoblast and hiNSC seeded gels in spatially segregated patterns difficult to form with the proliferative C2C12 and NG108-15 cell lines we used multi-ink printing to pattern both cell types in 3D. To begin these trials, we used a Scientist 3D printer to print lines of myoblasts and neurons in cross patterns in similar dimensions as would be found on orthogonal suspended gels. We first incubated both cell types in unique cell tracking dyes, and then used a silk-gelatin ink with glycerol stabilization [123]. This allowed us to pattern regularly interspersed human myoblast and hiNSC cell lines with minimum resolution of 300μm as determined by profilometry lines (figure 3.27C). Ultimately this patterning procedure proved difficult to employ further as inks would not adhere to tissue culture plastic in longer term systems required for cell growth and cocultured differentiation.

3.4.5 Coculture and Analysis of hiNSC-Derived Motoneuron-like Cells and Differentiating Human Skeletal Muscle Myoblasts

As an upgrade to the 3D suspended coculture design where gel types are heterogeneously mixed in the sacrificial gel based culture (figure 3.16-18) human myoblast-seeded silk-collagen gels were pipetted around printed silk cantilevers to provide better anchorage and gel stability. Silk-collagen hydrogels compacts arounds the base of cantilevers and then will compact gradually pull against the cantilevers in a similar method as embedded 3D cantilevers aligning cells though uniaxial tension (figure 3.10). These circular constructs could be pipetted or printed, and importantly can be designed for input of motorneuron-like cell gels to provide better spatial segregation.

The evolved strategy has been to combine differentiated hiNSCs with separately differentiated hSKMs in silk-collagen hydrogels, followed by cocultured differentiation

in media identical to 2D plated culture. In IF analysis there appeared to be diffuse alpha-bungarotoxin staining throughout extended myoblasts, but no specific localization in punctate areas or plagues could be appreciated (figure 3.28). It is possible that low-level alpha-bungarotoxin staining is sufficient for synaptic connectivity with motorneuron-like cells, as positive labeled myoblasts are thought to be in an advanced or mature more functional myotube-like state [124]. Diffuse staining of alpha-bungarotoxin has been seen in prior reports of 3D cultured myotubes [94] and the only report with limited evidence of acetylcholine receptor clustering in 3D also reported the first spontaneous human myotube contraction in 3D [55]. Future experiments aim to explore addition of recombinant agrin to 3D constructs which has been previously shown to advance the maturity of alpha-bungarotoxin clusters and thus increase the potential for downstream innervation of 3D myoblast-seeded constructs [41].

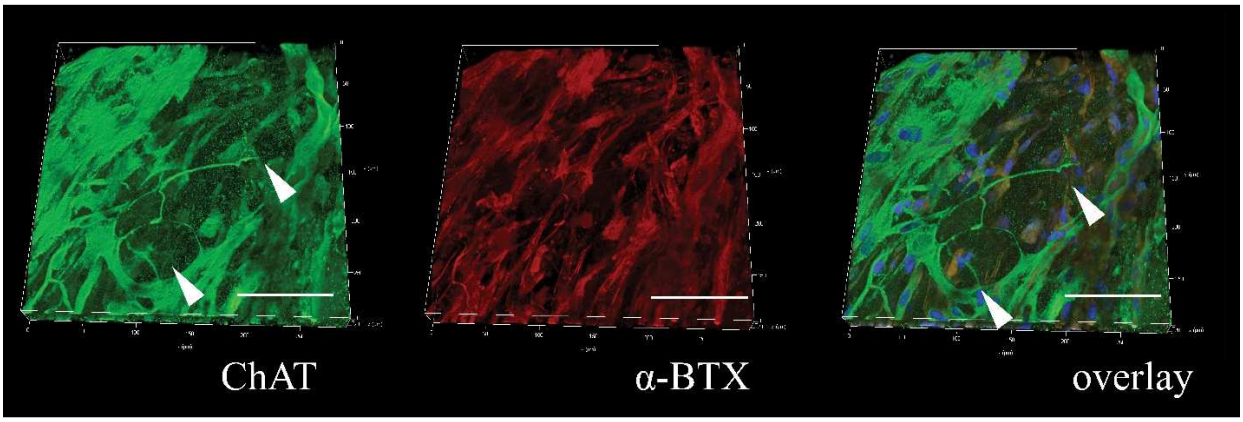

Figure 3.28: Three Dimensionality of Skeletal Muscle Myotubes and Potential for Synaptic Contact with Infiltrating Neuronal Cells**.** Split channel views of 3D culture gels cocultured for 14 days in suspended 3D culture with human skeletal muscle myoblasts differentiating anisotropically. (left) ChAT positive neurites extending from neural cell bodies. (center) Differentiated alpha-bungarotoxin positive myotubes shown in red. (right) Differentiated alpha-bungarotoxin positive myotubes contact hiNSCs propagating neurites co-localizing or extending along differentiated myoblast tracts. X and Y axes 600µm long with 50µm gridlines. Scale bars 100 µm.

As co-localization had been previously hard to detect in the heterogeneously cell-laden 3D suspended gels, methods which employ the same gel compositions as the 2.5D chip culture, where cells remain spatially segregated, were pursued. These experiments used controlled migration of motorneuron-like cells to differentiated 3D myoblast cultures after 14 days of monoculture by manual addition through pipetting. Differentiated motorneuron-like cells were concentrated through trypsinization and centrifugation to 5μL of $1*10^7$ cells/mL and directly pipetted on top of 3D freestanding constructs with culture media aspiration for more precise addition and to enable cells to adhere to the constructs without being mixed in culture solution. Cocultured constructs were then differentiated for seven to 14 additional days in motorneuron differentiation media or in 1:1 ratio of hiNSC and phenol-free myoblast differentiation media.

To test for the ability of hiNSC-derived cells to move through silk-collagen gels and interact with developing myoblasts, first myoblasts were shown to anisotropically differentiate in silk-collagen gels after four days of differentiation and compaction between silk cantilevers (figure 3.28A). The same hydrogel was also shown to be supportive of hiNSC-derived motoneuron-like cells as these cells spread β-III tubulin (Tuj1) positive neurites through the gel depth (figure 3.28B).

Differentiated myoblasts (both myosin heavy chain and alpha-bungarotoxin positive) were found to have remained extended throughout the seeded hydrogel with distinct localization from motorneuron-like cells which propagated regionally throughout the construct and stained positive for choline acetyltransferase. Specifically labeled motorneuron-like cells were visualized with 10X magnification, and thin (<1μm) ChAT+

neurites could be seen independently expressing specific ChAT staining, thought be indicative of the cholinergic property of motoneurons [125] (figure 3.28).

Moreover, the cocultured constructs could be reasonably viewed with brightfield microscopy during the cocultured differentiation and while cell types cannot be identified conclusively with this method, it was found that processes similar to what motorneuron-like cells extend in 2D culture were found extending from the 3D free-standing constructs, indicating possible proof-of-concept for potential orthogonal connection of motorneuron-like cells (figure 3.29).

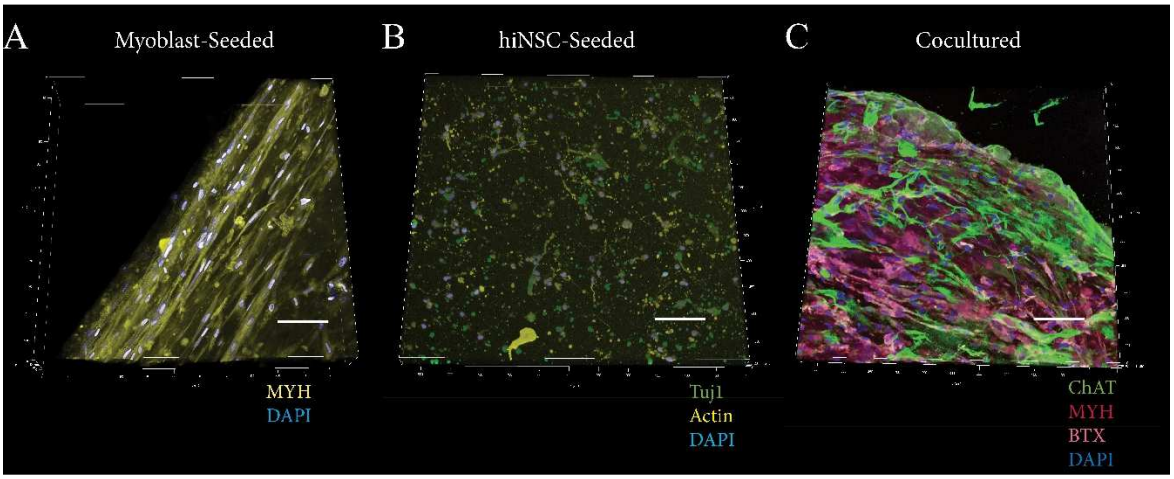

Figure 3.29: Three Dimensional Extension of Monocultured Myoblasts, Neurons and Coculture**.** (A) 3D culture gels grown for 14 days in suspended 3D culture with human skeletal muscle myoblasts differentiating anisotropically. DAPI (nuclear stain) - blue, MYH-yellow. (B) Differentiated hiNSCs propagating neurites in silk-collagen. Tuj1-green, actin-yellow, DAPI-blue. (C) HiNSC extending co-localizing or extending along differentiated myoblast tracts in coculture. X and Y axes 600µm long with 50µm gridlines.Scale bars 100 µm.

As cells processes exhibiting cell-specific synaptic machinery were found to colocalize in the cocultured 3D gels, the focus became proving that mono and cocultured constructs could be stimulated and demonstrate functionality. It was first found that after incubation with Fluo-4, live staining of mono and cocultured constructs demonstrated calcium flux along putative syncytia of myofibers in response to an acetylcholine bolus

of 10mM acetycholine to a final concentration of 100µM acetycholine after media agitation. The calcium movement was apparent in uniaxial fiber tracts in both mono and cocultured constructs (figure 3.30), indicating mature myotube formation with both construct types. However, it remained unclear what the contribution of the hiNSC-derived motoneuron-like was to the activation of calcium transients.

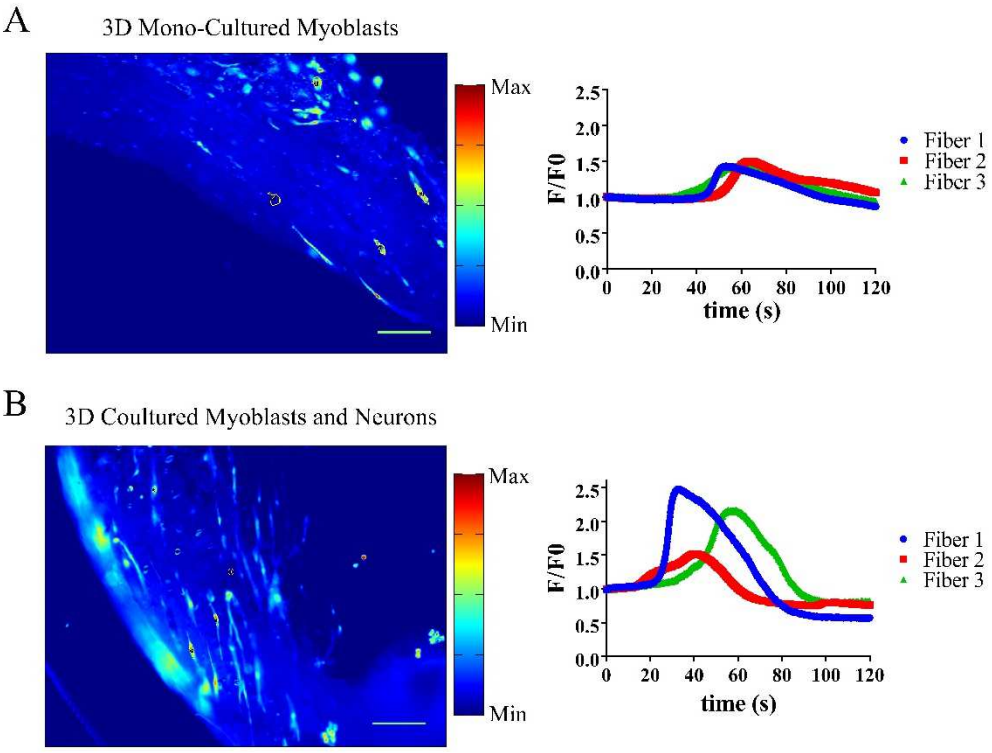

Figure 3.30: Calcium Flux Responses to Acetylcholine Bolus in Mono- and Cocultured 3D Human Cell-Derived Engineered Constructs**.** (A) 3D monoculture myoblast-seeded gels grown for 28 days in suspended 3D culture, incubated for one hour with Fluo-4 (Fluo-4 Calcium Imaging Kit, Thermo-Fisher) at 37°C. Individual wells on 12 well plates, containing constructs containing 1L of HBSS were given a 100mM acetylcholine chloride bolus and recording was started five seconds following the bolus. Standard deviation Z-projection of AVI file with 5 frames per second and total recording length of 120s. Image is show in "Jet" lookup table (LUT) (ImageJ) with red shift indicating movement, and blue shift showing low deviation (left). Graph of 3 cells outlined as regions of interest (yellow outline, left) shown in traces on right, with time 0 on chart indicating t=5s after acetylcholine bolus. Three traces are shown and are normalized to dark background (ROI # 4) as well as to baseline, taken as an average of 5 seconds at end of recording. (B) Same as above with imaging of hiNSCs and hSKMs differentiated for 14 days before Fluo-4 incubation. Scale bars 200µm.

To start to decouple the neuronal involvement in stimulation, differentiated neurons on poly-D-lysine were exposed to 1.5mM glutamate, and were recorded with a high-frame rate microscope. Activation was apparent at a 5 second timelapse (figure 3.31), but longer 160 second timelapses were necessary to determine the overall width of the calcium transient (figure 3.31B). In theory, if motoneuron-like cells are responsive to glutamate, a myogenic response in coculture to glutamate would be highly indicative of a neuronal origination of stimulation.

Cocultured constructs were first examined without acetylcholine or glutamate, and imaged for 120 seconds after 1 hour Fluo-4 incubation. There appeared to be a small amount of calcium transient visible in one cell, although the trend seemed to be generally one of deexcitation (figure 3.32A). However, 5 seconds post glutamate addition, cells could be observed showing calcium transients, although to a lesser fluorescence intensity (F/F_0) degree than with acetylcholine stimulation (figure 3.32B).

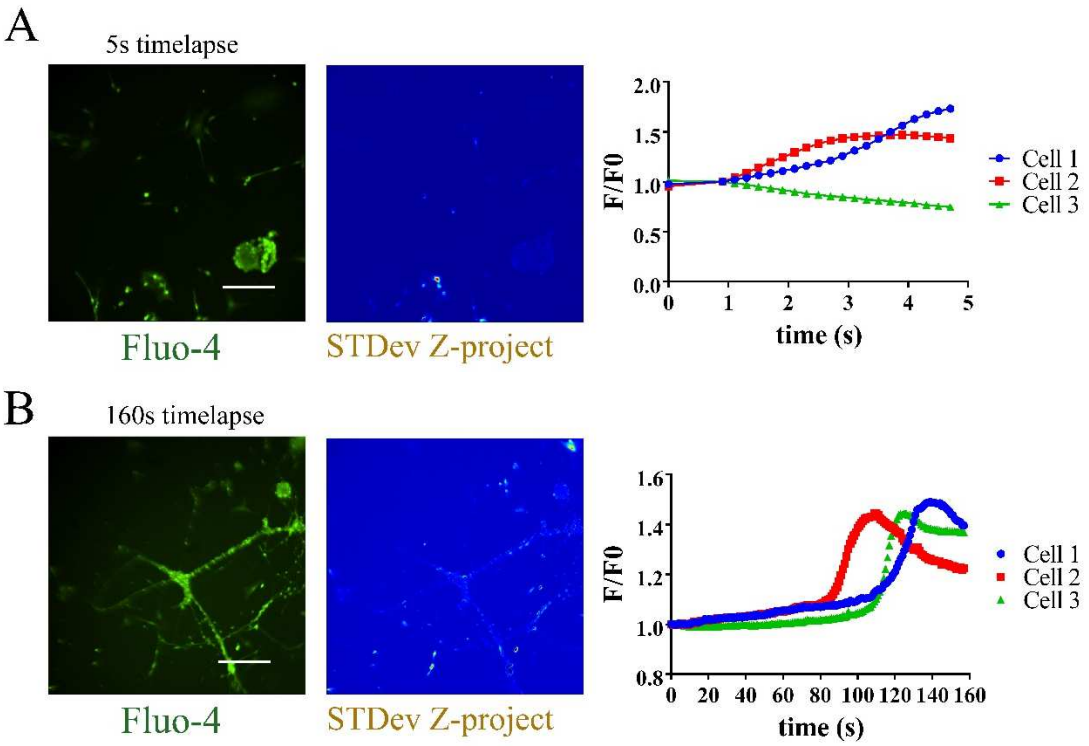

Figure 3.31: HiNSC-Derived Motoneuron Response to 1.5mM Glutamate Treatment. (A) hiNSC cells seeded on poly-D-lysine for 14 days, incubated for one hour with Fluo-4 (Fluo-4 Calcium Imaging Kit, Thermo-Fisher) at 37℃. were given a L-glutamic acid bolus and recording was started five seconds following the bolus. (A) Flou-4 snapshot and standard deviation Z-projection of AVI file with 5 frames per second and total recording length of 5s. STDev is show in "Jet" lookup table (LUT) (ImageJ) with red shift indicating change in fluorescence intensity, and blue shift showing low deviation (left). Graph of 3 cells outlined as regions of interest (yellow outline, left) shown in traces on right, with time 0 on chart indicating t=5s after L-glutamic acid bolus. Three traces are shown and are normalized to dark background (ROI # 4) as well as to baseline, taken as an average of 5 seconds at beginning of recording. (B) Same as above with imaging of hiNSCs taken for 2.5 minute timelapse to detect length of excitement peaks. Scale bar 100μm.

To fully decouple the neuronal origin of stimulation one needs to also demonstrate the stimulation is blocked when the nerve – muscle coupling is blocked. Curare, a potent neuromuscular blocking agent, was added to post glutamate stimulated samples. While calcium transients were too infrequent post glutamate addition to prove curare had an effect, one can look at the standard deviation of the timelapse to look for suspicion of an effect. In this instance, pre-curare and post-curare timelapse seem to shift

the transient relative to areas of identified cells. As neural cells were given incubation with a cell tracer before coculture, we could see that in this case, the transient standard deviation had an increase in an area of the construct with dense neural localization (figure 3.32C) and a relative decrease in unlabeled cells, or putative myocytes. Upon quantification of outlined cells over the timecourse, it was found that myocytes which should show a change in response after curare blocking had a higher decrease in fluorescence intensity shift over the timecourse than the neurons, identified through localization with cell tracking dyes.

While not a conclusive method, the use of cell tracking dyes to identify specific cell populations in 3D culture after seeding serves to illustrate a decoupling method for complicated and intertwined stimulation of densely coculture 3D constructs. If one can localize the cell origin and determine specific biochemical activation, this would lead to strong conclusions on the role of an integrating cell type in a new form of 3D coculture.

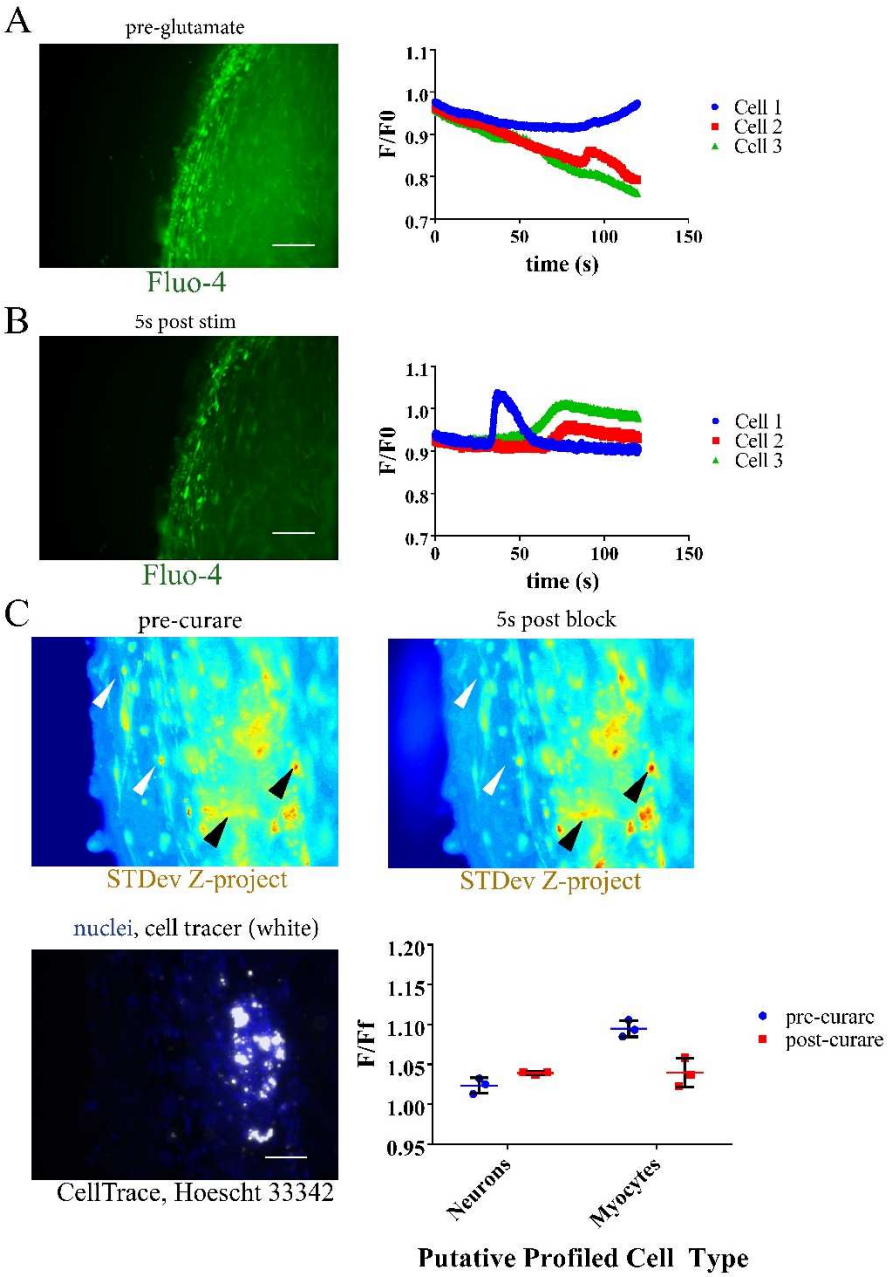

Figure 3.32: Decoupling Stimulation Response of Cocultures to L-glutamic Acid (A) hiNSCs and hSKMs differentiated for 14 days in 3D silk-collagen, incubated for one hour with Fluo-4 (Fluo-4 Calcium Imaging Kit, Thermo-Fisher) at 37℃. were recorded for 120s before and after stimulation (A) Flou-4 snapshot (left) and graph of 3 cells outlined as regions of interest (yellow outline, left) shown in traces on right, with time 0 on chart indicating start of recording t=5s after L-glutamic acid bolus. Three traces are shown and are normalized to dark background (ROI # 4) as well as to baseline, taken as an average of 5 seconds at beginning of recording. (B) Same as above with imaging beginning 5s after a L-glutamic acid bolus. (C) Pre- and post-curare addition, with cell tracer added to neural cells prior to coculture shown in white, Hoescht 33342 live cell dye shown in white. Quantified cell-specific change in fluorescence over 120s (bottom left). Scale bars 100µm.

Chapter 4: Discussion

4.1 Alignment of Human Skeletal Muscle Myoblasts

Tissue engineering methods exploring the connection between motoneurons and myotubes have advanced substantially over the past decade, and have developed into an increasing complexity of techniques utilizing both 2D and 3D culture. Numerous 2D coculture systems have been developed with distinct human cell types co-plated in tissue culture plastic and coated glass/coverslips. However, 2D systems generally suffer from a lack of recapitulation of the 3D architecture of normal tissue, and contain cells growing isotropically, in which myotubes are aligned parallel only in localized patchy regions [126]. While some 3D systems have shown reproducible alignment, both current 2D and 3D systems have drawbacks including the use of animal cell lines, and a lack of anisotropy in engineered muscle tissue. To date, the authors have seen no report of an aligned human cell-derived 3D coculture system for studying the NMJ and neuromuscular functionality.

The method described in the present work provides a system where motoneuron-like cells can be integrated into aligned 3D human myoblast-laden hydrogels, with healthy myotube formation and neurite extension through the gel. This method is introduced with a tunable system whereby cells can be seeded into hydrogels compacting around custom designed 3D cantilever-supported freestanding 3D cultures, while maintaining use of standard tissue culture techniques and materials.

We began early phases of research attempting to establish a method which could both reproducibly align and differentiate human myoblasts, with a focus on methods which could integrate neuronal inputs after viable differentiation of myotubes. Initial efforts focused on using directionally frozen lamellar scaffolds, which have a layered

structure of porous sheets, thought to be able to provide guidance cues towards cell alignment. Scaffolds were fabricated and analyzed for geometrical guidance cues and durability of common extracellular matrix coatings. These scaffolds were frozen into molds which would allow for inputs of tubular scaffolds developed by other lab members, previously designed for nerve conduits of chick dorsal root ganglia. When seeding trials showed low reproducibility of alignment, other means of 3D cell culture in biocompatible substrates were explored.

Subsequent tests were focused on analysis of extracellular matrix components with the effect of myoblast elongation, growth, and viability in 2D and 3D. It was first found that common extracellular matrix-based coating solutions on 2D significantly increased outgrowth of human myoblasts as compared to TCP, up to 8 days after initial cell seeding. It was also found that in 3D, the additional of matrigel in static culture increased the viability of expanding human myoblasts, and that cells oriented circumferentially around compacting static gels. To determine means of evaluating conditions which would lead to healthy myoblast growth and differentiation in encapsulated 3D gels, two automated systems for delivering and patterning cell-laden hydrogels were developed.

The first system involved bioplotting at regular sub-millimeter intervals to examine the repeatability of viable growth of C2C12 myoblasts in encapsulated hydrogels. It was found that two gel blends led to relatively high cell viability, and 500μm spacing of cell bundles lead to geometrically confined spacing. Bioprinting of thin lines of encapsulated cell solutions of concentrated C2C12 myoblasts also led to successful confinement of cells, although determining morphology of alignment of

individual cells proved difficult. 2D FFT methods of alignment analysis were able to show some specificity and ability for signal generation in analysis of 3D cultured embedded myoblasts, but later efforts improved alignment analysis through automated profiling and analysis of identified cells.

Further expansion of bioprinting methods expanded on FDM and cell printing processes enabling segregated patterning of silk-collagen gel blends in tissue culture materials, as opposed to embedded bioprinting of cells in thick gels. These techniques showed proof of concept of both high viability of C2C12 myoblasts as found in other reports [43,44], as well as advanced differentiation marker expression in differentiated myotubes.

The next step towards reproducibly aligned myotubes in 3D culture with capacity of neural integration involved using sacrificial cavities from wires removed through cooled and congealed Gelatin as a support for polymerization of cell-laden silk-collagen hydrogel solutions. These 3D cultures were cast in PDMS and designed for static strain between two cantilevers and for the ability for orthogonally seeded gels to potentially provide neuronal integration of developing myotubes. This system was shown to support the growth and elongation of C2C12 myoblasts, (as well as NG108-15 motoneuron-like cells in independent trials) and further experiments aimed to show utility for anisotropic differentiation of human skeletal myoblasts characterized for myogenic differentiation. Human skeletal muscle myoblasts purchased commercially were characterized to show myogenic lineage through both IF imaging of differentiation markers and analysis of Desmin+ percentage of differentiated myoblasts in 2D cell culture surfaces and 3D silk-collagen gels. Human myoblasts were also shown to expand align along the axis of the

sacrificial cavities between PDMS cantilevers in a similar degree as in C2C12 myoblasts in the same device.

We next wanted to show that differentiating myoblasts would have the ability for functional contact with integrating neuronal cells, and thus we stained for alpha-bungarotoxin, which binds to acetycholine receptors, demonstrating a high degree of differentiation of myoblasts into myotubes on thin silk-collagen gels, in which the human myotubes produced distinct acetylcholine receptor plaque formation after 4 weeks of differentiation. Other experiments showed human skeletal myoblasts in thin silk-collagen gels could be moved away from quiescence and towards higher degrees of differentiation through the use of molecules thought to stimulate myoblasts: IGF-1 and recombinant agrin [127,128]. Recombinant agrin was also shown to upregulate AGRN, thought to be responsible for the aggregation of acetylcholine receptors involved in synaptogenesis with contacted motor axons.

Further investigation of the static strain model previously shown in proof of concept to align human myoblasts involved a newly developed method of freeform silk printing, which formed silk cantilevers supporting the polymerization and gel compaction of human myoblast seeded hydrogels. The next aim was to show that this method of static strain in compacting myoblast-laden hydrogels reproducibly aligned 3D constructs as opposed to hydrogels seeded without substrate providing directed compaction and testing. Reproducible anisotropic alignment of hSKMs in 3D silk-collagen hydrogels cast around sterile bioprinted silk cantilevers in tissue culture wells was analyzed through differentiation for three weeks with constructs fixed at selected timepoints. This technique showed significant increases in the percentage of cells falling within 20° of the

gel axis at all timepoints with the printing cantilever method and advanced neuronal integration experiments were undertaken with constructs differentiated in this manner.

4.2 Coculture of Motoneuron-like Cells with Differentiating Myoblasts

Several research groups have explored 3D coculture systems with neuronal cells producing uni-axially oriented cells, allowing for the measure of gross contraction of the construct, but such models presently rely on rat or murine primary cells or cell lines [74,86,89]. Murine-derived cells are typically used in this context due to the additional expense and complexity involved in human primary cell culture, however more widely commercially available primary human cells are becoming an attractive option to further translational relevance through human cell-derived tissue engineering strategies.

Our 3D coculture NMJ model was designed from the start to maximize reproducibility, emphasizing longer-term culture with a focus on exploring the potential of nerve-originated contractions to explore neuromuscular unit functions. Initial experiments using motoneuron-like cells to provide neural input into differentiation myotubes began through exploration of NG108-15 cell lines, which could be induced to promote axonal outgrowth. The NG108-15 cells were first shown to have potential for co-plating with differentiating C2C12 myotubes, although the pattern of acetylcholine aggregation in C2C12 myotubes was not immediately identifiable to specific cell contact as both cell lines are known to have a high degree of growth, common to several immortalized cell lines. Attempts were also employed to spatially segregate cell lines using previously described bioprinting methods, although difficulties with poorly regulated expansion of cell lines precluded further evaluation.

NG108-15 cells were shown to have successful and specific growth with human skeletal myoblasts in culture in plated thin 3D silk-collagen gels, although methods which could provide segregation of cell types, allowing for more direct analysis of axon outgrowth and muscle differentiation, were explored. These methods included silk films in transwells, seeded with one cell type per side. Fully human coculture was also desired for novelty at this point and human coculture began in thin 3D gels seeded with human induced neural stem cells, which differentiated into mature cholinergic motorneuron phenotype. This phenotype was shown through positive expression of cholinergic and neuronal markers after 14 days of specific differentiation with shh agonist, and in thin 3D gel culture, ChAT positive hiNSC-derived motoneuron-like cells cocultured with Desmin and alpha-bungarotoxin positive hSKMs. After success with differentiated 3D thin gel culture (existing in static planar monolayers), we aimed to demonstrate feasibility of growing mature innervated human myotubes in our 3D system.

The initial plan for establishing the suspended 3D NMJ model relied on the integration of two human cell types in the sacrificial gel cavity-seeded cantilevers to be stable in culture for a long enough period for mature differentiation of both cell types. Unfortunately, while this technique showed initial promise as overlapping orthogonal 3D suspended gels were seen in culture after sacrificial gelatin was removed and replaced with culture media, this technique suffered from a few major drawbacks. The first issue was that the gels seemed to have decreasing stability in culture media over time, and the process of labeling for fluorescence imaging often destroyed the gel intersection. Secondly, the fidelity of each cell type moving through its own channel was in question, as it is possible to view the injected gel moving into adjacent orthogonal channels while

being injected. Immunofluorescence studies have shown that there is increased migration of motorneuron-like cells into areas thought to be occupied exclusively by myoblasts. To more fully elucidate how hiNSC-derived motorneurons and human myoblasts would integrate, a 2.5D chip culture allowing for imaging without sacrifice, and the use of two separate media inputs was used, as well as a bioprinting system with cell tracking of both cell types.

While other systems were explored, the use of the printed silk cantilever system with proven alignment of human muscle cells enabled successful myogenic differentiation as well as the use of precisely added hiNSC derived cells in coculture. These motorneuron-like cells were added into a myoblast seeded 3D matrix to mimic growth cone-directed axonal outgrowth into contact muscle similar to surgical muscular reinnervation by double fascicular transfer in patients with brachial plexus injuries [129] and ventral root outgrowth in embryonic development. After hiNSCs were added to muscle-seeded constructs in high density aliquots, cocultures were differentiated towards cholinergic motoneuron-like cell maturation, with widespread neurite extension.

Confocal z-stacking was first used to investigate the nature of the mono- and cocultured constructs, and mature myotubes were present over several layers of the short axes of stacked cells (<50 μm) indicating differentiation in 3D. Staining for alpha-bungarotoxin also showed co-localized AChRs along myotubes with ChAT positive neurites in the construct thickness, illustrating the potential for synaptic connectivity of cholinergic neurons and acetylcholine receptors. Through coculture in engineered 3D suspended gels, we aimed to show viable NMJ formation both through co-localization of immunofluorescence of cell specific machinery, and with functional changes using

stimulation with acetylcholine and L-glutamic acid, thought to stimulation myocytes and neurons, respectively. Video analysis showed calcium transients along uniaxially oriented myotube tracts after acetylcholine stimulation. Using video analysis with ImageJ, we were able to measure myotube stimulation through calcium fluxes in myofibers in both mono- and coculture models. In neuronal monoculture, excitation was shown after L-glutamic acid addition, although activation appeared only after longer delays than expected. L-glutamic acid was used in stimulation experiments with cocultured constructs, where we aimed to induce stimulation of baseline calcium fluxes, which could be subsequently blocked by curare addition, which inhibits acetylcholine receptors on the postsynaptic membrane. There appeared to be some degree of stimulation through L-glutamic acid addition in cocultured constructs, although the relatively slow timecourse of the calcium transient and infrequence of flux made it difficult to determine a significant difference from baseline. Addition of curare with neuronal cells previously incubated with cell tracking dyes aimed to show that calcium transients after L-glutamic acid could be reproducibly blocked, but here again, the relatively low level of stimulation made it difficult to determine if there was a significant difference. However, it was suggested that the relative change in degree of calcium transient was downregulated on unlabeled (myoblast-derived) cells after curare addition and upregulated in colocalization with labeled (neuronal-derived) cells.

This novel *in vitro* model of cocultured human myoblasts and motoneuron-like cells provides advancement towards a platform for medium to high-throughput predictive pharmacological testing and functional assaying of synaptic strength, plasticity, and contraction strength of muscle culture without limitation of encapsulating hydrogel used,

assuming the availability of standard tissue culture-ware and materials. Further development of this tissue model may serve as a potential alternative to costly animal studies and as a means for real-time analysis of patient specific response to therapeutics. Currently functional acetylcholine receptor clustering within engineering innervated skeletal muscle constructs allows for analysis of physiological neuron-muscle connectivity as well as a means to monitor the variety of pathological neuromuscular conditions in a controlled lab environment.

While the system in this work presents a novel functional toolkit and fills a needed gap for neuromuscular analysis, models for the study of NMJs still have significant roadblocks before they are routinely used for translational and diagnostic purposes. This system does not currently have a precise method of integration of Schwann cells, which are known to be present at human NMJs. Precise segregation of neural cell bodies would also increase relevance to how motoneurons exist in the spinal cord. Further engineering methods could be added to this model that would allow for more cell types in coculture as well as more precise introduction of cell types to segregate cell bodies to address this need.

4.3 Future Work

The model described here may be useful in preclinical studies of human neuromuscular disease through defining new methods to combine human neurons and muscle in 3D and providing initial evidence of synaptic contact in novel constructs. This novel technique and finding was designed from the beginning to be available to most research labs, although potentially more useful to labs with basic bioprinting devices and biomaterials available.

While human primary myoblasts and limited forms of human motoneuron progenitors derived from human embryonic stem cells are currently available commercially, in future research satellite cells from muscle biopsies of disease mutation-carrying donors could be used to create human disease models as demonstrated with preliminary aneural models of the muscular dystrophies [130]. Disease model human motoneurons will likely need to be terminally differentiated from induced pluripotent stem cells, as has been accomplished for the differentiation of iPSCs from spinal muscular atrophy patients into disease-recapitulating neurons. It also possible that it will no longer be necessary to obtain primary cells from patients to study disease mutations, as rapidly evolving gene editing technology such as Clustered Regularly Interspaced Short Palindromic Repeats (CRISPR) will allow disease genotypes to be derived from wild-type cell lines. However, before the use of disease model cells in similar 3D coculture, there are several elements of future work that will need to be carried out to increase the translational nature of the coculture construct, and increase the robust analysis of synaptic connectivity in human constructs.

The first future aim will be to increase differentiation towards functional contractility of human myotubes through a combined program of mechanical and electrical stimulation. The hypothesis is that mechanical and electrical stimulation can be applied to form longitudinal striated myotubes in both aneural and cocultured constructs. To this end, an electrical stimulation set-up is near complete, which will deliver constructs with 2 ms pulses separated by a 2 μs interruption in applied current, at a frequency of 10 Hz for 8 hours per 24 hours period for three days in a protocol that has shown positive benefits in myonuclear density, myoblast differentiation and release of

neurotrophins [128]. After a period of three days or longer in coculture, tissues will be incubated with Fluo-4, then stimulated with acetylcholine and L-glutamic acid, and finally tissues will be fixed for immunostaining and confocal analysis, as well as qPCR analysis of targets described above.

The second form of stimulation which is predicted to yield similar results in terms of contractility of human myotubes and longitudinal striation of cultured muscle is cyclic mechanical strain, which can be applied to 3D tissue constructs alone or in combination with electrical stimulation. To apply mechanical stimulation, we will continue setting up a linear motion actuator/bioreactor which will apply simple mechanical stretch and loading on the 3D printed cantilevers. A program of strain delivery at 10% strain at 0.5 Hz for 1 h alternated with 5 h of relaxation will be applied to 3D aneural and cocultured myoblasts, which has been previously shown to induce myoblast differentiation [131]. We hypothesize both electrical and mechanical stimulation individually will induce advanced longitudinally striated cytoarchitecture, and combined protocols likely have some additive effect, although likely not a fully additive effect as both mechanical and electrical stimulation activate the same contractile machinery and may reach an upper limit of stimulation and metabolic requirements. We also predict that along with an increase in the number of myotubes with longitudinally striated cytoarchitecture, staining for alpha-bungarotoxin may illustrate the presence of plaque formation on differentiated myotubes, likely correlated with the percentage of myotubes displaying longitudinally striated contractile machinery, including apposition of ryanodine receptors and T-tubules.

One further aim to improve the cell specificity of stimulation as a future improvement on 3D models will use optogenetic actuators to specifically stimulate cell

types in 3D NMJ models. The hypothesis is that transfected motoneuron-like cells in 3D coculture will be stimulated by blue light through transfection with channelrhodopsin-2 (ChR2) allowing a muscle response to blue light only with specifically transfected 3D cocultures. HiNSC-derived motoneuron cells will be first transfected with Lipofectamine 2000 and ChR2 vector, providing cells with blue light actuation. These transfected cells will be added in high density to myoblast-seeded 3D constructs as described earlier, and then exposed to blue light through an open-hardware light plate apparatus [132], which is in the final stages of construction and troubleshooting in our lab (figure 4.1). While monochromatic blue light has been shown to have mild effect on some model skeletal muscles systems including chick muscle [133], it is predicted that the optogenetic activator-transduced neurons cocultured with myoblast 3D constructs will show significant activation response of blue wavelengths in myotube calcium transients and possibly in visible contractile response. Contractile response to optogenetically induced myotubes has been previous shown in C2C12 myotubes in 3D [74,79,134], as well as in 2D human cocultures [126]. Demonstration of neuron-to-muscle activation in human 3D cocultures through optogenetic stimulation would be a significant advance both in tissue engineering and neuromuscular research, and such technology may have potential impact in clinics and laboratories, which could use patient-derived cells to reproducibly recreate and stimulate the human neuromuscular connection *in vitro,* with the ability for testing of novel therapeutics with an eye towards cell specific responses. While the direction and utility of *in vitro* 3D culture techniques remains to be elucidated, it is likely that development of such systems in a low-cost and high-throughput manner could lead to

vastly more widespread use and potential benefit in tailoring individual therapeutics to personalized response of treatments.

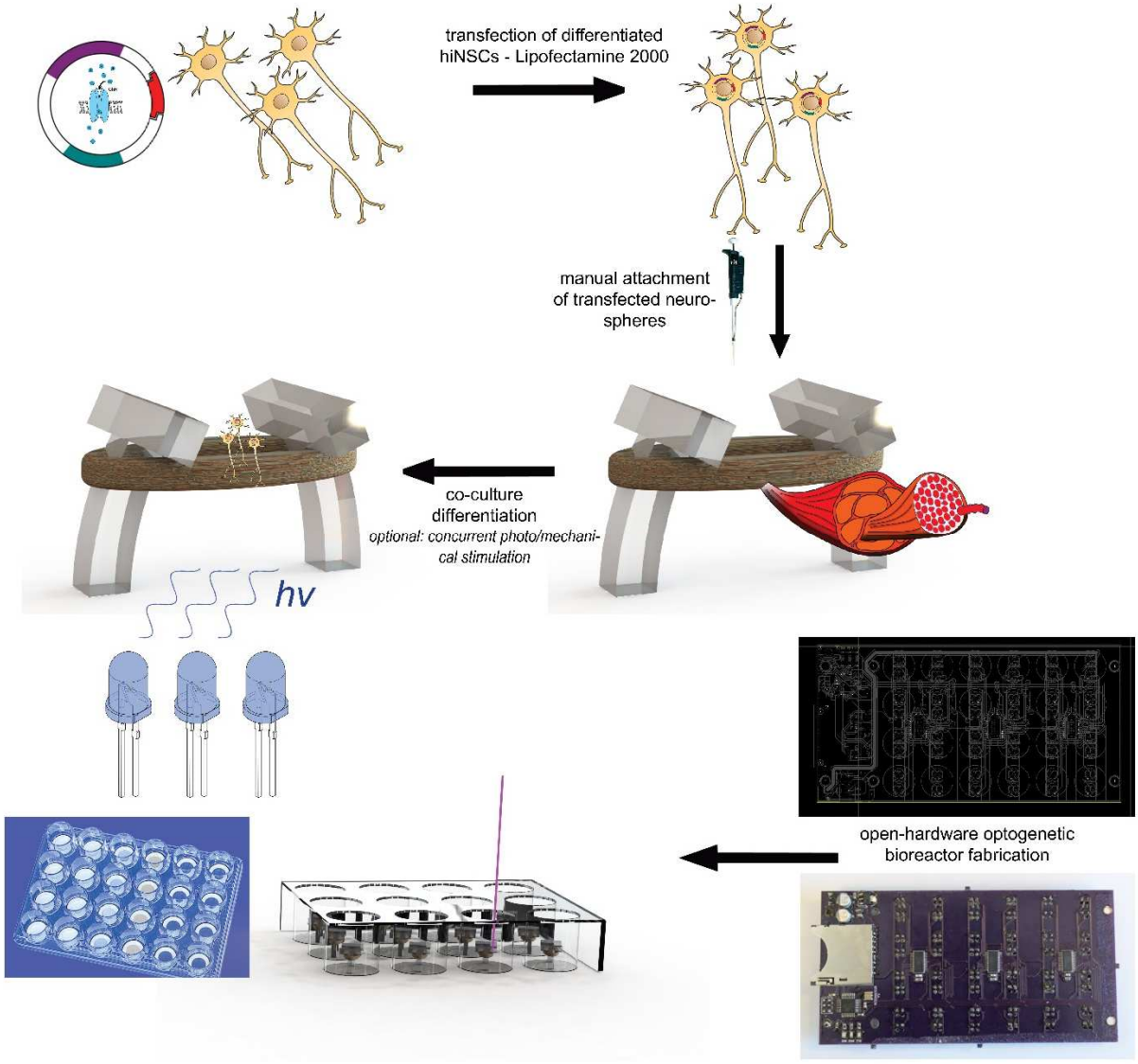

Figure 4.1. Schematic for Functional Determination of Coculture Through Incorporation of ChannelRhodopsin2 in hiNSCs and Manufacture of Optogenetic Stimulator**.** From Top left: Differentiated human induced neural stem cells are transfected with channelrhodopsin optogenetic actuator through lipofectamine 2000 transduction. Transduced hiNSCs added to 3D human muscle constructs as described previously. Open hardware device for stimulation of 24 well plates [132] is currently in the final stages of fabrication and can used to provide optogenetic conditioning as well as used in imaging platforms to stimulate with blue light and look for evidence of muscle activity derived from neural activation in 3D cocultured constructs with inlaid flexible freeform printed silk cantilevers.

Chapter 5: Appendix

5.1: Deconvolution Method for Removing Imaging Artifacts from 2D FFT Analysis

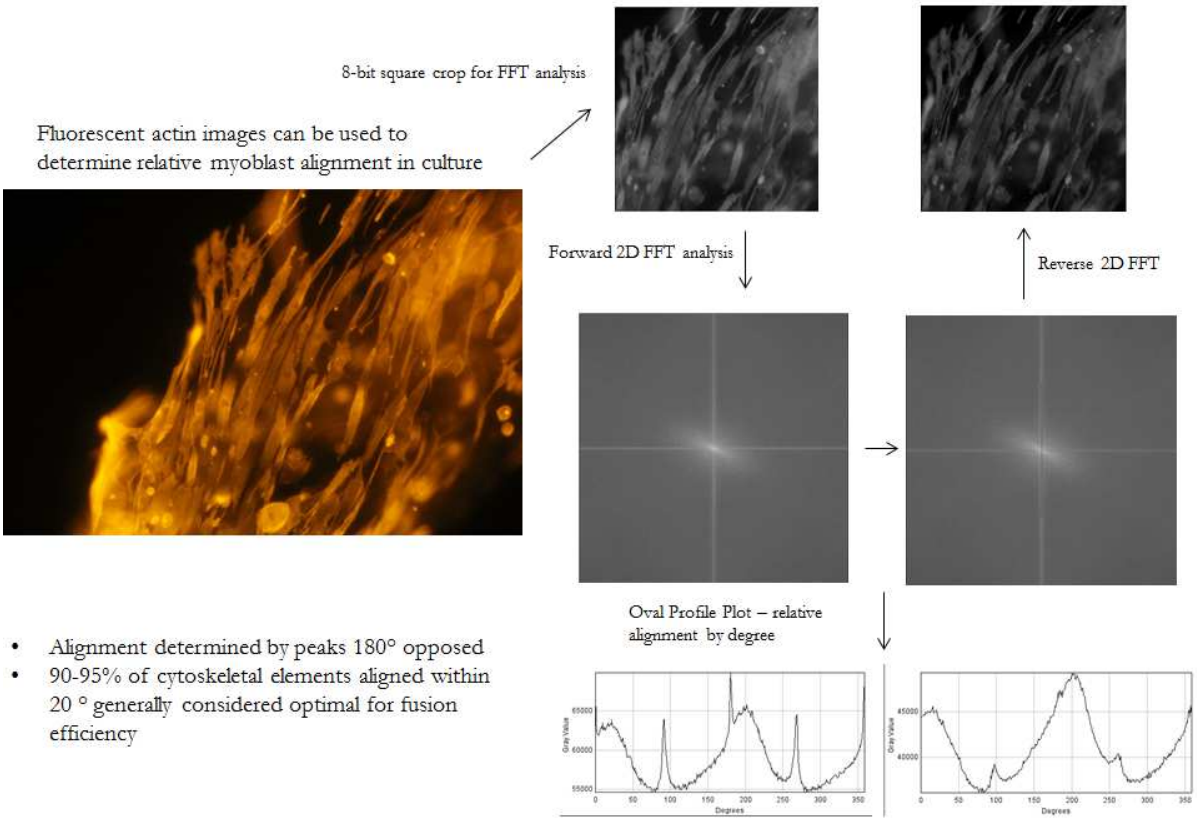

Figure 5.1: Flowchart for Removing Artifacts from Fluorescent Images for 2D FFT Alignment Analysis. Fluorescent actin images taken from myoblasts grown in 3D culture are cropped to square images and converted to grayscale. Forward 2D FFT and alignment plots show X and Y axis lines corresponding to pixel image scanning method. Using thin black lines on X and Y axis, a reverse 2D FFT shows cell structure intact (top) left and reduced peaks at 90 and 270̊ corresponding to artifacts of imaging.

5.2: Robotically Deposited 3D Culture Loading onto Flexible Cantilevers

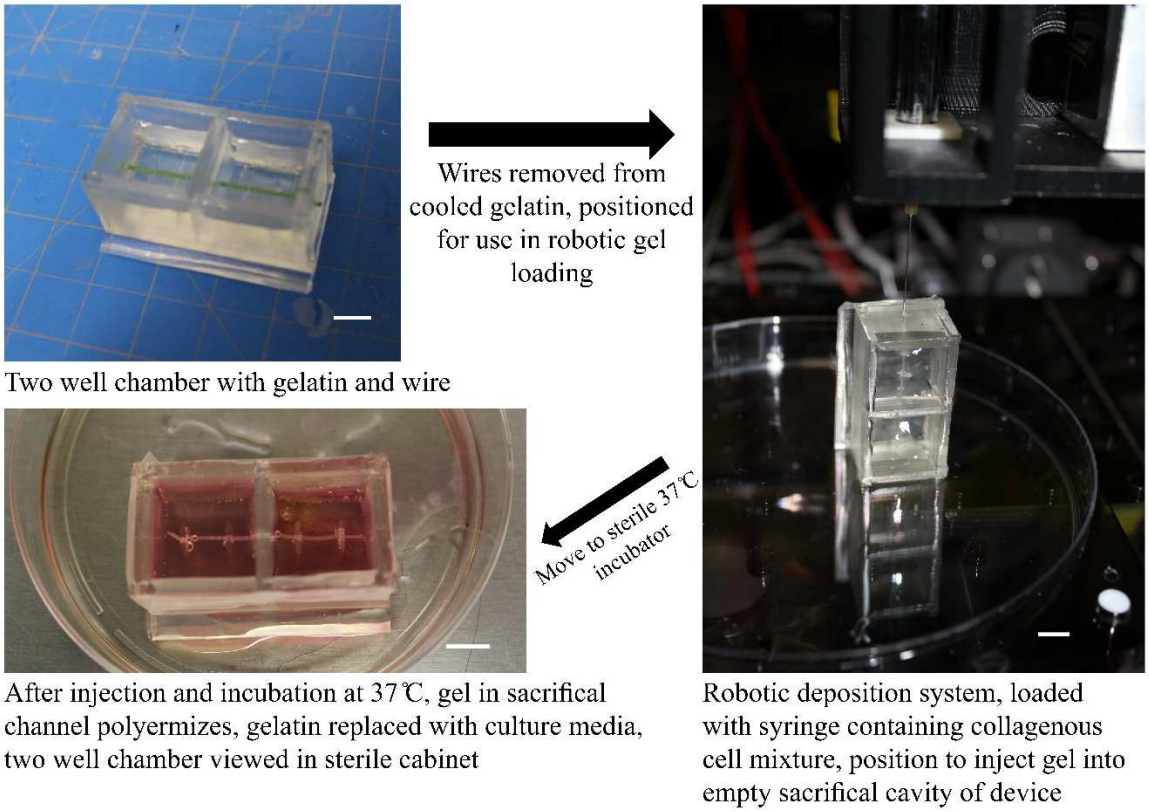

Two well chamber with gelatin and wire

After injection and incubation at 37℃, gel in sacrifical channel polyermizes, gelatin replaced with culture media, two well chamber viewed in sterile cabinet

Robotic deposition system, loaded with syringe containing collagenous cell mixture, position to inject gel into empty sacrifical cavity of device

Figure 5.2: Schematic and Flowchart for Automated Loading of Sacrificial Free Standing Gels in PDMS Culture Device. (top left) Two well PDMS culture device with cooled gelatin and inlaid PTFE-coated wires. (right) Wires removed from culture device leaving empty channel through gelatin in-between cantilevers. Syringe holder of robotic deposition system shown on top, with syringe tip extending into PDMS. (bottom left) PDMS device transferred to incubator and fluid gelatin replaced with culture media.

5.3: G-code Setup Sample for Printing with Repetier-Host

generated by Slic3r 1.2.9 on 2017-03-28 at 12:32:32

; external perimeters extrusion width = 0.10mm
; perimeters extrusion width = 0.11mm
; infill extrusion width = 0.11mm
; solid infill extrusion width = 0.11mm
; top infill extrusion width = 0.11mm
; support material extrusion width = 0.10mm

M107 ; disable fan

G92 X0;
G92 Y0;
G92 Z0;

G21 ; set units to millimeters
G90 ; use absolute coordinates
M83 ; use relative distances for extrusion
M761
G1 Z0.100 F1200.000 ; move to next layer (0)
M760
G1 X5.915 Y1.058 F1200.000 ; move to first brim point
G1 X5.915 Y-1.060 E0.00235 F300.000 ; brim

Chapter 6: Bibliography

(1) Ijkema-Paassen, J.; Gramsbergen, A. Development of postural muscles and their innervation. *Neural Plast.* **2005**, *12* (2–3), 141-51-72 DOI: 10.1155/NP.2005.141.

(2) Fidzianska, A. Human Ontogenesis: II. Development of the Human Neuromuscular Junction. *J. Neuropathol. Exp.* **1980**.

(3) Sanes, J. R.; Lichtman, J. W. Development of the vertebrate neuromuscular junction. *Annu. Rev. Neurosci.* **1999**, *22*, 389–442 DOI: 10.1146/annurev.neuro.22.1.389.

(4) Pratt, S. J. P.; Shah, S. B.; Ward, C. W.; Inacio, M. P.; Stains, J. P.; Lovering, R. M. Effects of *in vivo* injury on the neuromuscular junction in healthy and dystrophic muscles. *J. Physiol.* **2013**, *591* (2), 559–570 DOI: 10.1113/jphysiol.2012.241679.

(5) Larkindale, J.; Yang, W.; Hogan, P. F.; Simon, C. J.; Zhang, Y.; Jain, A.; Habeeb-Louks, E. M.; Kennedy, A.; Cwik, V. A. Cost of illness for neuromuscular diseases in the United States. *Muscle Nerve* **2014**, *49* (3), 431–438 DOI: 10.1002/mus.23942.

(6) Fan, L.; Simard, L. R. Survival motor neuron (SMN) protein: role in neurite outgrowth and neuromuscular maturation during neuronal differentiation and development. *Hum. Mol. Genet.* **2002**, *11* (14), 1605–1614 DOI: 10.1093/hmg/11.14.1605.

(7) Ohlendieck, K.; Ervasti, J. M.; Matsumura, K.; Kahl, S. D.; Leveille, C. J.; Campbell, K. P. Dystrophin-related protein is localized to neuromuscular junctions of adult skeletal muscle. *Neuron* **1991**, *7* (3), 499–508 DOI: 10.1016/0896-6273(91)90301-F.

(8) Oki, K.; Wiseman, R. W.; Breedlove, S. M.; Jordan, C. L. Androgen receptors in muscle fibers induce rapid loss of force but not mass: Implications for spinal bulbar muscular atrophy. *Muscle Nerve* **2013**, *47* (6), 823–834 DOI: 10.1002/mus.23813.

(9) Wirtz, P. W.; Sotodeh, M.; Nijnuis, M.; Van Doorn, P. A.; Van Engelen, B. G. M.; Hintzen, R. Q.; De Kort, P. L. M.; Kuks, J. B.; Twijnstra, A.; De Visser, M.; et al. Difference in distribution of muscle weakness between myasthenia gravis and the Lambert-Eaton myasthenic syndrome. *J. Neurol. Neurosurg. Psychiatry* **2002**, *73* (6), 766–768 DOI: 10.1136/JNNP.73.6.766.

(10) Verschuuren, J. J. G. M.; Huijbers, M. G.; Plomp, J. J.; Niks, E. H.; Molenaar, P. C.; Martinez-Martinez, P.; Gomez, A. M.; De Baets, M. H.; Losen, M. Pathophysiology of myasthenia gravis with antibodies to the acetylcholine receptor, muscle-specific kinase and low-density lipoprotein receptor-related protein 4. *Autoimmun. Rev.* **2013**, *12* (9), 918–923 DOI: 10.1016/j.autrev.2013.03.001.

(11) Marzetti, E.; Leeuwenburgh, C. Skeletal muscle apoptosis, sarcopenia and frailty at old age. *Exp. Gerontol.* **2006**, *41* (12), 1234–1238 DOI: 10.1016/j.exger.2006.08.011.

(12) Sharples, A. P.; Player, D. J.; Martin, N. R. W.; Mudera, V.; Stewart, C. E.; Lewis, M. P. Modelling *in vivo* skeletal muscle ageing *in vitro* using three-dimensional

bioengineered constructs. *Aging Cell* **2012**, *11* (6), 986–995 DOI: 10.1111/j.1474-9726.2012.00869.x.
(13) Johnson, A. M.; Connor, N. P. Effects of electrical stimulation on neuromuscular junction morphology in the aging rat tongue. *Muscle Nerve* **2011**, *43* (2), 203–211 DOI: 10.1002/mus.21819.
(14) Bernet, J.; Doles, J.; Hall, J.; Tanaka, K.; Carter, T. p38 MAPK signaling underlies a cell-autonomous loss of stem cell self-renewal in skeletal muscle of aged mice. *Nat. Med.* **2014**.
(15) Lee, M.; Vasioukhin, V. Cell polarity and cancer–cell and tissue polarity as a non-canonical tumor suppressor. *J. Cell Sci.* **2008**.
(16) Guo, X.; Greene, K.; Akanda, N.; Smith, A. S. T.; Stancescu, M.; Lambert, S.; Vandenburgh, H.; Hickman, J. J. In vitro differentiation of functional human skeletal myotubes in a defined system. *Biomater. Sci* **2014**, No. 2 DOI: 10.1039/c3bm60166h.
(17) Tanaka, H.; Furuya, T.; Kameda, N.; Kobayashi, T.; Mizusawa, H. Triad proteins and intracellular Ca2+ transients during development of human skeletal muscle cells in aneural and innervated cultures. *J. Muscle Res. Cell Motil.* **2000**, *21* (6), 507–526 DOI: 10.1023/A:1026561120566.
(18) Oleaga, C.; Bernabini, C.; Smith, A. S. T.; Srinivasan, B.; Jackson, M.; McLamb, W.; Platt, V.; Bridges, R.; Cai, Y.; Santhanam, N.; et al. Multi-Organ toxicity demonstration in a functional human in vitro system composed of four organs. *Sci. Rep.* **2016**, *6*, 20030 DOI: 10.1038/srep20030.
(19) Andriani, Y.; Chua, J. M.-W.; Chua, B. Y.-J.; Phang, I. Y.; Shyh-Chang, N.; Tan, W. S. Polyurethane acrylates as effective substrates for sustained in vitro culture of human myotubes. *Acta Biomater.* **2017** DOI: 10.1016/j.actbio.2017.04.022.
(20) Pantic, B.; Borgia, D.; Giunco, S.; Malena, A.; Kiyono, T.; Salvatori, S.; De Rossi, A.; Giardina, E.; Sangiuolo, F.; Pegoraro, E.; et al. Reliable and versatile immortal muscle cell models from healthy and myotonic dystrophy type 1 primary human myoblasts. *Exp. Cell Res.* **2016**, *342* (1), 39–51 DOI: 10.1016/j.yexcr.2016.02.013.
(21) Takayama, Y.; Wagatsuma, A.; Hoshino, T. Micropatterning C2C12 myotubes for orderly recording of intracellular calcium transients. *Med. ...* **2013**.
(22) Charest, J. L.; Eliason, M. T.; García, A. J.; King, W. P. Combined microscale mechanical topography and chemical patterns on polymer cell culture substrates. *Biomaterials* **2006**, *27* (11), 2487–2494 DOI: 10.1016/j.biomaterials.2005.11.022.
(23) Bettadapur, A.; Suh, G. C.; Geisse, N. A.; Wang, E. R.; Hua, C.; Huber, H. A.; Viscio, A. A.; Kim, J. Y.; Strickland, J. B.; McCain, M. L. Prolonged Culture of Aligned Skeletal Myotubes on Micromolded Gelatin Hydrogels. *Sci. Rep.* **2016**, *6*, 28855 DOI: 10.1038/srep28855.
(24) Rhim, C.; Lowell, D. A.; Reedy, M. C.; Slentz, D. H.; Zhang, S. J.; Kraus, W. E.; Truskey, G. A. Morphology and ultrastructure of differentiating three-dimensional mammalian skeletal muscle in a collagen gel. *Muscle Nerve* **2007**, *36* (1), 71–80 DOI: 10.1002/mus.20788.
(25) Powell, C. A.; Smiley, B. L.; Mills, J.; Vandenburgh, H. H. Mechanical stimulation improves tissue-engineered human skeletal muscle. *Am. J. Physiol. Cell Physiol.* **2002**, *283* (5), C1557-65 DOI: 10.1152/ajpcell.00595.2001.
(26) Rhim, C.; Cheng, C. S.; Kraus, W. E.; Truskey, G. A. Effect of MicroRNA

Modulation on Bioartificial Muscle Function. DOI: 10.1089/ten.tea.2009.0601.
(27) Khodabukus, A.; Baar, K. Defined electrical stimulation emphasizing excitability for the development and testing of engineered skeletal muscle. *Tissue Eng. Part C Methods* **2011**.
(28) Jockenhoevel, S.; Zund, G. Fibrin gel–advantages of a new scaffold in cardiovascular tissue engineering. *J. cardio- ...* **2001**.
(29) Engler, A. J.; Griffin, M. A.; Sen, S.; Bönnemann, C. G.; Sweeney, H. L.; Discher, D. E. Myotubes differentiate optimally on substrates with tissue-like stiffness. *J. Cell Biol.* **2004**, *166* (6), 877–887 DOI: 10.1083/jcb.200405004.
(30) Chaudhuri, O.; Mooney, D. Stem-cell differentiation: Anchoring cell-fate cues. *Nat. Mater.* **2012**.
(31) Cheng, C. S.; Davis, B. N.; Madden, L.; Bursac, N.; Truskey, G. A. Physiology and metabolism of tissue-engineered skeletal muscle. *Exp. Biol. Med.* **2014**, *239* (9), 1203–1214 DOI: 10.1177/1535370214538589.
(32) Sengupta, D.; Gilbert, P.; Johnson, K. Protein□Engineered Biomaterials to Generate Human Skeletal Muscle Mimics. *Advanced* **2012**.
(33) Bozek, K.; Wei, Y.; Yan, Z.; Liu, X.; Xiong, J.; Sugimoto, M. Exceptional evolutionary divergence of human muscle and brain metabolomes parallels human cognitive and physical uniqueness. *PLoS Biol* **2014**.
(34) Perniconi, B.; Coletti, D. Skeletal muscle tissue engineering: best bet or black beast? *Front. Physiol.* **2014**, *5*, 255 DOI: 10.3389/fphys.2014.00255.
(35) Li, Y.; Huang, G.; Zhang, X.; Wang, L.; Du, Y.; Lu, T. J.; Xu, F. Engineering cell alignment in vitro. *Biotechnol. Adv.* **2014**, *32* (2), 347–365 DOI: 10.1016/j.biotechadv.2013.11.007.
(36) Zhao, Y.; Zeng, H.; Nam, J. Fabrication of skeletal muscle constructs by topographic activation of cell alignment. *Biotechnol.* **2009**.
(37) Kim, M. S.; Lee, B.; Kim, H. N.; Bang, S.; Yang, H. S.; Kang, S. M.; Suh, K.-Y.; Park, S.-H.; Jeon, N. L. 3D tissue formation by stacking detachable cell sheets formed on nanofiber mesh. *Biofabrication* **2017**, *9* (1), 15029 DOI: 10.1088/1758-5090/aa64a0.
(38) Grabowska, I.; Szeliga, A.; Moraczewski, J. Comparison of satellite cell□derived myoblasts and C2C12 differentiation in two□and three□dimensional cultures: changes in adhesion protein expression. *Cell Biol.* **2011**.
(39) Ahadian, S.; Ramón-Azcón, J.; Estili, M.; Liang, X. Hybrid hydrogels containing vertically aligned carbon nanotubes with anisotropic electrical conductivity for muscle myofiber fabrication. *Sci. Rep.* **2014**.
(40) Bian, W.; Bursac, N. Soluble miniagrin enhances contractile function of engineered skeletal muscle. *FASEB J.* **2012**, *26* (2), 955–965 DOI: 10.1096/fj.11-187575.
(41) Wang, L.; Shansky, J.; Vandenburgh, H. Induced formation and maturation of acetylcholine receptor clusters in a defined 3D bio-artificial muscle. *Mol. Neurobiol.* **2013**, *48* (3), 397–403 DOI: 10.1007/s12035-013-8412-z.
(42) Choi, Y.-J.; Kim, T. G.; Jeong, J.; Yi, H.-G.; Park, J. W.; Hwang, W.; Cho, D.-W. 3D Cell Printing of Functional Skeletal Muscle Constructs Using Skeletal Muscle-Derived Bioink. *Adv. Healthc. Mater.* **2016**, *5* (20), 2636–2645 DOI: 10.1002/adhm.201600483.

(43) Merceron, T. K.; Burt, M.; Seol, Y.-J.; Kang, H.-W.; Lee, S. J.; Yoo, J. J.; Atala, A. A 3D bioprinted complex structure for engineering the muscle--tendon unit. *Biofabrication* **2015**, *7* (3), 35003.
(44) Costantini, M.; Testa, S.; Mozetic, P.; Barbetta, A.; Fuoco, C.; Fornetti, E.; Tamiro, F.; Bernardini, S.; Jaroszewicz, J.; Święszkowski, W.; et al. Microfluidic-enhanced 3D bioprinting of aligned myoblast-laden hydrogels leads to functionally organized myofibers in vitro and in vivo. *Biomaterials* **2017**, *131*, 98–110 DOI: 10.1016/j.biomaterials.2017.03.026.
(45) Chaturvedi, V.; Naskar, D.; Kinnear, B. F.; Grenik, E.; Dye, D. E.; Grounds, M. D.; Kundu, S. C.; Coombe, D. R. Silk fibroin scaffolds with muscle-like elasticity support *in vitro* differentiation of human skeletal muscle cells. *J. Tissue Eng. Regen. Med.* **2016** DOI: 10.1002/term.2227.
(46) Cheema, U.; Yang, S.; Mudera, V. 3□D in vitro model of early skeletal muscle development. *Cell Motil.* **2003**.
(47) Huang, Y.; Dennis, R.; Larkin, L. Rapid formation of functional muscle in vitro using fibrin gels. *J. Appl.* **2005**.
(48) Smith, A.; Passey, S.; Greensmith, L. Characterization and optimization of a simple, repeatable system for the long term in vitro culture of aligned myotubes in 3D. *J. Cell.* **2012**.
(49) Lam, M. T.; Huang, Y.-C.; Birla, R. K.; Takayama, S. Microfeature guided skeletal muscle tissue engineering for highly organized 3-dimensional free-standing constructs. *Biomaterials* **2009**, *30* (6), 1150–1155 DOI: 10.1016/j.biomaterials.2008.11.014.
(50) Heher, P.; Maleiner, B.; Prüller, J.; Teuschl, A. H.; Kollmitzer, J.; Monforte, X.; Wolbank, S.; Redl, H.; Rünzler, D.; Fuchs, C. A novel bioreactor for the generation of highly aligned 3D skeletal muscle-like constructs through orientation of fibrin via application of static strain. *Acta Biomater.* **2015**, *24*, 251–265 DOI: 10.1016/j.actbio.2015.06.033.
(51) Park, S.-H.; Koh, U. H.; Kim, M.; Yang, D.-Y.; Suh, K.-Y.; Shin, J. H. Hierarchical multilayer assembly of an ordered nanofibrous scaffold via thermal fusion bonding. *Biofabrication* **2014**, *6* (2), 24107 DOI: 10.1088/1758-5082/6/2/024107.
(52) Smith, A. S. T.; Long, C. J.; McAleer, C.; Bobbitt, N.; Srinivasan, B.; Hickman, J. J. Utilization of microscale silicon cantilevers to assess cellular contractile function in vitro. *J. Vis. Exp.* **2014**, No. 92, e51866 DOI: 10.3791/51866.
(53) Lee, P. H. U.; Vandenburgh, H. H. Skeletal Muscle Atrophy in Bioengineered Skeletal Muscle: A New Model System. *Tissue Eng. Part A* **2013**, *19* (19–20), 2147–2155 DOI: 10.1089/ten.tea.2012.0597.
(54) Gholobova, D.; Decroix, L.; Muylder, V. Van; Desender, L.; Gerard, M.; Carpentier, G.; Vandenburgh, H.; Thorrez, L. Endothelial Network Formation Within Human Tissue-Engineered Skeletal Muscle. DOI: 10.1089/ten.tea.2015.0093.
(55) Madden, L.; Juhas, M.; Kraus, W. E.; Truskey, G. A.; Bursac, N. Bioengineered human myobundles mimic clinical responses of skeletal muscle to drugs. *Elife* **2015**, *4*, e04885 DOI: 10.7554/eLife.04885.
(56) Davis, B. N.; Santoso, J. W.; Walker, M. J.; Cheng, C. S.; Koves, T. R.; Kraus, W.

E.; Truskey, G. A. Human, Tissue-Engineered, Skeletal Muscle Myobundles to Measure Oxygen Uptake and Assess Mitochondrial Toxicity. DOI: 10.1089/ten.tec.2016.0264.

(57) Ostrovidov, S.; Hosseini, V.; Ahadian, S.; Fujie, T.; Parthiban, S. P.; Ramalingam, M.; Bae, H.; Kaji, H.; Khademhosseini, A. Skeletal Muscle Tissue Engineering: Methods to Form Skeletal Myotubes and Their Applications. DOI: 10.1089/ten.teb.2013.0534.

(58) Dutton, E.; Uhm, C.; Samuelsson, S. Acetylcholine receptor aggregation at nerve-muscle contacts in mammalian cultures: induction by ventral spinal cord neurons is specific to axons. *J.* **1995**.

(59) Merlie, J.; Sanes, J. Concentration of acetylcholine receptor mRNA in synaptic regions of adult muscle fibres. **1985**.

(60) Wagner, S.; Dorchies, O.; Stoeckel, H.; Warter, J. Functional maturation of nicotinic acetylcholine receptors as an indicator of murine muscular differentiation in a new nerve-muscle co-culture system. *Pflügers Arch.* **2003**.

(61) Dhawan, V.; Lytle, I.; Dow, D.; Huang, Y. Neurotization improves contractile forces of tissue-engineered skeletal muscle. *Tissue* **2007**.

(62) Harrison, R. G.; Greenman, M. J.; Mall, F. P.; Jackson, C. M. Observations of the living developing nerve fiber. *Anat. Rec.* **1907**, *1* (5), 116–128 DOI: 10.1002/ar.1090010503.

(63) Dimauro, S.; Arnold, S.; Miranda, A. McArdle disease: the mystery of reappearing phosphorylase activity in muscle culture—a fetal isoenzyme. *Ann.* **1978**.

(64) Tahmoush, A.; Askanas, V.; Nelson, P.; Engel, W. Electrophysiologic properties of aneurally cultured muscle from patients with myotonic muscular atrophy. *Neurology* **1983**.

(65) Miranda, A.; Mongini, T. Duchenne muscle culture: current status and future trends. *Neuromuscul. Dis. G. Serratrice, D. Cros, C.* **1984**.

(66) Askanas, V.; Kwan, H.; Alvarez, R. B.; Engel, W. K.; Kobayashi, T.; Martinuzzi, A.; Hawkins, E. F. De novo neuromuscular junction formation on human muscle fibres cultured in monolayer and innervated by foetal rat spinal cord: Ultrastructural and ultrastructural-cytochemical studies. *J. Neurocytol.* **1987**, *16* (4), 523–537 DOI: 10.1007/BF01668506.

(67) Campenot, R. B. [25] Independent control of the local environment of somas and neurites; 1979; pp 302–307.

(68) Tong, Z.; Seira, O.; Casas, C.; Reginensi, D.; Homs-Corbera, A.; Samitier, J.; Del Río, J. A.; Guo, X.; Hickman, J. J.; Vanhoutte, P.; et al. Engineering a functional neuro-muscular junction model in a chip. *RSC Adv.* **2014**, *4* (97), 54788–54797 DOI: 10.1039/C4RA10219C.

(69) Southam, K. A.; King, A. E.; Blizzard, C. A.; McCormack, G. H.; Dickson, T. C. Microfluidic primary culture model of the lower motor neuron–neuromuscular junction circuit. *J. Neurosci. Methods* **2013**, *218* (2), 164–169 DOI: 10.1016/j.jneumeth.2013.06.002.

(70) Ionescu, A.; Zahavi, E. E.; Gradus, T.; Ben-Yaakov, K.; Perlson, E. Compartmental microfluidic system for studying muscle–neuron communication and neuromuscular junction maintenance. *Eur. J. Cell Biol.* **2016**, *95* (2), 69–88 DOI: 10.1016/j.ejcb.2015.11.004.

(71) Smith, A. S. T.; Long, C. J.; Pirozzi, K.; Najjar, S.; McAleer, C.; Vandenburgh, H. H.; Hickman, J. J. *A multiplexed chip-based assay system for investigating the functional development of human skeletal myotubes in vitro*; 2014; Vol. 185.
(72) Smith, A. S. T.; Long, C. J.; Pirozzi, K.; Hickman, J. J. A functional system for high-content screening of neuromuscular junctions in vitro. *Technology* **2013**, *1* (1), 37–48 DOI: 10.1142/S2339547813500015.
(73) Rabieh, N.; Ojovan, S. M.; Shmoel, N.; Erez, H.; Maydan, E.; Spira, M. E. On-chip, multisite extracellular and intracellular recordings from primary cultured skeletal myotubes. *Sci. Rep.* **2016**, *6*, 36498 DOI: 10.1038/srep36498.
(74) Uzel, S. G. M.; Platt, R. J.; Subramanian, V.; Pearl, T. M.; Rowlands, C. J.; Chan, V.; Boyer, L. A.; So, P. T. C.; Kamm, R. D. Microfluidic device for the formation of optically excitable, three-dimensional, compartmentalized motor units. *Sci. Adv.* **2016**, *2* (8).
(75) Guo, X.; Gonzalez, M.; Stancescu, M.; Vandenburgh, H. H.; Hickman, J. J. Neuromuscular junction formation between human stem cell-derived motoneurons and human skeletal muscle in a defined system. *Biomaterials* **2011**, *32* (36), 9602–9611 DOI: 10.1016/j.biomaterials.2011.09.014.
(76) Yoshida, M.; Kitaoka, S.; Egawa, N.; Yamane, M.; Ikeda, R.; Tsukita, K.; Amano, N.; Watanabe, A.; Morimoto, M.; Takahashi, J.; et al. *Modeling the Early Phenotype at the Neuromuscular Junction of Spinal Muscular Atrophy Using Patient-Derived iPSCs*; 2015; Vol. 4.
(77) Pawlina, W.; Ross, M.; Kaye, G. Histology: a text and atlas: with cell and molecular biology. *Hagerstown, Maryl. Lippincott Williams* **2003**.
(78) Hinds, S.; Bian, W.; Dennis, R.; Bursac, N. The role of extracellular matrix composition in structure and function of bioengineered skeletal muscle. *Biomaterials* **2011**.
(79) Asano, T.; Ishizuka, T.; Morishima, K.; Yawo, H. Optogenetic induction of contractile ability in immature C2C12 myotubes. *Sci. Rep.* **2015**, *5* (1), 8317 DOI: 10.1038/srep08317.
(80) Demestre, M.; Orth, M.; Föhr, K. J.; Achberger, K.; Ludolph, A. C.; Liebau, S.; Boeckers, T. M. Formation and characterisation of neuromuscular junctions between hiPSC derived motoneurons and myotubes. *Stem Cell Res.* **2015**, *15* (2), 328–336 DOI: 10.1016/j.scr.2015.07.005.
(81) Puttonen, K. A.; Ruponen, M.; Naumenko, N.; Hovatta, O. H.; Tavi, P.; Koistinaho, J. Generation of Functional Neuromuscular Junctions from Human Pluripotent Stem Cell Lines. *Front. Cell. Neurosci.* **2015**, *9*, 473 DOI: 10.3389/fncel.2015.00473.
(82) Duffy, R.; Feinberg, A. Engineered skeletal muscle tissue for soft robotics: fabrication strategies, current applications, and future challenges. *Wiley Interdiscip. Rev.* **2014**.
(83) Norman, J.; Desai, T. Control of cellular organization in three dimensions using a microfabricated polydimethylsiloxane–collagen composite tissue scaffold. *Tissue Eng.* **2005**.
(84) Aubin, H.; Nichol, J. W.; Hutson, C. B.; Bae, H.; Sieminski, A. L.; Cropek, D. M.; Akhyari, P.; Khademhosseini, A. Directed 3D cell alignment and elongation in microengineered hydrogels. *Biomaterials* **2010**, *31* (27), 6941–6951 DOI:

10.1016/j.biomaterials.2010.05.056.
(85) LARKIN, L. M.; VAN DER MEULEN, J. H.; DENNIS, R. G.; KENNEDY, J. B. FUNCTIONAL EVALUATION OF NERVE–SKELETAL MUSCLE CONSTRUCTS ENGINEERED IN VITRO. *Vitr. Cell. Dev. Biol. - Anim.* **2006**, *42* (3), 75 DOI: 10.1290/0509064.1.
(86) Morimoto, Y.; Kato-Negishi, M.; Onoe, H.; Takeuchi, S. Three-dimensional neuron-muscle constructs with neuromuscular junctions. *Biomaterials* **2013**, *34* (37), 9413–9419 DOI: 10.1016/j.biomaterials.2013.08.062.
(87) R.W., M.; L., P.; J., P.; MuderaVivek; BaarKeith; GreensmithLinda; P., L. Neuromuscular Junction Formation in Tissue-Engineered Skeletal Muscle Augments Contractile Function and Improves Cytoskeletal Organization. *http://www.liebertpub.com/tea* **2015** DOI: 10.1089/TEN.TEA.2015.0146.
(88) Takahashi, H.; Shimizu, T.; Nakayama, M.; Yamato, M.; Okano, T. Anisotropic Cellular Network Formation in Engineered Muscle Tissue through the Self-Organization of Neurons and Endothelial Cells. *Adv. Healthc. Mater.* **2015**, *4* (3), 356–360 DOI: 10.1002/adhm.201400297.
(89) Smith, A. S. T.; Passey, S. L.; Martin, N. R. W.; Player, D. J.; Mudera, V.; Greensmith, L.; Lewis, M. P. Creating Interactions between Tissue-Engineered Skeletal Muscle and the Peripheral Nervous System. *Cells. Tissues. Organs* **2016**, *202* (3–4), 143–158 DOI: 10.1159/000443634.
(90) Vilmont, V.; Cadot, B.; Ouanounou, G.; Gomes, E. R. A system for studying mechanisms of neuromuscular junction development and maintenance. *Development* **2016**, *143* (13).
(91) Guo, X.; Colon, A.; Akanda, N.; Spradling, S.; Stancescu, M.; Martin, C.; Hickman, J. J. Tissue engineering the mechanosensory circuit of the stretch reflex arc with human stem cells: Sensory neuron innervation of intrafusal muscle fibers. *Biomaterials* **2017**, *122*, 179–187 DOI: 10.1016/j.biomaterials.2017.01.005.
(92) Wray, L.; Rnjak-Kovacina, J.; Mandal, B.; Schmidt, D. A silk-based scaffold platform with tunable architecture for engineering critically-sized tissue constructs. *Biomaterials* **2012**.
(93) Ziv, K.; Nuhn, H.; Ben-Haim, Y.; Sasportas, L.; Kempen, P. A tunable silk–alginate hydrogel scaffold for stem cell culture and transplantation. *Biomaterials* **2014**.
(94) Scott, J. B.; Ward, C. L.; Corona, B. T.; Deschenes, M. R.; Harrison, B. S.; Saul, J. M.; Christ, G. J. Achieving Acetylcholine Receptor Clustering in Tissue-Engineered Skeletal Muscle Constructs In vitro through a Materials-Directed Agrin Delivery Approach. *Front. Pharmacol.* **2016**, *7*, 508 DOI: 10.3389/fphar.2016.00508.
(95) Dellavalle, A.; Sampaolesi, M.; Tonlorenzi, R.; Tagliafico, E.; Sacchetti, B.; Perani, L.; Innocenzi, A.; Galvez, B. G.; Messina, G.; Morosetti, R.; et al. Pericytes of human skeletal muscle are myogenic precursors distinct from satellite cells. *Nat. Cell Biol.* **2007**, *9* (3), 255–267 DOI: 10.1038/ncb1542.
(96) Zheng, B.; Cao, B.; Crisan, M.; Sun, B.; Li, G.; Logar, A.; Yap, S.; Pollett, J. B.; Drowley, L.; Cassino, T.; et al. Prospective identification of myogenic endothelial cells in human skeletal muscle. *Nat. Biotechnol.* **2007**, *25* (9), 1025–1034 DOI: 10.1038/nbt1334.

(97) Rockwood, D. N.; Preda, R. C.; Yücel, T.; Wang, X.; Lovett, M. L.; Kaplan, D. L. Materials fabrication from Bombyx mori silk fibroin. *Nat. Protoc.* **2011**, *6* (10), 1612–1631 DOI: 10.1038/nprot.2011.379.
(98) Cairns, D. M.; Chwalek, K.; Moore, Y. E.; Kelley, M. R.; Abbott, R. D.; Moss, S.; Kaplan, D. L. Expandable and Rapidly Differentiating Human Induced Neural Stem Cell Lines for Multiple Tissue Engineering Applications. *Stem cell reports* **2016**, *7* (3), 557–570 DOI: 10.1016/j.stemcr.2016.07.017.
(99) Hu, X.; Park, S.-H.; Gil, E. S.; Xia, X.-X.; Weiss, A. S.; Kaplan, D. L. The influence of elasticity and surface roughness on myogenic and osteogenic-differentiation of cells on silk-elastin biomaterials. *Biomaterials* **2011**, *32* (34), 8979–8989 DOI: 10.1016/j.biomaterials.2011.08.037.
(100) Borg, T. K.; Caulfield, J. B. Morphology of connective tissue in skeletal muscle. *Tissue Cell* **1980**, *12* (1), 197–207 DOI: 10.1016/0040-8166(80)90061-0.
(101) Snyman, C.; Goetsch, K. P.; Myburgh, K. H.; Niesler, C. U. Simple silicone chamber system for in vitro three-dimensional skeletal muscle tissue formation. *Front. Physiol.* **2013**, *4*, 349 DOI: 10.3389/fphys.2013.00349.
(102) Vandenburgh, H. High-Content Drug Screening with Engineered Musculoskeletal Tissues. *Tissue Eng. Part B Rev.* **2010**, *16* (1), 55–64 DOI: 10.1089/ten.teb.2009.0445.
(103) Juhas, M.; Engelmayr, G. C.; Fontanella, A. N.; Palmer, G. M.; Bursac, N. Biomimetic engineered muscle with capacity for vascular integration and functional maturation in vivo. *Proc. Natl. Acad. Sci. U. S. A.* **2014**, *111* (15), 5508–5513 DOI: 10.1073/pnas.1402723111.
(104) Alberti, K. A.; Xu, Q. Slicing, Stacking and Rolling: Fabrication of Nanostructured Collagen Constructs from Tendon Sections. *Adv. Healthc. Mater.* **2013**, *2* (6), 817–821 DOI: 10.1002/adhm.201200319.
(105) Alberti, K. A.; Hopkins, A. M.; Tang-Schomer, M. D.; Kaplan, D. L.; Xu, Q. The behavior of neuronal cells on tendon-derived collagen sheets as potential substrates for nerve regeneration. *Biomaterials* **2014**, *35* (11), 3551–3557 DOI: 10.1016/j.biomaterials.2013.12.082.
(106) Komarova, G. A.; Starodubtsev, S. G.; Khokhlov, A. R. Investigation of physical-chemical properties of agarose hydrogels with embedded emulsions. *J. Phys. Chem. B* **2009**, *113* (45), 14849–14853 DOI: 10.1021/jp901255c.
(107) Jose, R. R.; Rodriguez, M. J.; Dixon, T. A.; Omenetto, F.; Kaplan, D. L. Evolution of Bioinks and Additive Manufacturing Technologies for 3D Bioprinting. *ACS Biomater. Sci. Eng.* **2016**, *2* (10), 1662–1678 DOI: 10.1021/acsbiomaterials.6b00088.
(108) Neal, D.; Sakar, M. S.; Ong, L.-L. S.; Harry Asada, H.; Suh, K.-Y.; Reyes, M.; Kim, D.-H.; Chen, D. Z.; Rosen, E. D.; Xu, Z.; et al. Formation of elongated fascicle-inspired 3D tissues consisting of high-density, aligned cells using sacrificial outer molding. *Lab Chip* **2014**, *14* (11), 1907 DOI: 10.1039/c4lc00023d.
(109) Hogan, Q. Size of Human Lower Thoracic and Lumbosacral Nerve Roots. *J. Am. Soc. Anesthesiol.* **1996**, *85* (1), 37–42.
(110) J. LAWSON-SMITH, M.; K. McGEACHIE, J. The identification of myogenic cells in skeletal muscle, with emphasis on the use of tritiated thymidine autoradiography and desmin antibodies. *J. Anat.* **1998**, *192* (2), 161–171.

(111) Bigot, A.; Jacquemin, V.; Debacq-Chainiaux, F.; Butler-Browne, G. S.; Toussaint, O.; Furling, D.; Mouly, V. Replicative aging down-regulates the myogenic regulatory factors in human myoblasts. *Biol. Cell* **2008**, *100* (3), 189–199 DOI: 10.1042/BC20070085.
(112) Hopkins, A. M.; De Laporte, L.; Tortelli, F.; Spedden, E.; Staii, C.; Atherton, T. J.; Hubbell, J. A.; Kaplan, D. L. Silk Hydrogels as Soft Substrates for Neural Tissue Engineering. *Adv. Funct. Mater.* **2013**, *23* (41), 5140–5149 DOI: 10.1002/adfm.201300435.
(113) Whitemarsh, R. C. M.; Pier, C. L.; Tepp, W. H.; Pellett, S.; Johnson, E. A. Model for studying Clostridium botulinum neurotoxin using differentiated motor neuron-like NG108-15 cells. *Biochem. Biophys. Res. Commun.* **2012**, *427* (2), 426–430 DOI: 10.1016/j.bbrc.2012.09.082.
(114) Choi, R. C. .; Yam, S. C. .; Hui, B.; Wan, D. C. .; Tsim, K. W. . Over-expression of acetylcholinesterase stimulates the expression of agrin in NG108–15 cells. *Neurosci. Lett.* **1998**, *248* (1), 17–20 DOI: 10.1016/S0304-3940(98)00320-6.
(115) Chen, S.-S.; Lin, C.-H.; Chen, T.-J. Lead-induced attenuation in the aggregation of acetylcholine receptors during the neuromuscular junction formation. *Toxicol. Lett.* **2005**, *159* (1), 89–99 DOI: 10.1016/j.toxlet.2005.04.011.
(116) Torrejais, M. M.; Soares, J. C.; Matheus, S. M. M.; Cassel, F. D.; Mello, J. M.; Basso, N. A. Histochemical and SEM evaluation of the neuromuscular junctions from alcoholic rats. *Tissue Cell* **2002**, *34* (2), 117–123.
(117) Desaki, J.; Uehara, Y. The overall morphology of neuromuscular junctions as revealed by scanning electron microscopy. *J. Neurocytol.* **1981**, *10*, 101–110.
(118) Magin, C. M.; Alge, D. L.; Anseth, K. S. Bio-inspired 3D microenvironments: a new dimension in tissue engineering. *Biomed. Mater.* **2016**, *11* (2), 22001 DOI: 10.1088/1748-6041/11/2/022001.
(119) Shamir, E. R.; Ewald, A. J. Three-dimensional organotypic culture: experimental models of mammalian biology and disease. *Nat Rev Mol Cell Biol* **2014**, *15* (10), 647–664.
(120) Wu, W.; Manz, A.; Xu, W.; Güse, K.; Abell, C.; Hollfelder, F.; Revzin, A. Rapid manufacture of modifiable 2.5-dimensional (2.5D) microstructures for capillary force-driven fluidic velocity control. *RSC Adv.* **2015**, *5* (87), 70737–70742 DOI: 10.1039/C5RA13407B.
(121) Di Buduo, C. A.; Wray, L. S.; Tozzi, L.; Malara, A.; Chen, Y.; Ghezzi, C. E.; Smoot, D.; Sfara, C.; Antonelli, A.; Spedden, E.; et al. Programmable 3D silk bone marrow niche for platelet generation ex vivo and modeling of megakaryopoiesis pathologies. *Blood* **2015**, *125* (14).
(122) Vickerman, V.; Blundo, J.; Chung, S.; Kamm, R. Design, fabrication and implementation of a novel multi-parameter control microfluidic platform for three-dimensional cell culture and real-time imaging. *Lab Chip* **2008**, *8* (9), 1468–1477 DOI: 10.1039/b802395f.
(123) Rodriguez, M. J.; Brown, J.; Giordano, J.; Lin, S. J.; Omenetto, F. G.; Kaplan, D. L. Silk based bioinks for soft tissue reconstruction using 3-dimensional (3D) printing with in vitro and in vivo assessments. *Biomaterials* **2017**, *117*, 105–115 DOI: 10.1016/j.biomaterials.2016.11.046.
(124) Charest, J. L.; García, A. J.; King, W. P. Myoblast alignment and differentiation on

cell culture substrates with microscale topography and model chemistries. *Biomaterials* **2007**, *28* (13), 2202–2210 DOI: 10.1016/j.biomaterials.2007.01.020.
(125) Zorlutuna, P.; Jeong, J. H.; Kong, H.; Bashir, R. Stereolithography-Based Hydrogel Microenvironments to Examine Cellular Interactions. *Adv. Funct. Mater.* **2011**, *21* (19), 3642–3651 DOI: 10.1002/adfm.201101023.
(126) Steinbeck, J. A.; Jaiswal, M. K.; Calder, E. L.; Kishinevsky, S.; Weishaupt, A.; Toyka, K. V; Goldstein, P. A.; Studer, L. Functional Connectivity under Optogenetic Control Allows Modeling of Human Neuromuscular Disease. *Cell Stem Cell* **2016**, *18* (1), 134–143 DOI: 10.1016/j.stem.2015.10.002.
(127) Sato, M.; Ito, A.; Kawabe, Y.; Nagamori, E.; Kamihira, M. Enhanced contractile force generation by artificial skeletal muscle tissues using IGF-I gene-engineered myoblast cells. *J. Biosci. Bioeng.* **2011**, *112* (3), 273–278 DOI: 10.1016/j.jbiosc.2011.05.007.
(128) Zhang, B. G. X.; Quigley, A. F.; Bourke, J. L.; Nowell, C. J.; Myers, D. E.; Choong, P. F. M.; Kapsa, R. M. I. Combination of agrin and laminin increase acetylcholine receptor clustering and enhance functional neuromuscular junction formation *In vitro*. *Dev. Neurobiol.* **2016**, *76* (5), 551–565 DOI: 10.1002/dneu.22331.
(129) Ray, W. Z.; Pet, M. A.; Yee, A.; Mackinnon, S. E. Double fascicular nerve transfer to the biceps and brachialis muscles after brachial plexus injury: clinical outcomes in a series of 29 cases. *J. Neurosurg.* **2011**, *114* (6), 1520–1528 DOI: 10.3171/2011.1.JNS10810.
(130) Smith, A. S. T.; Davis, J.; Lee, G.; Mack, D. L.; Kim, D.-H. Muscular dystrophy in a dish: engineered human skeletal muscle mimetics for disease modeling and drug discovery. *Drug Discov. Today* **2016**, *21* (9), 1387–1398 DOI: 10.1016/j.drudis.2016.04.013.
(131) Cheng, C. S.; El-Abd, Y.; Bui, K.; Hyun, Y.-E.; Hughes, R. H.; Kraus, W. E.; Truskey, G. A. Conditions that promote primary human skeletal myoblast culture and muscle differentiation in vitro. *Am. J. Physiol. - Cell Physiol.* **2014**, *306* (4).
(132) Gerhardt, K. P.; Olson, E. J.; Castillo-Hair, S. M.; Hartsough, L. A.; Landry, B. P.; Ekness, F.; Yokoo, R.; Gomez, E. J.; Ramakrishnan, P.; Suh, J.; et al. An open-hardware platform for optogenetics and photobiology. *Sci. Rep.* **2016**, *6*, 35363 DOI: 10.1038/srep35363.
(133) Halevy, O.; Biran, I.; Rozenboim, I. Various light source treatments affect body and skeletal muscle growth by affecting skeletal muscle satellite cell proliferation in broilers. *Comp. Biochem. Physiol. Part A Mol. Integr. Physiol.* **1998**, *120* (2), 317–323 DOI: 10.1016/S1095-6433(98)10032-6.
(134) Sakar, M. S.; Neal, D.; Boudou, T.; Borochin, M. A.; Li, Y.; Weiss, R.; Kamm, R. D.; Chen, C. S.; Asada, H. H. Formation and optogenetic control of engineered 3D skeletal muscle bioactuators. *Lab Chip* **2012**, *12* (23), 4976 DOI: 10.1039/c2lc40338b.